
**Addis Ababa University**
**College of Technology and Built Environment**
**School of Electrical and Computer Engineering**

# Stability Challenges and Solutions in High-PV Penetration Grids: A Case Study of Ethiopia and Kenya HVDC link.

**By Teshome Hambissa Dimbassa**

A dissertation submitted to the Graduate School of Electrical and Computer Engineering in partial fulfillment of the requirements for the Degree of Doctor of Philosophy (Ph.D.) in Electrical Engineering (Electrical Power Engineering).

**July 16, 2025**

**Addis Ababa, Ethiopia**



## Supervisor

**Getachew Biru (Ph.D.)**
Addis Ababa University,
College of Engineering and Environmental Built,
Addis Ababa,
Ethiopia

## Supervisor

**Mehrdad Ghandhari (Professor.)**
KTH Royal Institute of Technology,
Stockholm,
Sweden

# Addis Ababa University
# College of Technology and Built Environment
# School of Electrical and Computer Engineering

---

## Stability Challenges and Solutions in High-PV Penetration Grids: A Case Study of Ethiopia and Kenya HVDC link.

---


**By Teshome Hambissa Dimbassa**

## Supervisor

**Getachew Biru (Ph.D.)**
Addis Ababa University,
College of Engineering and Environmental Built,
Addis Ababa,
Ethiopia

## Supervisor

**Mehrdad Ghandhari (Professor.)**
KTH Royal Institute of Technology,
Stockholm,
Sweden

# Approved by Examining Committee

| | | |
|---|---|---|
| **Dean, School of Graduate Studies** | **Signature** | **Date** |
| | | |
| **Advisor** | | |
| | | |
| **Internal Examiner** | | |
| | | |
| **External Examiner** | | |
| | | |

# Declaration

This Ph.D. dissertation is a presentation of my work and any material used from other sources has been clearly identified and properly acknowledged and cited.

# Acknowledgments

First and foremost, I would like to express my heartfelt gratitude to Almighty God for blessing me with guidance and support throughout this journey. I would like to extend my sincere appreciation to my supervisors, Dr. Getachew Biru and Prof. Mehrdad Ghandhari. I sincerely appreciate all the guidance, support, knowledge, and considerable time and effort you have devoted to me. I have learned a great deal from both of you regarding what a Ph.D. entails, and I look forward to the opportunity to work with you again. I would also like to thank the staff members at my school and the members of the Control Chair and Power Chair, Dr. Mengesha Mamo and Prof. N.P. Singh, for their valuable insights and feedback on my work throughout this process. My deepest gratitude goes to my sponsor, the honored SIDA of Ethio-Sweden Capacity Building, for their continuous support through this journey.

I would also like to acknowledge my best friend, Mr. Mesfin Tilahun, for his unwavering support and best friendship, both during my time in Sweden and in my home country. His encouragement and ideas have been invaluable in my journey. With a distinct personality, I have always been influenced by those around me. Moving to Sweden and starting a new chapter was a significant challenge. I especially want to express my gratitude to Danilo Obradovic for his unwavering support and encouragement throughout my thesis work. I also want to thank all my friends who continued their research with me in Sweden. Thank you very much for sharing the best times and for your encouragement throughout this journey. Additionally, I would like to thank KTH Royal Institute of Technology for providing everything necessary for my work during my time in Sweden. Special thanks to my supervisor, Prof. Mehrdad Ghandhari, for your unwavering support.

Finally, I would like to acknowledge my family, especially my beloved wife, for standing by me and supporting me throughout this journey. Your love and encouragement have been my greatest source of strength. Thank you all for being part of this journey.

In loving memory of my sister.

# Abstract

The Ethiopia-Kenya HVDC project represents a significant advance in power transmission, establishing a ±500 kV bipolar HVDC link with a capacity of 2000 MW to enhance regional energy integration and promote sustainable development. This ambitious initiative facilitates the export of Ethiopia's substantial hydroelectric resources while addressing the growing demand for electricity in East Africa. As Ethiopia prioritizes renewable energy sources, including hydro, wind, and solar, its power system faces opportunities and challenges in integrating large-scale photovoltaic (LSP) systems. Although LSP systems promise carbon-free electricity and improved grid resilience, their integration introduces complexities such as reduced system inertia, increased frequency oscillations, and dependence on advanced inverter technologies.

This thesis explores advanced methodologies for enhancing the stability and resilience of the Ethiopian power grid amid the increasing integration of renewable energy sources, particularly photovoltaic (PV) systems. The transition from traditional Synchronous generators (SGs) to large scale PV plants has reduced system inertia, amplifying the challenges associated with transient stability and frequency control. To address these concerns, three distinct yet interconnected studies are presented.

First, the modeling of the Ethiopia-Kenya HVDC link using DIgSILENT software demonstrates that the implementation of HVDC technology significantly improves transient stability. Next, the research evaluates FACTS-based supplementary control strategies, including Power Oscillation Damping (POD) and a novel Control Lyapunov Function (CLF) approach integrated with STATCOM to mitigate electromechanical oscillations in grids with high PV penetration. Simulations of severe three-phase faults near the HVDC rectifier terminal reveal that the CLF-based controller outperforms POD in damping ratio enhancement and dynamic response evaluation, particularly in high PV scenarios. Third, the study proposes Battery Energy Storage Systems (BESS) as a fast frequency control (FFC) solution to counteract the diminished inertial response of PV systems, effectively reducing the Instantaneous Frequency Deviation (IFD) during disturbances. The simulations convincingly demonstrate that the proposed BESS frequency control scheme effectively reduces the maximum frequency deviation and suppresses significant frequency excursions under various disturbance and PV penetration conditions.

In general, this thesis emphasizes the integration of advanced control strategies, including HVDC, FACTS-based supplementary controls, and BESS, to ensure a stable and reliable power system in the face of the burgeoning adoption of renewable energy. The findings underscore the necessity of adaptive control frameworks to mitigate risks posed by reduced inertia and transient instability, safeguarding grid resilience as Ethiopia transitions toward a renewable-dominated energy future.

**Keywords:** large-scale photovoltaic, supplementary control, fast frequency control, instantaneous frequency deviation, and battery energy storage systems.

# Contents

*

# List of Figures

# List of Tables

# Acronyms

| | |
|---|---|
| **BESS** | **B**attery Energy Storage Systems |
| **CCT** | **C**ritical clearing time |
| **CIGRE** | **I**nternational Council on Large Electric Systems |
| **CLF** | **C**ontrol Lyapunov Function |
| **CSC** | **C**urrent source converter |
| **CO2** | **C**arbon dioxide |
| **DSL** | **D**IgSILENT Simulation Language |
| **EMT** | **E**lectromagnetic transient |
| **FACTS** | **F**lexible Alternating Current Transmission System |
| **FCR** | **F**requency Containment Reserves |
| **FFC** | **F**ast Frequency Control |
| **FFR** | **F**ast Frequency Response |
| **HVDC** | **H**igh Voltage Direct Current |
| **IGBT** | **I**nsulated Gate Bipolar Transistor |
| **IFD** | **I**nstantaneous Frequency Deviation |
| **LCC** | **L**ine Commutated Converter |
| **LSP** | **L**arge-Scale Photovoltaic |
| **OLTCs** | **O**oad tap changers |
| **PCC** | **P**oint of common coupling |
| **PFC** | **P**ower frequency control |
| **PLL** | **P**hase locked loop |
| **POD** | **P**ower oscillating damping |
| **PV** | **P**hotovoltaic |
| **PI** | **P**roportional Integral |
| **PWM** | **P**ulse width modulation |
| **RMS** | **R**oot Mean Sqaure |
| **RESs** | **R**enewable Energy Sources |
| **RoCoF** | **R**ate-of-Change of Frequency |
| **SGs** | **S**ynchronous generators |
| **SOC** | **S**tate of charge |
| **SOs** | **S**ystem Operators |
| **SSFD** | **S**teady-State Frequency Deviation |
| **SSFD** | **S**teady-State Frequency Deviation |
| **TSO** | **T**ransmission System Operator |
| **ULTC** | **U**nder load tap changers |

# Nomenclature

| | |
|---|---|
| $U_{sr}$ | **R**ectifier RMS AC voltage |
| $U_{si}$ | **I**nverter RMS AC voltage |
| $U_{dr}$ | **R**ectifier DC voltage |
| $U_{di}$ | **I**nverter DC voltage |
| $I_d$ | **D**C line current |
| $\alpha$ | **F**iring angle of the rectifier |
| $\gamma$ | **I**nverter extinction angle rectifier |
| $N$ | **N**o. of 6-pulse bridges |
| $T$ | **T**transformation turn ratio |
| $R_L$ | **R**esistance of the HVDC line |
| $R_r$ | **R**esistance of the rectifier |
| $R_i$ | **R**esistance of the inverer |
| $P_{ac}$ | **A**ctive power from AC to DC |
| $Q_{ac}$ | **R**reactive power from AC to DC |
| $P_{dcr}$ | **D**C power injected from rectifier converter |
| $I_d$ | **C**urrent of the DC line |
| $f_0$ | **N**ominal frequency |
| $T_w$ | **W**ash time constant |
| $T_1$ | **A** time constant for the lead part of the filter |
| $T_2$ | **A** time constant for the lag part of the filter |
| $P_{elec}$ | **E**lectrical power |
| $P_{mech}$ | **M**echanical power |
| $Rect$ | **R**ectifier |
| $Inv$ | **I**nverter |

# 1 Introduction

## 1.1 Background

Power systems represent one of humanity's most significant technical achievements, evolving from their initial role of providing electricity for prestigious facilities to delivering reliable power to a vast portion of the global population. This remarkable growth is the result of sustained engineering advancements, scientific development, and market integration, reflecting the essential role power systems play in societal progress. However, the pursuit of a fair and secure energy future is fraught with challenges, as the benefits of these systems often reach only a limited segment of the population [1]. Global warming has become a significant concern in recent decades, primarily driven by greenhouse gas emissions, particularly CO2. The increase in industrial development and the increasing demands for energy have exacerbated these emissions, leading to pollution and erratic environmental changes. Society's efforts to address global warming have prompted essential actions to reduce emissions and promote system sustainability and security [2].

To address global warming, power systems are increasingly incorporating RES to supplement and replace conventional fossil fuel and nuclear generation. The integration of Low-Cost LCC HVDC technology is crucial in this process, as it allows for the efficient transmission of electricity over long distances with minimal energy loss, connecting remote renewable energy sources like wind farms and solar arrays to urban centers. LCC HVDC enhances stability and reliability by quickly adjusting to fluctuations in power generation, ensuring a steady supply despite the intermittent nature of RES. Additionally, it enables interconnection between different power grids, allowing for the sharing of renewable energy across regions and improving overall resilience. With reduced transmission losses compared to traditional AC systems, LCC HVDC is more efficient for transporting electricity from RES, which is particularly important as their share in the energy mix increases. Furthermore, it supports decentralized generation, empowering local energy production and consumption. Overall, the combination of RES integration with LCC HVDC technology is vital for transitioning to a more sustainable energy future while effectively addressing the challenges posed by global warming [3].

The transition to renewable energy sources is crucial for modern power systems, particularly in regions like Ethiopia, where the integration of LSP systems and HVDC links presents both significant opportunities and challenges. The Ethiopia-Kenya HVDC project, a ±500 kV

bipolar link spanning approximately 1045 km, aims to facilitate power exchange and enhance regional integration, enabling the import of electricity from Ethiopia's abundant hydropower resources. With Ethiopia's impressive hydropower potential of 45 GW, alongside growing contributions from wind and solar energy, the country prioritizes the generation of clean and sustainable electricity [4].

However, the increased penetration of RESs, particularly photovoltaic systems, introduces complexities related to transient stability and frequency control within the grid. The intermittent nature of RES can lead to reduced system inertia, affecting the power system's ability to maintain synchronism during disturbances [5]. This concern is echoed in studies examining the effects of HVDC links on transient stability under various fault conditions [6]. As the electricity demand continues to rise, maintaining system stability becomes critical, necessitating the development of robust control strategies and the integration of technologies like BESS [7], [8]. In addition to these considerations, there are several mitigation techniques proposed by the author. One approach involves using FACTS-based supplementary control for POD and CLF controllers to address electromechanical damping oscillations, along with BESS for rapid frequency control. The emphasis is on evaluating how different levels of LSP integration impact rotor angle dynamics and fluctuations in active power output near the rectifier terminal bus after a fault, while also assessing the effectiveness of the chosen FACTS-based controllers. Furthermore, the analysis includes the performance of BESS during load or generation contingencies under varying levels of PV integration.

This paper aims to create a detailed model of the Ethiopia-Kenya HVDC link to study the stability of the power system using DIgSILENT simulation software and to evaluate the impact of integrating LSP systems on the transient stability of the Ethiopian power grid. By assessing varying levels of LSP integration, the effects on rotor angle dynamics, active power output and frequency stability will be analyzed. The findings will provide valuable information on the role of renewable energy in modern power systems, particularly about fault conditions and system stability, while addressing the challenges of high PV penetration and the integration of battery energy storage systems for frequency regulation in low-inertia power systems.

## 1.2 problem Statement

The increasing integration of PV systems into power grids has led to significant challenges in maintaining system stability, particularly as traditional synchronous generators are phased out. This transition results in reduced system inertia, which exacerbates frequency deviations and destabilizes power operations during disturbances. Additionally, the use of LCC HVDC systems, while beneficial for long-distance power transmission, presents challenges related to reactive power consumption. LCC HVDC systems require a significant amount of reactive power for their operation, which can strain the existing grid and further complicate stability under high renewable penetration scenarios. Furthermore, the growing variability of renewable energy sources creates additional complexities in power management. Existing solutions to address these challenges are limited, highlighting a critical gap in understanding how advanced technologies, such as LCC HVDC, BESS, and FACTS-based supplementary control strategies can be effectively utilized. This research seeks to explore integrating these technologies to enhance grid reliability and performance, ultimately mitigating the adverse effects of high renewable energy penetration.

## 1.3 Research Objectives

In recent years, the global transition towards renewable energy sources has significantly influenced power system dynamics. Particularly in regions like Ethiopia, where LSP systems are being integrated, the displacement of traditional SGs has led to challenges in maintaining system stability and frequency control. As the penetration of PV increases, the overall inertia of the power grid decreases, exacerbating issues related to frequency deviations and transient stability. This necessitates the exploration of advanced control strategies and technologies, such as HVDC systems, BESS to support the evolving grid requirements.

### 1.3.1 General Objective

The general objective of this research is to improve the transient stability and frequency regulation of the Ethiopian power grid in light of the growing integration of variable renewable energy sources.

### 1.3.2 Specific Objective

To achieve this, the study focuses on the following specific objectives.

1. Analyze the effectiveness of HVDC systems in improving the transient stability of the grid.
2. Developing and validating fast frequency control techniques for BESS to mitigate frequency deviations caused by high PV penetration.
3. Investigating the implementation of FACTS-based supplementary controllers to address the instability arising from reduced system inertia and enhance overall grid reliability.

By achieving these objectives, the research aims to provide valuable insights and effective strategies for maintaining grid stability in the face of a rapidly changing energy landscape.

## 1.4 Major contribution of the research

As the global energy landscape shifts towards renewable sources, the integration of LSP systems has become increasingly prevalent. Although this transition offers environmental benefits, it also introduces significant challenges to the stability of the power system. The displacement of traditional synchronous generators reduces the inertia of the system, leading to increased frequency deviations and instability during disturbances. The existing literature highlights these issues, yet there remains a notable gap in understanding how advanced technologies, such as HVDC systems, BESS, and FACTS-based supplementary controllers, can effectively mitigate these challenges. This research aims to address this gap by exploring innovative control strategies that improve the stability and reliability of power systems amid the increase in renewable energy penetration.

The major contributions of this thesis address gaps identified in the existing literature and fulfill the three specific objectives outlined in the research context of the Ethiopian power grid. These contributions include the following key points.

1. Enhanced Understanding of HVDC Systems: This thesis provides a comprehensive analysis of how LCC HVDC systems can improve transient stability in the Ethiopian power grid, offering a framework for similar applications in other regions, typically neighboring countries or countries with similar grid structures.

2. Development of Frequency Control Techniques: The introduction of an FFC technique for BESS contributes to the body of knowledge on mitigating frequency deviations in grids with high PV penetration, demonstrating effective modeling and implementation strategies.

3. Insights into Power Oscillation Damping and Control Lyapunov Function: The exploration of FACTS-based supplementary controllers for POD and CLF highlights the importance of integrating advanced control technologies to enhance system stability and reliability, particularly in the context of reduced inertia from conventional generators.

## 1.5 Significance of the study

This thesis work holds significant importance as it tackles the pressing challenges that modern power systems face due to the increasing integration of renewable energy sources, particularly LSP systems, and the impact of HVDC on the existing legacy of HVAC systems. As these renewable technologies are adopted, traditional synchronous generators are being displaced, which leads to a decrease in system inertia. This reduction can cause instability in the power grid, resulting in frequency deviations and other operational challenges.

By investigating advanced solutions such as HVDC systems, BESS, and advance controller design, this research aims to provide different strategies for enhancing the stability and reliability of the Ethiopian power grid. The study highlights how these technologies can effectively mitigate the adverse effects of high penetration of photovoltaic energy, ensuring that the power system can maintain performance during disturbances and fluctuations. Furthermore, the findings of this study will be valuable for policymakers, engineers, and stakeholders involved in power system planning and management. By offering a framework for the implementation of these advanced technologies, the research will guide decision-making processes and support the transition to a more sustainable energy infrastructure. Ultimately, this study contributes to the broader goal of achieving a resilient and efficient energy system that can accommodate the growing share of renewable energy while ensuring a reliable electricity supply.

## 1.6 Thesis outline

The outline of the rest of this thesis work is as follows:

**Chapter 2** presents a literature review on HVDC technologies and power system stability, focusing on rotor angle and frequency stability.

**Chapter 3** discusses the modeling and simulation of the power grid in DIgSILENT, including a a transient stability analysis with and without HVDC links. In this chapter, the modeling focuses Ethipiaan grid modeling and LCC HVDC modeling for transient stability study.

**Chapter 4** explores FACTS solutions for power oscillation damping, detailing the modeling and simulation results.

**Chapter 5** examines frequency control challenges in the Ethiopian grid caused by PV integration and different disturbances, with a focus on the integration of BESS.

**Chapter 6** concludes the study and outlines future research directions.

## 1.7 List of Appended Publications

This dissertation is based on the papers listed below:

I ***Modeling of Ethiopia-Kenya HVDC for Power System Stability Study***
**Teshome Hambissa**, Getachew Biru, Mehrdad Ghandhari
*AFRICON Conference (2023).* This paper has been published in the 2023 IEEE AFRICON.

II ***Analysis of Fast Frequency Control Using Battery Energy Storage Systems in Mitigating Impact of Photovoltaic Penetration in Ethiopia-Kenya HVDC Link***.
**Teshome Hambissa**, Getachew Biru, Mehrdad Ghandhari
This paper has been published in International Journal of Electrical Power & Energy Systems (ELSEVIER), *Journal (2024)*

III ***Enhancing Transient Stability in Renewable-Integrated Power Grids through FACTS-based Power Oscillation Damping***.
**Teshome Hambissa**, Getachew Biru, Mehrdad Ghandhari. This article has been reviewed in the International Journal of Electrical Power & Energy Systems (ELSEVIER)

Paper *I* and *II* have been published in the 2023 IEEE AFRICON and International Journal of Electrical Power & Energy Systems (ELSEVIER), respectively, and Paper *III* is under review in International Journal of Electrical Power & Energy Systems (ELSEVIER).

# 2 Literature Review

## 2.1 Background

This chapter outlines the history of the LLC HVDC link within the grid and examines the stability of power systems. The review also looks into recently proposed solutions by researchers aimed at enhancing system stability through the use of HVDC, BESS, and FACTS-based POD and CLF.

## 2.2 Technologies of HVDC Links

The development of HVDC transmission systems began in the 1930s with the invention of mercury arc rectifiers. In 1941, the first contract for a commercial HVDC system was established to supply 60 MW to Berlin via a 115 km underground cable. Although the system was completed in 1945, it was dismantled due to the end of World War II and never became operational. It was not until 1954 that the first HVDC transmission system, with a capacity of 10 MW, was commissioned in Gotland. Since the 1960s, HVDC technology has matured significantly, playing a crucial role in long-distance power transmission and the interconnection of electrical systems [9]. HVDC transmission systems, once implemented, frequently serve as the foundation of an electric power network. They offer high reliability and have a long operational lifespan. The key component of these systems is the power converter, which acts as the interface with the AC transmission network. The conversion between AC and DC, and the reverse, is accomplished using controllable electronic switches (valves) arranged in a 3-phase bridge configuration. Various types of HVDC links based on the methods of AC to DC conversion are introduced in [9], [10]. LCC and VSC are the two distinct technologies in HVDC transmission systems. LCC HVDC utilizes current source converters with line-commutated thyristor valves, necessitating 50%-60% reactive power compensation. It requires a minimum short circuit capacity greater than twice the converter rating and offers fast active power control with conversion losses around 0.6%. In contrast, VSC HVDC employs voltage source converters featuring self-commutated IGBT valves, which do not require reactive power compensation (only about 15% harmonic filtering). This technology is suitable for weak grid and can facilitate black start operations. It is also more compact, providing rapid active and reactive power control, although it has higher conversion losses of approximately 1.6%. Overall, while LCC HVDC is robust and efficient for

large-scale applications, VSC technology offers greater flexibility and adaptability in various system conditions [11].

## 2.3 HVDC and its primary benefits.

The electrical industry is currently witnessing a significant competition between direct current (DC) and alternating current (AC) solutions. As energy demand and generation continue to rise, there has been an increasing shift toward AC systems. However, challenges persist, particularly in raising the voltage levels of submarine cables, which limits their high-power transmission capabilities. Additionally, the development of high-capacity hydroelectric projects in remote areas complicates the conventional use of AC for power transmission, as transmitting AC over long distances raises concerns about static stability and leads to higher power losses. Presently, the two primary technologies for HVDC are LCC, also known as CSC using thyristors, and VSC-HVDC, which utilize IGBT transistors. Both technologies are suitable for a variety of applications [12].

For long-distance and high-capacity transmission links, CSC-HVDC technology offers greater efficiency and higher power transfer capacity compared to traditional AC solutions. In scenarios involving power transmission from offshore plants or remote locations with space constraints, VSC-HVDC is the preferred option due to its excellent capabilities for active and reactive power control. The modern iterations of HVDC systems are based on technologies that were extensively developed in the 1930s, such as mercury-arc valves, in Sweden and Germany. Early commercial applications of HVDC include a system established in the Soviet Union in 1951, connecting Moscow and Kashira, as well as a 100 kV, 20 MW link between Gotland and mainland Sweden in 1954 [12]. Thyristor valves were first utilized in HVDC applications in the 1970s, effectively addressing many of the limitations associated with mercury-arc technology. The Eel River Converter Station in Canada, commissioned in 1972, was the first LCC-HVDC system to be put into operation [13].

HVDC transmission is predominantly adopted for economic reasons, offering several advantages:

- Cost Efficiency: HVDC systems can be more economical than AC transmission lines, particularly over long distances. The effective range for overhead lines is typically between 600 to 800 kilometers, which is shorter for submarine cables, where it is approximately 50 kilometers [14].
- Environmental Impact: HVDC transmission has benefits over AC in terms of lower

environmental and electromagnetic interference, along with reduced electric and magnetic fields.

- Back-to-Back Stations: A back-to-back station is a facility where converters are situated within the same building, allowing for efficient interconnection of different AC systems. There is typically no fixed-phase relationship between the systems.
- High Control Capability: HVDC technology offers significant control over power transmission.

In the case of LCC in HVDC links, it is important to note that the reactive power is not fully controllable. The converters tend to consume reactive power in proportion to the active power transmitted.In LCC-HVDC links, converters consume roughly 50-60% reactive power for every 100% of active power transmitted [15]. This reactive power consumption is inherent to the line-commutated converter technology and is not fully controllable. The high demand for reactive power and the need for harmonic filters are notable disadvantages of LCC HVDC transmission when compared to AC systems. Despite this, most of the currently installed HVDC capacity utilizes LCC technology due to its superior transmission capacity over VSC technology [16]. HVDC links are essential for efficient long-distance power transmission and integration of renewable energy sources.

## 2.4 Power system stability

Power system stability is the ability of an electric power system, for a given initial operating condition, to regain a state of operating equilibrium after being subjected to a physical disturbance, with most system variables bounded so that practically the entire system remains intact [17]. Understanding the types and magnitudes of disturbances is crucial for power system stability. SOs analyze historical data and use simulation models to categorize these disturbances, focusing on the most severe ones, such as equipment failures or natural events. By applying the N-1 stability criterion, SOs design control strategies to ensure that the system can withstand the loss of any single critical component without destabilizing. This proactive approach improves the resilience of the system, minimizes risks, and ensures reliable power delivery even in the face of unexpected challenges [18].

## 2.5 Classification of power system stability

Power system stability is fundamentally a single issue. However, power systems can encounter different types of instabilities that cannot be effectively resolved by approaching them as a singular problem. Classifying system stability into specific categories aids in analyzing

stability, pinpointing causes of instability, and developing strategies for improvement. The classification of power system stability is based on several factors, including the magnitude of disturbances, the physical characteristics of the resulting instability modes, the devices and processes involved, and the time frame considered for stability assessment. This framework allows for a comprehensive understanding of how various disturbances affect the system and how stability can be evaluated effectively [17]. Figure 2.1 describes the various forms of power system stability.

- Rotor angle stability
- Frequency stability
- Voltage stability

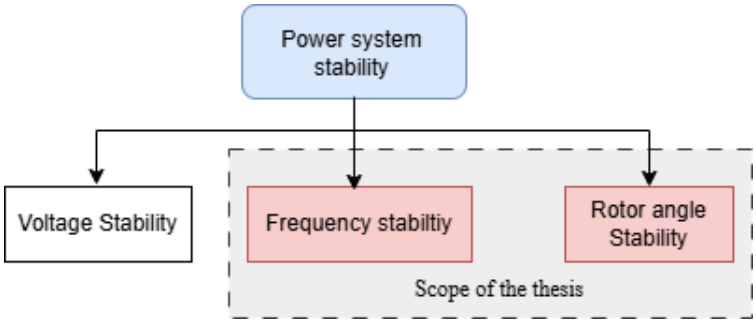


**Figure 2.1:** Classification of Power system stability [17]

### 2.5.1 Rotor angle stability

Rotor angle stability refers to the ability of synchronous machines of an interconnected power system to remain in synchronism after being subjected to a disturbance. The instability that may result occurs in the form of increasing angular swings of some generators, leading to their loss of synchronism with other generators. Loss of synchronism can occur between one machine and the rest of the system or between groups of machines, with synchronism maintained within each group after separating from each other [19].

Rotor angle stability involves maintaining a balance between the input mechanical torque and the output electrical torque of each generator. When this balance is disrupted, the generator's rotor may accelerate or decelerate, altering its angular position and leading to angular separation. If this separation exceeds a certain limit, it can trigger further instability. The electromagnetic torque in a synchronous machine after a disturbance consists of two components: synchronizing torque (aligned with rotor angle deviation) and damping torque (aligned with speed deviation). A lack of sufficient synchronizing torque can cause periodic instability, while inadequate damping torque leads to oscillatory instability. To better understand rotor angle stability issues, it can be categorized into two subtypes:

- **Small-disturbance stability:** focuses on a power system's ability to maintain synchronism when subjected to minor disturbances and mostly depends on initial operating state. These disturbances are deemed small enough to allow for the linearization of system equations for analysis. This type of stability is commonly known as Small Signal Stability. Small-disturbance rotor angle stability issues can be classified as either local or global. Local rotor angle oscillation modes are influenced by the strength of the transmission system, generator excitation control systems, and the output of the plants. In contrast, global rotor angle oscillations, known as interarea mode oscillations, arise from interactions among large groups of generators. These oscillations involve groups of generators connected by relatively weak tie-lines [17].

- **Large-disturbance rotor angle stability**, or transient stability, refers to a power system's ability to maintain synchronism during severe disturbances, such as a transmission line short circuit. This stability is influenced by the system's initial operating state and the disturbance's intensity. Transient instability typically manifests as periodic angular separation due to inadequate synchronizing torque, known as first swing instability. It may arise from the combination of a slow inter-area swing mode and a local plant swing mode, leading to significant rotor angle deviations following the initial swing [17].

### 2.5.2 Frequency stability

Frequency Stability refers to a power system's capacity to sustain a consistent frequency following a significant disturbance, such as a large imbalance between electricity generation and demand. This capability is crucial because frequency deviations can lead to instability, which manifests as prolonged oscillations in frequency. These oscillations can ultimately trigger the disconnection of generating units and/or loads to protect the system from further damage. The maintenance and restoration of equilibrium between generation and load are vital components of frequency stability. When a disruption occurs, the system must quickly adjust to re-establish balance without incurring excessive loss of load. This involves not only the generation of electricity but also the effective management of demand-side resources [17],[19]. Several factors influence frequency stability, including

- System Responsiveness: The ability of generation resources to react quickly to changes in demand or generation. Fast-responding resources, such as gas turbines or battery storage, can help stabilize frequency more effectively than slower resources.

- Inertia: The physical inertia of rotating machinery in the power system provides a buffer against rapid frequency changes. Higher inertia can dampen frequency oscillations following disturbances.

- Control Mechanisms: Advanced control strategies, such as automatic generation control (AGC) and frequency-responsive demand-side management, are essential for maintaining balance in real time.
- Grid Interconnections: The interconnection of multiple power systems can improve stability through the sharing of resources and load diversity. However, it also requires careful coordination to prevent cascading failures.

### 2.5.3 Voltage stability

Voltage stability is defined as a power system's capacity to sustain steady voltages at all buses following a disturbance from a specific initial operating condition. It relies on the system's ability to maintain or restore equilibrium between load demand and supply. Voltage instability can lead to load losses or the tripping of transmission lines and other elements due to their protective systems, potentially resulting in cascading outages. The most prevalent form of voltage instability is a gradual decline in voltage levels, although overvoltage instability can also occur [17], [19].

## 2.6 Impact of Renewable Integration on Rotor Angle and Frequency Stability

The increasing incorporation of large-scale renewable energy sources significantly affects the dynamics of the power system. Consequently, it is crucial to assess both the steady state and dynamic performance of the power system in different scenarios involving installations of renewable power plants, especially photovoltaic systems. Traditional power systems rely on synchronous machines to provide inertia, which is essential to maintain grid stability by resisting frequency changes during disturbances. These machines have considerable rotational inertia, which helps dampen frequency fluctuations by absorbing and releasing kinetic energy during various contingencies [20]. In contrast, large-scale renewable energy sources, typically interfaced through power electronics, contribute little or no inertia, increasing the vulnerability of the grid to frequency deviations [21].

High penetration of PV systems, along with the location and dynamic characteristics of adjacent systems, complicates rotor angle stability. Depending on system configurations and control strategies, this situation can either improve stability under certain conditions or exacerbate rotor angle oscillations while diminishing the damping in other generators [22]. Notably, during fault conditions, a high share of RES can lead to marked increases in rotor angle oscillations, with oscillatory modes displaying low frequencies, such as 1.85

Hz, indicating poor damping and extended periods of instability [23]. These observations highlight the need for further research into the stability of the rotor angle to ensure the overall stability of power systems in various scenarios and levels of penetration. Thus, a deeper analysis of the rotor angle stability is essential, particularly with regard to different situations and penetration levels, to maintain the stability of the entire system.

## 2.7 Potential Solutions for Enhancing Power System Stability

The rapid development and integration of large-scale renewable energy sources into the power system have led to bottlenecks in power flow and increased complexity in maintaining system security. This transition has also created a demand for higher power transfer capacity across the network. Many transmission networks are now being operated closer to their physical limits, posing a risk to the N-1 security criteria. Consequently, system enhancements will be essential. However, due to challenges in gaining support for the construction of new transmission lines, more advanced solutions must be implemented to achieve the necessary improvements. The concept of FACTS was first introduced by N.G. Hingorani in 1988 [24]. These devices are power electronic-based systems that can control various electrical parameters, thereby providing enhanced controllability and increasing power transfer capability.

The integration of large-scale renewable energy sources into the grid poses significant challenges, particularly regarding rotor angle and frequency stability in long-distance AC transmission networks. The variability of renewable generation can lead to fluctuations in power supply, adversely affecting synchronous operation and grid stability. To address these issues, FACTS devices and HVDC links have become essential solutions. FACTS devices enhance controllability by dynamically managing reactive power, voltage regulation, and power flow, thereby stabilizing rotor angles and improving overall reliability. Meanwhile, HVDC technology is advantageous for long-distance transmission, allowing efficient power transfer with minimal losses and providing excellent control over power flows [25]. Together, FACTS devices and HVDC links form a robust framework that enhances grid performance and maintains stability, enabling the successful integration of large-scale renewables while minimizing risks to system security [26]. As the demand for electricity continues to rise, maintaining system stability becomes critical, necessitating the development of robust control strategies and the integration of technologies like BESS [7], [8]. Besides these considerations, there are effective mitigating techniques. Notably, FACTS-based POD has been shown to significantly improve transient stability compared to traditional FACTS solutions, especially in the context of renewable energy integration. Meanwhile, HVDC technology is advantageous

for long-distance transmission, allowing efficient power transfer with minimal losses and providing excellent control over power flows. Together, FACTS devices and HVDC links form a robust framework that enhances grid performance and maintains stability, enabling the successful integration of large-scale renewables while minimizing risks to system security.

While existing studies highlight the role of FACTS and HVDC in improving grid stability, critical gaps remain in the context of hybrid AC/DC grids with high renewable penetration. First, most transient stability studies focus on conventional synchronous generators, neglecting the dynamic role of PV systems in replacing inertia-less generation during severe disturbances (e.g., three-phase faults or line outages). The findings demonstrate that LCC-HVDC enhances transient stability in the Ethiopia-Kenya interconnection, but the dynamic interaction effects of PV-based active power support during frequency deviations remain unexplored. Second, while HVDC improves fault recovery, the coordinated control of PV systems and HVDC to simultaneously address frequency regulation and rotor angle stability is lacking. Therefore, the main gaps obtained from the literature studies are:

1. Developing and validating a detailed simulation model of the Ethiopia-Kenya HVDC-linked grid in DIgSILENT, tested under both load and generation imbalance and large disturbances.

2. There is a lack of comprehensive analysis on the performance of LCC HVDC systems in conjunction with renewable energy sources under various disturbance scenarios, particularly in the Ethiopian context.

3. Proposing a dual-role PV control strategy: (a) active power injection for frequency stabilization and (b) synchronous generator replacement for transient angle stability.

4. Current research does not adequately address the interaction between renewable energy integration and transient stability during specific disturbances, such as three-phase faults or line outages, which is crucial for understanding system behavior.

5. Demonstrating how PV-HVDC coordination can enhance stability margins beyond traditional FACTS solutions, offering a scalable approach for renewable-rich grids. This work directly addresses the underexplored intersection of renewable integration, HVDC dynamics, and hybrid stability control, providing actionable insights for grid operators in developing economies.

# 3 Power Grid Modeling

## 3.1 Background

DIgSILENT PowerFactory is recognized as a premier simulation tool designed to address the complexities of modern integrated electric power networks. As the demand for comprehensive simulation capabilities increases, PowerFactory stands out for its extensive functionalities that cater to various applications in generation, transmission, distribution, and industrial systems. It integrates all necessary functions for effective power system modeling and analysis, including power flow analysis, fault analysis, RMS stability, and small signal analysis. These features are essential for understanding the flow of electrical power, assessing the impact of faults, evaluating stability under normal and disturbed conditions, and analyzing responses to minor disturbances [27]. Furthermore, the software supports integration with modern technologies such as power electronic devices, including FACTS and HVDC links, as well as renewable energy sources like wind generation systems. Additionally, PowerFactory offers interfaces for SCADA integration, allowing for real-time monitoring and control of power systems, and is compatible with PSS/E, facilitating seamless data exchange and analysis across different platforms. In summary, DIgSILENT PowerFactory is a robust tool that not only meets the current demands of power system analysis but also adapts to emerging technologies, making it an essential resource for engineers and researchers in the field.

Modeling the power grid with LCC HVDC technology is crucial for understanding the integration and performance of large-scale renewable energy sources, such as hydropower. LCC HVDC systems offer significant advantages, including reduced transmission losses, enhanced stability, and the ability to connect asynchronous grids. These systems are particularly beneficial in long-distance transmission scenarios as they can efficiently transport large amounts of electricity over vast distances while minimizing the impact of voltage drops and reactive power losses. Accurate modeling of LCC HVDC systems involves sophisticated simulations that take into account the dynamic behavior of the converters, control strategies, and the overall interaction with the AC grid. This modeling is essential for optimizing system design, ensuring reliability, and facilitating the seamless operation of interconnected power networks.

The Ethiopia-Kenya transmission line, part of the East African Power Pool (EAPP) master plan, connects the national power grids of both countries [28], leveraging Ethiopia's substantial hydropower potential. Spanning 433 km in Ethiopia and 612 km in Kenya, this line

enables Nairobi to import electricity from Ethiopian hydroelectric projects, with a power transportation capacity of 2,000 MW in either direction. As the first ±500 kV LCC HVDC line in the region, the project aims to promote power trade, regional integration and contribute to the social and economic development of East African countries. The HVDC used is the bipolar LCC-HVDC system consisting of two poles: a positive pole and negative pole, each operating at high DC voltage (±500 kV ). The rectifier station converter AC power from the Ethiopia grid into DC power, which flows through both poles. The positive pole carries current from the rectifier's positive terminal to the inverter's positive terminal, while the negative pole transmits current in the opposite direction ( rectifier's negative terminal to inverter's negative terminal). The earth or a metallic return can serve as a neutral path if one fails. At the inverter station, the DC power is converted back to AC and fed into the receiving grid (Kenya equivalent).

Power utilities have begun to integrate HVDC schemes into their networks due to the inherent advantages of HVDC systems over HVAC lines for bulk power transmission over long distances [29]. With increasing demand for energy and the construction of large generation units in Ethiopia, particularly through the opening of electric power markets, the provision of stable and controlled electric power is becoming increasingly important in the current environment. The impact of HVDC links on the operation of the power system, particularly the transient stability [30],[31], is a major source of concern and interest. Several case studies in the Netherlands, Belgium, Denmark, and China examined how HVDC links affected transient stability under various fault conditions and HVDC link configurations[32].

The stability of the power system is divided into several components. One of the most important types of stability phenomena is the stability of the transient or large signal rotor angle[33]. Transient stability refers to the ability of the power system to maintain synchronism after being subjected to severe disturbances, such as a short circuit in a transmission line[17]. Several recent studies [6] [34] describe in detail the effect of HVDC on the transient stability of the power system. According to the author in [35], appropriate HVDC power modulation can minimize synchronous machine acceleration during power swing circumstances following a significant contingency and avoid system instability. Experimental evidence of the parallel DC link's capacity to enhance transient stability dates back to the 1960s [36]. The enhancement of the transient stability margin was later found to be influenced by the duration of the increase in current [37].

The primary objective of this thesis part is to create a detailed model of the Ethiopia-Kenya LCC HVDC link for a study of power system stability using DIgSILENT simulation software. The Kenya networks are replaced by an equivalent Thevenin voltage source and impedance [38]. The authors were forced to utilize this since the data from Kenya's side wasn't available. Second, using a time-domain RMS / EMT simulation, a detailed evaluation of the impact of the proposed model system on the transient stability of the Ethiopian power grid is performed

for model validation. The impact of the transient stability of the Ethiopian grid is studied using CCT by comparing two scenarios: the case where an HVDC link is installed between Ethiopia and Kenya, and the case without HVDC interconnection.

## 3.2 Modeling and control of LCC HVDC link

The LCC HVDC link model utilized in this research is based on the CIGRE benchmark model. Figure 3.1 illustrates the single-line diagram of the LCC HVDC link as modeled in DIgSILENT PowerFactory. The associated converter control models and corresponding parameter data are detailed in the Appendix 7.4.

### 3.2.1 HVDC Modeling

Modeling of LCC HVDC systems is essential for analyzing their performance, stability, and control characteristics. It involves the development of mathematical representations that capture the dynamics of the converters, transmission lines, and associated components. These models help in simulating the system's response under various operating conditions, providing insights into power flow, voltage regulation, and harmonic distortion. The HVDC system model for this investigation was quite detailed and took into account the components details for the Ethiopian AC network, including the converter transformer, converter, filter bank, the DC side system and the rectifier and inverter control system. The data for these components are obtained from Ethiopia Electric Power (EEP) and included in Appendix 7.4. The bipolar LCC HVDC link facilitates power transfer between Ethiopia and Kenya, enabling a total capacity of 2000 MW, with each pole (positive and negative) transferring 1000 MW. Operating at a voltage rating of +500 kV on the positive pole and -500 kV on the negative pole, the system employs a 12-pulse configuration consisting of two 6-pulse valves connected in series to enhance the DC voltage level for efficient power transmission. The total line length spans 1045 km, with 433 km within the Ethiopian network and the remainder in Kenya. The rectifier side connects to a complex grid in Ethiopia, comprising various generation sources and loads, while the inverter side links to a Thevenin equivalent voltage source and equivalent reactance in Kenya, representing the grid or load it serves. Each converter, both rectifier and inverter, is designed to minimize harmonic distortion and improve overall efficiency through the 12-pulse arrangement. Furthermore, the system's neutral point is grounded to ensure safety and stability during operation. This LCC HVDC link represents a significant infrastructure advancement for the Ethiopia-Kenya electricity interconnection, enabling efficient power transfer over long distances and improving regional power supply reliability through its advanced technology.

The modeled HVDC system comprises several key components [17] :

1. **Converters**: The conversion between DC and AC is executed in the converter units. Each unit comprises two 6-pulse Thyristor bridges, each bridge consisting of six Thyristor valves. These units also feature built-in transformers equipped with tap changers, specifically designed to handle high harmonic currents and withstand AC/DC voltage stress.

2. **AC and DC Side Filters**: In a 12-pulse converter, harmonics of the order $12k \pm 1$ (where k = 0, 1, 2, 3, ...) manifest on the AC side. Consequently, a typical 12-pulse Thyristor terminal necessitates filters for the $11^{th}$, $13^{th}$, $23^{th}$, $25^{th}$ harmonics, etc., on the AC side. Some HVDC designs that employ overhead lines also incorporate DC filters.

3. **Reactive Power Compensation** : The LCC HVDC link exhibits a significant reactive power demand, which fluctuates with the DC power levels. Typically, up to 60% of the DC power rating must be compensated through filter banks, with the remainder supplied by switchable capacitor banks or FACTS based devices like STATCOM or SVC.

4. **Smoothing Reactors**: The DC side of the converter includes smoothing reactors, primarily aimed at reducing harmonics, preventing commutation failures, and protecting the valves during post-fault conditions. The specifications for these reactors are generally based on factors such as DC fault current, communication failures, and dynamic stability [38].

### 3.2.2 HVDC Controller performance

The performance analysis of the Line Commutated Converter (LCC) in High Voltage Direct Current (HVDC) systems begins with understanding its control objectives and strategies. These objectives include maintaining stable operation, regulating active and reactive power flow, ensuring voltage stability, and minimizing harmonic distortion. To achieve these goals, various control strategies are employed. Constant DC voltage control is used to maintain a fixed voltage at the converter terminals, while droop control adjusts the voltage based on the power flow conditions. Additionally, current control strategies, such as current limiting and reference current tracking, help protect the system from overcurrent conditions. Active and reactive power control mechanisms are implemented to respond dynamically to changes in power demand, ensuring that the system remains stable and efficient. Ultimately, these strategies work together to fulfill the operational requirements of the HVDC system [39]. In the context of fault conditions, the Voltage Dependent Current Order Limit (VDCOL) plays a crucial role. When a fault occurs on the rectifier side, it can lead to a significant drop in

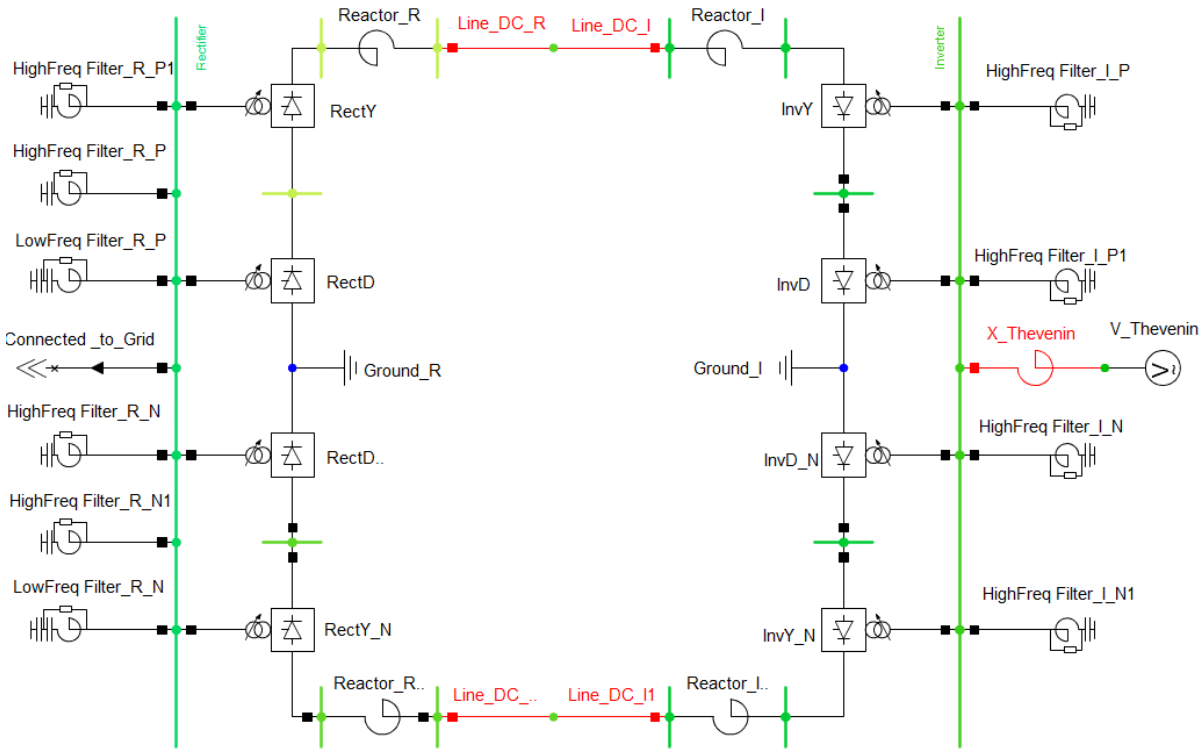


**Figure 3.1:** The LCC HVDC single line diagram modeled in DIgSILENT

rectifier voltage, subsequently affecting the rectifier current. This drop can result in unstable operation and potential damage to the system. The VDCOL mechanism helps manage these situations by adjusting the current limit based on the available voltage at the rectifier. As the rectifier voltage decreases, VDCOL lowers the current order limit, preventing the inverter from attempting to draw excessive current that the rectifier cannot supply. This coordinated response helps maintain stability during rectifier faults, allowing the inverter to operate within safe limits and minimizing the risk of further complications. Ultimately, active and reactive power control mechanisms, along with VDCOL, work together to ensure that the system remains stable and efficient, even in fault conditions [40].

In the event of a fault on the inverter side of an LCC HVDC system, several critical impacts and responses need to be considered. When a fault occurs, it can lead to a sudden drop in inverter output voltage, which affects the overall power flow and stability of the system. This voltage drop can cause the inverter to lose its ability to effectively control the DC voltage and current, potentially leading to commutation failures and further instability in the system. To mitigate the effects of an inverter-side fault, control strategies like VDCOL remain essential. VDCOL can adjust the current limit in response to the decreased inverter voltage, thereby preventing the system from attempting to draw more current than the inverter can handle. This helps protect both the inverter and the connected AC grid from damage due to overcurrent conditions. Additionally, protective relays are activated to isolate the faulted

section of the inverter, ensuring that the rest of the system remains operational. These relays can quickly disconnect the faulty inverter from the grid, allowing for safe operation and minimizing the risk of cascading failures. By implementing these measures, including the use of VDCOL and robust protection schemes, the system can maintain stability and reliability, even in the face of inverter-side faults [41], [42].

Dynamic performance and stability are critical aspects of LCC HVDC systems, particularly under varying load conditions and disturbances. The ability of the system to respond to transient events, such as sudden changes in load or faults, is vital for maintaining reliability. The performance analysis often involves evaluating the system's response time and settling time during disturbances. A well-designed controller should facilitate quick recovery to steady-state conditions while minimizing oscillations. Stability analysis, including small-signal and large-signal stability assessments, is essential to understand how the system will behave under different operating conditions. Effective control strategies contribute to enhancing the dynamic performance, ensuring that the system can withstand fluctuations without compromising stability [43].

AC faults can have profound effects on the operation of LCC HVDC systems, given their reliance on the AC grid for commutation. During an AC fault, voltage levels may drop significantly, which can lead to commutation failures and destabilize the converter operation. The performance analysis of LCC HVDC systems must include evaluations of how the system reacts to various types of AC faults, such as short circuits or voltage sags. The system's response can lead to difficulties in maintaining the desired power flow and may necessitate protective measures to prevent damage. Understanding the impact of AC faults is essential for designing resilient control strategies that can quickly restore stable operation while minimizing disruptions to the power network.

### 3.2.3 Impact of rectifier fault on controller performance

The impact of a three-phase AC fault on the rectifier side of a Line Commutated Converter (LCC) in HVDC systems can significantly affect controller performance and overall system stability. When a three-phase fault occurs, it typically results in a substantial drop in voltage at the rectifier terminals. This voltage reduction directly influences the rectifier's ability to convert AC power to DC, leading to a decrease in output DC voltage and potentially causing commutation failures. As the rectifier voltage drops, the control system must respond rapidly to maintain stability. Current control strategies, such as current limiting and reference current tracking, may struggle to manage the sudden changes in power flow, leading to oscillations or instability in the DC link. This condition can exacerbate the fault, affecting the inverter side as well, as it may attempt to draw more current than the rectifier can supply. The VDCOL can play a critical role during this situation by adjusting the current limits based

on the available voltage. However, if the fault persists, the VDCOL may not be sufficient to prevent instability, as the inverter could face difficulties in maintaining its operational parameters. Additionally, protective relays are activated to isolate the fault, but the response time and effectiveness of these protections are crucial. In summary, a three-phase AC fault on the rectifier side can lead to significant disruptions in LCC HVDC controller performance, affecting voltage stability, increasing the risk of commutation failures, and challenging the current control mechanisms. Properly designed control strategies and protective measures are essential to mitigate these impacts and ensure the reliable operation of the HVDC system.

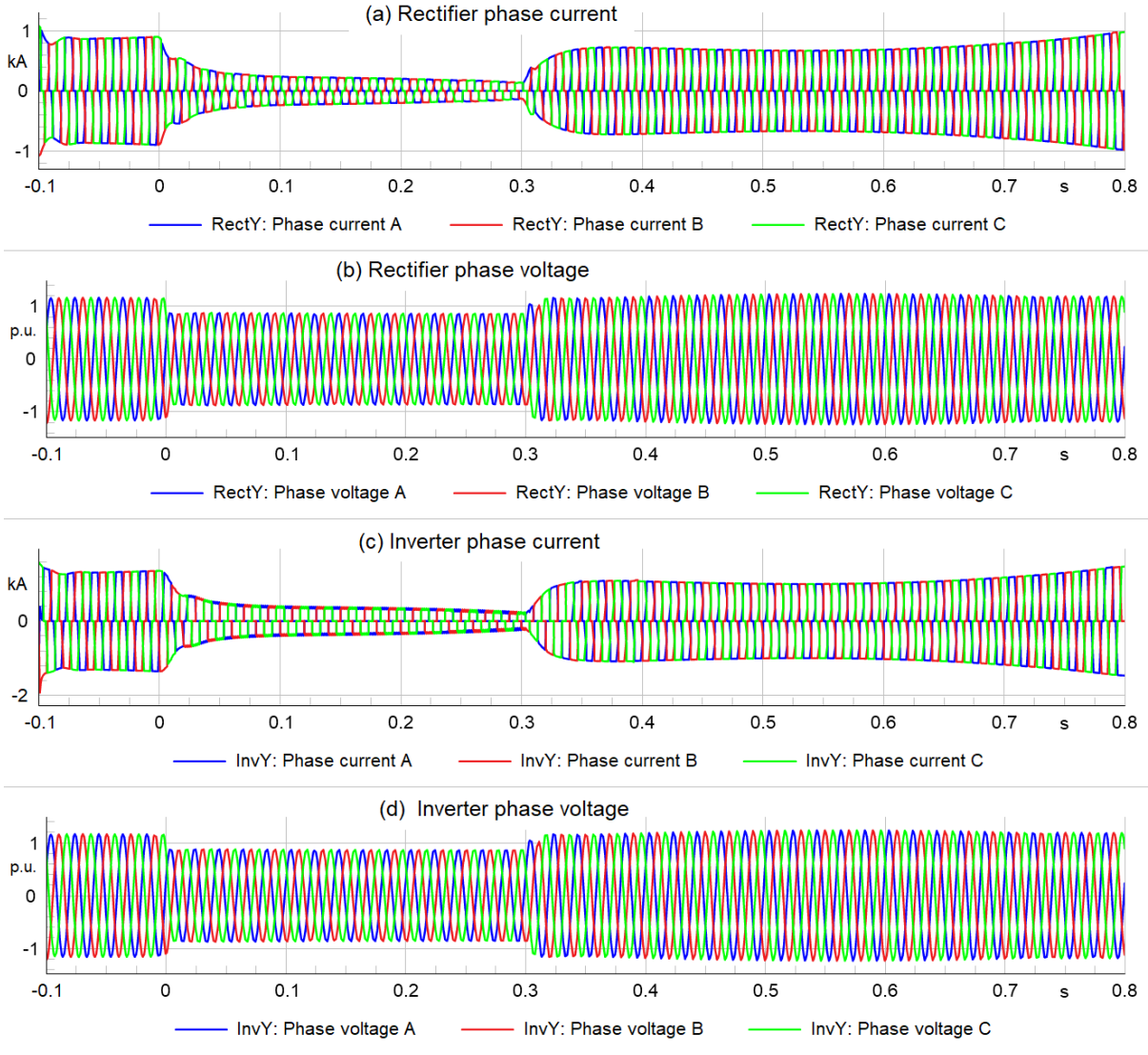


**Figure 3.2:** Rectifier and Inverter side of a LCC HVDC system

The simulation result shown in Figure 3.2 illustrates the behaviour of the rectifier and inverter currents and voltages during a three-phase fault at the rectifier terminals, which occurs at 0 and is cleared after 400 ms. The fault impedance is set to j20$\Omega$ to minimize com-

mutation failures, and the simulation captures the initial condition state of electromagnetic transients or instantaneous values, characterized by relatively small transient times.

- **Figure 3.2 (a)** shows the phase currents at the rectifier terminals. During the fault, these currents exhibit significant fluctuations, reflecting the instability introduced by the fault condition. The rapid changes indicate the rectifier's struggle to maintain current flow due to the dropping voltage caused by the fault.

- **Figure (b)** presents the rectifier phase voltages, which demonstrate a marked decrease during the fault period. This drop critically impacts the rectifier's ability to convert AC power to DC, potentially leading to commutation failures if the voltage falls below necessary levels, however, there is fault impedance to prevent such a drop.

- **Figure (c)** depicts the phase currents at the inverter terminals. These currents may experience erratic changes as the inverter responds to the altered conditions at the rectifier. The inverter attempts to draw current despite the reduced supply, further exacerbating system instability.

- **Figure (d)** shows the phase voltages at the inverter terminals. Similar to the inverter currents, these voltages may fluctuate due to the fault condition, reflecting the challenges the inverter faces in maintaining operational stability in light of the rectifier's compromised performance.

During a three-phase fault at the rectifier terminal, both the measured and the filtered voltage magnitude exhibits a drop immediately after the fault occurs, indicating a significant disturbance in the voltage supply. The filtered voltage shows a delayed response due to the filtering process as the fault happened, and takes more time to recover to a steady state value as the fault is cleared. As can be seen in Figure 3.3, the measured voltage exhibits significant noise and fluctuations, especially during the fault event. This noise is typical in real-time measurements as it captures all transient behaviors, including rapid voltage spikes and drops caused by the fault. The high-frequency variations represent the electromagnetic transients occurring in the system, which can be attributed to the fault conditions. In contrast, the filtered voltage is smooth and free from noise. Filtering is a technique used to remove high-frequency components from a signal, allowing only the steady state or low-frequency variations to pass through. As can be seen in Figure 3.3 (b), the plot indicates that the rectifier voltage magnitude is always greater than that of the inverter voltage, both during the fault and after it is cleared. This consistent behavior highlights the operational dynamics between the rectifier and inverter in the system and also due to some voltage drop across the DC transmission line. From the simulation result of Figure 3.3 (c ), the current comparison shows a dramatic change when the fault occurs, with the rectifier controller current initially spiking

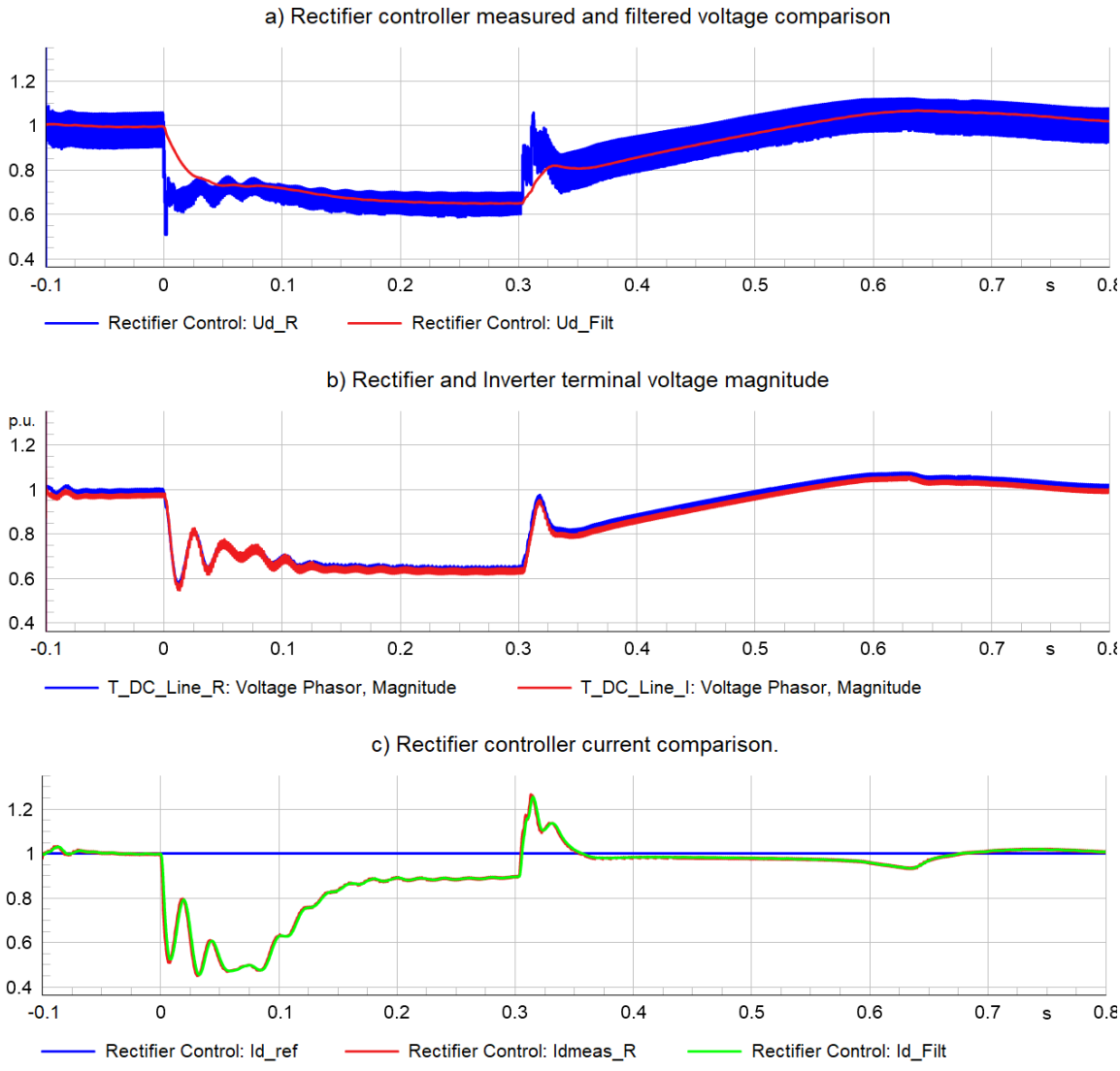


**Figure 3.3:** Rectifier and inverter controller current and voltage simulation result

before dropping significantly. This spike indicates a rush of current as the system responds to the fault. After the fault is cleared, the measured and the filtered current try to truck the reference current but remains lower than pre-fault levels for a some period. This transient response showcases the electromagnetic effects of the fault, where the system must adapt to sudden changes in current flow, highlighting the complexity of managing currents during faults.

The effect of a solid three-phase fault on SGs can be seen in Figure 3.4. During a three-phase fault at the rectifier terminal, most generators experience a sudden decrease in their rotor angles due to a rapid drop in electrical power output as they reduce their output to maintain stability. In contrast, G1, serving as the reference generator, maintains its output and angle, allowing it to remain stable during the disturbance. Once the fault is cleared, the affected generators begin to recover, increasing their rotor angles as they restore power

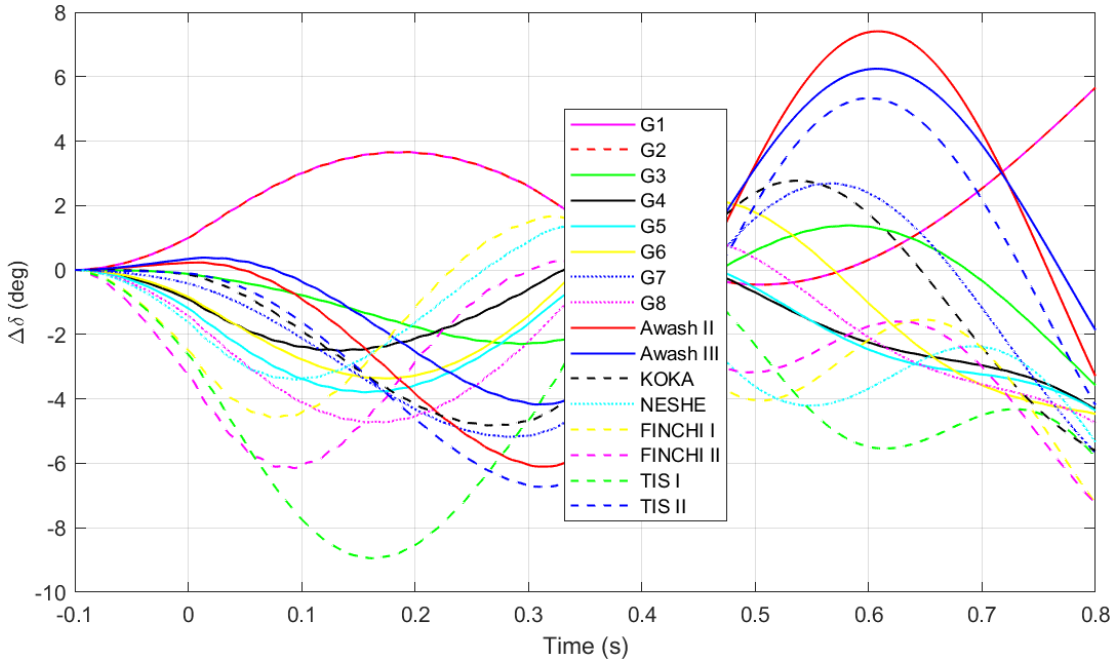


**Figure 3.4:** Rotor Angle Deviations Relative to G1 as the Reference Generator

output to pre-fault levels. This behavior reflects the dynamic response of the generators to faults and emphasizes the role of the reference generator in maintaining overall system stability.

### 3.2.4 HVDC control

The HVDC configuration in this paper is based on the CIGRE benchmark, which was modeled using the DIgSILENT PowerFactory simulation environment. The HVDC system controls are identical for both the positive and negative poles and are modeled independently of one another. The LCC HVDC converter is a CSC that features unique forms of control techniques for dynamic stability investigations. The CSC's control strategy may be separated into independent and coordinated control strategies based on several control goals. The coordinated control approach can regulate both the active and reactive power of one converter station, while the independent control strategy can only manage a single variable, such as DC current or DC voltage. The needs of the system determine the control technique to be used [44]. This research work uses an independent control strategy for CSC control. The common CSC control methods for LCC HVDC include DC current control for the rectifier converter and constant DC voltage control for the Inverter converter. According to equations (3.1) to (3.3), the independent control strategy for CSC is designed, as shown in Fig. 3.6, to include a constant DC current control and constant DC voltage control [45].

The schematics for the rectifier and inverter sides of the monopolar LCC HVDC system are shown in Figure 3.5. Except for the polarity of the voltage-dependent current-order

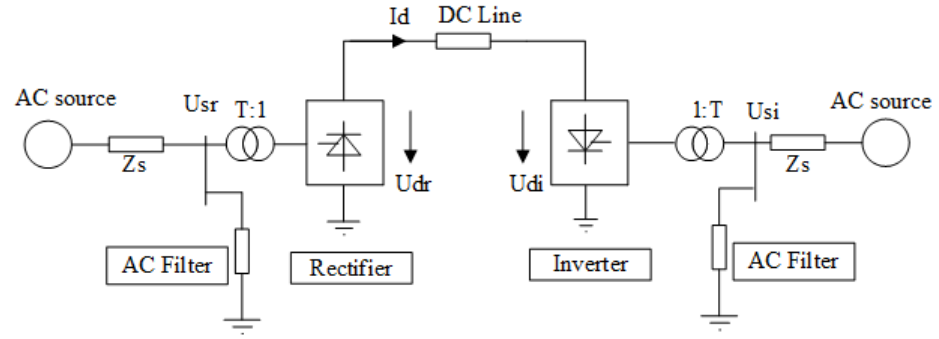


**Figure 3.5:** Rectifier and Inverter side of a LCC HVDC system

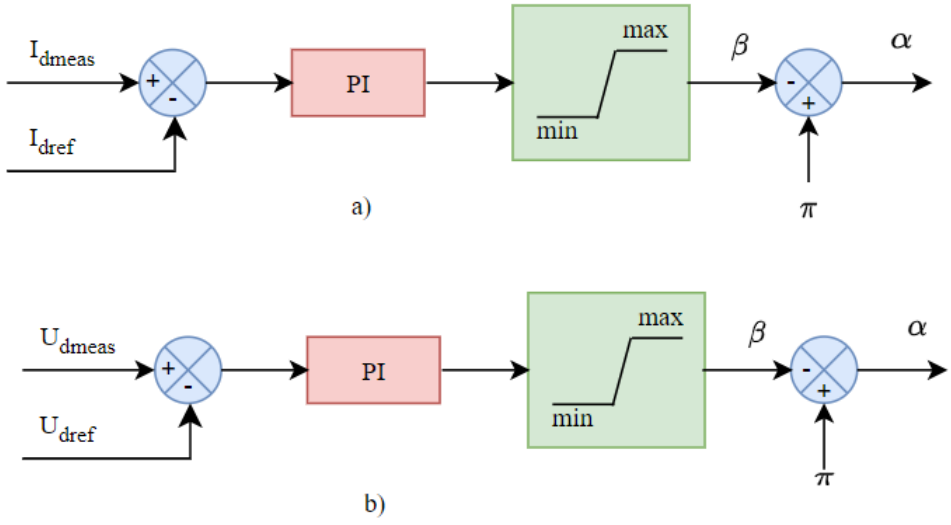


**Figure 3.6:** CSC's independent control methods. (A) Control of constant DC current. (b) Control of constant DC voltage.

configuration in the dynamic modeling utilizing DSL, bipolar HVDC modeling is nearly identical to monopolar LCC HVDC. The following equations can be used to model the HVDC link for the monopolar case [46]. In the LCC-HVDC system, the rectifier side adopts constant DC control, and the inverter side adopts constant DC voltage control, respectively.

$$U_{dr} = \frac{3\sqrt{2}}{\pi} U_{sr} NT \cos\alpha \tag{3.1}$$

$$U_{di} = \frac{3\sqrt{2}}{\pi} U_{si} NT \cos\gamma \tag{3.2}$$

$$I_d = \frac{U_{dr} - U_{di}}{R_r + R_i + R_L} \tag{3.3}$$

By using equations 3.1 to 3.3, we can find the DC power transferred along the DC line. Hence, the rectifier side DC model of power in steady state calculation is found by equation 3.4, in which an approximation was made in reactive power calculation and with losses neglected

[47]. The same calculation method is used for the steady state power of the inverter side.

$$\begin{cases} P_{dcr} = U_{dr} I_d \\ P_{ac} = P_{dcr} \\ Q_{ac} = P_{ac} \tan \alpha \end{cases} \tag{3.4}$$

## 3.3 Modeling of the system and simulation result

Ethiopian grid consists of 24 power plants, of which 18 are SGs, 3 wind turbines, 1 geothermal, and the remaining are diesel power plants with 572 bus bar systems. This grid was connected to the rectifier side, while the Kenyan power grid was connected to the inverter side. The HVDC link is connected between the Ethiopian and Kenyan substation at a voltage level of 400kV line-to-line.

PowerFactory is a software tool used to employ a general mathematical description of the power system, consisting of algebraic and differential equations, in this research work. The software models the power system by representing its components and their interconnections, incorporating the electrical characteristics, control systems, and operating parameters. This software automatically formulates the differential equations describing the dynamic behavior as represented in [48].

$$\begin{cases} \dfrac{dx}{dt} = f(x, y, u) \\ \\ \dfrac{du}{dt} = h(x, y, u) \end{cases} \tag{3.5}$$

The algebraic equations capturing the steady-state behavior, including power flow relationships, nodal balance, and network constraints [48]. The software then solves these equations to simulate the transient response and determine the steady-state operating points of the system. The corresponding algebraic equation is given in equation 3.6.

$$0 = g(x, y, u) \tag{3.6}$$

Where,

- x - represents the short-term state variables corresponding to fast dynamic states of generators, induction motor loads, FACTS, and HVDC controllers.
- y - corresponds to the algebraic variables related to the transmission system and steady-state models, including voltage magnitudes and phases at nodes, generator sources, and loads within the network.

- u - represents the long-term dynamic state variables of slow-acting devices, such as ULTC transformers, OLTCs, and secondary voltage controls.

The generalized system setup for the interconnection of Ethiopia and Kenya is shown in Figure 3.7. The power plant model of the entire system is detailed in Appendix 7.5. SGs are modelled together with exciter systems and governor-turbine systems. The generators exciters, governors, and other controller in Ethiopia system are modelled by DSL and their representative values used for the models are obtained from EEP and shown in Appendix 7.1. The voltage dependency of load modeling is built in power factory software so that the load model used is the static ZIP model. In the simulation, power plants with high generation capacity and directly connected to rectifier bus bar of the converter are shown in Figure 3.7, and the remaining are connected to the grid through AKAKI II and SEBETA substation.

## 3.4 Transient stability analysis

To assess the transient stability of the proposed model, disturbances were introduced by simulating solid three-phase to ground short circuit faults at various locations within the Ethiopian power grid. Specifically, the fault locations selected for this analysis are Bus 1, Bus 2, and Bus 5. The evaluation of transient stability is conducted for both scenarios: with and without HVDC link. The choice of fault location is a critical aspect of transient stability studies, as it significantly impacts the system's response. Buses 1, 2, and 5 were prioritized due to their proximity to the rectifier side of the converter. Notably, Bus 1 is home to the largest generator in the Ethiopian grid, making it a strategic point for analyzing fault impacts. The selection of these fault locations is also influenced by the overall network topology and the prevailing load flow conditions, which can vary across different areas of the grid. By focusing on these specific buses, the study aims to provide a comprehensive understanding of the transient stability dynamics under realistic fault scenarios in the Ethiopian power system.

### 3.4.1 Transient stability of Ethiopian grid without HVDC link

In this case, the transient stability in terms of CCT has been evaluated for three-phase faults in selected buses. As illustrated in Figure 3.7, the critical bus for the overall system is Bus 3, because all high-capacity generators are connected to this bus. The fault time is set to 1 second for all selected buses with the voltage level of 400kV, and the fault clearing time varies depending on the fault's location and the generator's capacity connected to the faulty bus. For the CCT of Table 3.1, for the three selected buses, the Ethiopian power grid release one generator, namely AWASH 3, depending on the CCT and fault location. It is the first generator out of step for the three faults location with a different CCT. Therefore, the impact

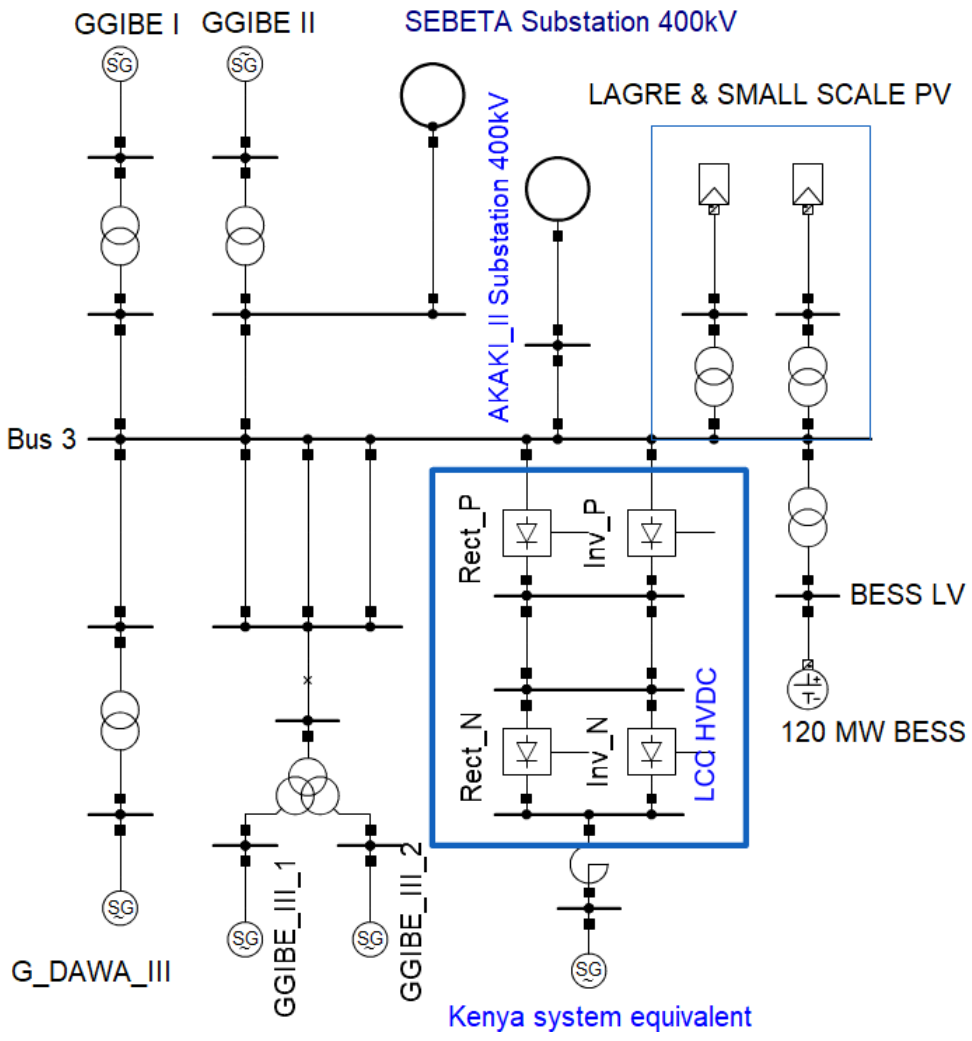


**Figure 3.7:** The topology of the overall Ethiopia-Kenya system

of the HVDC link on transient stability was performed based on this generator for all CCTs in Table 3.1.

Figure 3.8 shows the performance response of the Ethiopian power system in terms of active power through the lines connecting the generators to Bus 3.

- During a fault at Bus 1, the voltage collapses, and the connected generator cannot inject power into the grid (Active power drops to near zero).
- Generators continue receiving mechanical power from turbines during a fault, but electrical power output drops to zero (due to a short circuit). This imbalance ( $P_{mech} > P_{elec}$) causes rotor acceleration, increasing kinetic energy.
- Post-fault clearing at CCT = 0.989 sec, the generator restores power flow as the grid voltage recovers. The plot should show a rebound in active power (Gibe 3's curve rising after fault clearance).

- Accelerating power depends on the imbalance between mechanical power. If Gibe 3 (connected to bus 3) shows large amplitude oscillations in the plot:
  - It's more affected by the fault due to proximity to Bus 1 or lower inertia.
  - It has less damping or higher transient energy.
- If oscillations decay to zero after 0.989 sec, the system is stable.
- Higher amplitude oscillation in Gibe 3 indicates
  - It's more responsive to grid dynamics (e.g., larger machine or weaker grid connection).
  - Its power swings are more pronounced but still stabilize.
- The plot indicates Gibe 3's power oscillation heavily, but this is due to transient energy exchange. Since Gibe 3 is the largest generator from the grid, it likely absorbs more transient energy during the fault, causing larger swings.

**Table 3.1:** CCT with no HVDC in the system.

| No | Fault Location | $CCT_1$ (sec) |
|---|---|---|
| 1 | Bus 1 | 0.989 |
| 2 | Bus 2 | 0.974 |
| 3 | Bus 5 | 0.978 |

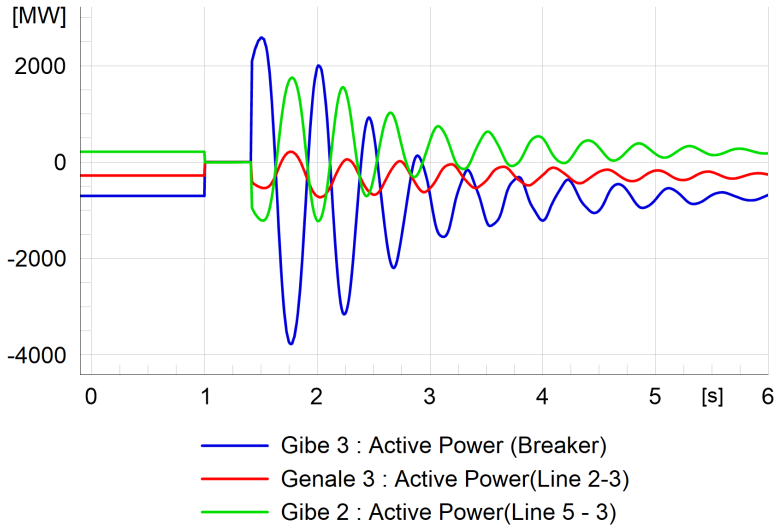


**Figure 3.8:** Active power injected to Bus 3 from the selected three generators via transmission lines, and for a phase fault that occurred at Bus 1

### 3.4.2 Transient stability of Ethiopian grid with HVDC link

Similar to the case without HVDC, the fault time for all selected buses is set to 1 second, and the clearing times for Bus 1, Bus 2, and Bus 5 are 0.989 sec, 0.974 sec and 0.978 sec, respectively. Table 3.2 depicts the effect of the LCC HVDC link on the transient stability of the Ethiopian power grid for solid three phase faults at Bus 1, Bus 2, and Bus 5. CCT has been improved in comparison to the initial CCT without the HVDC link between Ethiopia and Kenya. The improved CCT is $CCT_2$ and is given in Table 3.2 when the HVDC link was in the system. The simulation result of $CCT_2$ was obtained by increasing the clearing time further above the initial $CCT_1$. The stability margin was used to quantify the improvement in transient stability. It indicates how much the system's transient stability improves when an HVDC link is present. The stability margin refers to the ability of a power system to withstand disturbances without losing stability. It is often quantified by the time available to clear a fault before stability is compromised. A larger stability margin indicates that the system can tolerate disturbances better and return to a stable operating condition more effectively. For this paper, the transient stability margin ($S_M$) was formulated in terms $CCT_1$ and $CCT_2$,where $CCT_2$ is the CCT of case B when HVDC is install in the system. This stability margin, '$S_M$', will be defined as in [49] and given in equation 3.7:

$$S_M = \frac{CCT_2 - CCT_1}{CCT_2} \times 100\% \tag{3.7}$$

When a three-phase fault occurs on bus 1 with a fault time of one second, the CCT of the system without HVDC is 0.989 seconds. The Ethiopian power grid released one generator, Awash 3, during this period of interest. When HVDC is installed between Ethiopia and Kenya with the same fault time and CCT as in the absence of HVDC, the transient stability of Awash 3 is investigated. Figure 3.9 demonstrates how the rotor angle response of Awash 3 suddenly rises and becomes unstable in the absence of HVDC while being stable with the HVDC link. The active power injected by this generator is constant until the fault occurs. As soon as the fault was cleared, the power damping oscillation abruptly increase without HVDC, and the generator became unstable. This generator continuously injects active power until a fault develops. When the fault was fixed, the generator's instability was immediately followed by a sharp rise in the power damping oscillation. This demonstrates how unstable the generator was at this failure level.

Figure 3.10 depicts the response of Awash 3's rotor angle and active power response when the fault is now located on bus 5. The fault was cleared at CCT = 0.978 sec, and the response indicates that Awash 3 was unstable without HVDC and stable with HVDC link. The response characteristics of this result can be summarized as follows:

- Without HVDC: The angle of the rotor may exhibit large oscillations or diverge,

indicating instability. Active power may fluctuate significantly, leading to a potential loss of synchronism.

- With HVDC: The rotor angle would show damped oscillations or return to a steady state more quickly, while active power levels stabilize, demonstrating improved system resilience.

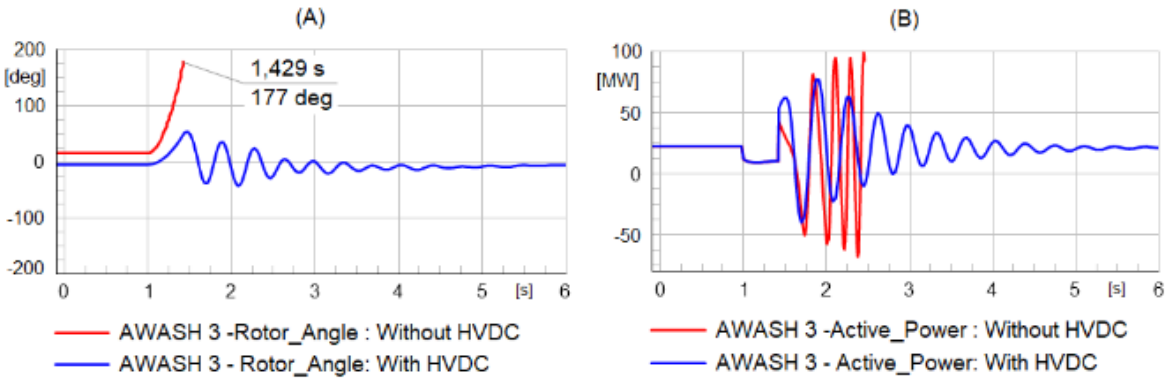


**Figure 3.9:** AWASH 3 (A) Rotor Angle (B) Active Power responses at $CCT_1$ = 0.989 sec and fault location at Bus 1

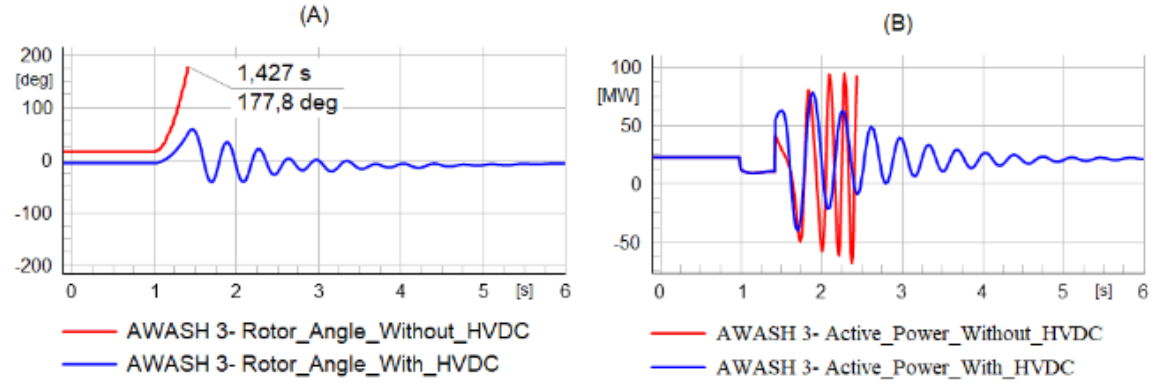


**Figure 3.10:** AWASH 3 (A) Rotor Angle (B) Active Power responses at $CCT_1$ = 0.978 sec and fault location at Bus 5

Figure 3.11 depicts the response of Awash 3's rotor angle and active power when the fault is on bus 2. In this case, the fault was cleared at CCT = 0.974 sec, and the response indicates that Awash 3 was unstable without HVDC and stable with HVDC. The active power response was an increase in damping and is unstable with no HVDC link in the system. Table 3.2 clearly shows the simulation results for selected buses in terms of CCT for both cases with and without the HVDC link. As shown in the Table, the CCT with an HVDC link outperformed the CCT without an HVDC link. The stability margin is used to quantify

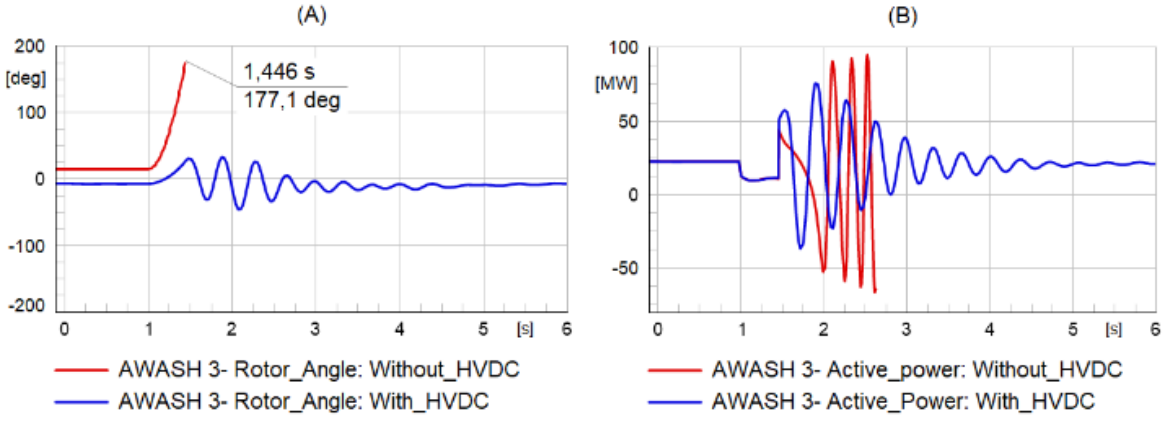


**Figure 3.11:** AWASH 3, (A) Rotor Angle and (B) Active Power responses at $CCT_1$ = 0.974 sec and fault at Bus 2

improvements in transient stability performance. When an HVDC link between Ethiopia and Kenya is installed, the stability margin indicates how much the stability improves. A higher stability margin suggests that the system can withstand disturbances for a longer period before becoming unstable. The stability margin can be seen to vary depending on the location of the fault. Gibe 3 has a lower stability margin than Gibe 2 and Genale 3. This is because Gibe 3 is the source of the majority of the electricity used in the Ethiopian grid, and the placement of the fault is also a significant element in this situation.

**Table 3.2:** Simulation result of CCT when HVDC is connected and is compared with the initial CCT.

| CCT(sec) | Cases | Bus 1 | Bus 2 | Bus 5 |
|---|---|---|---|---|
| $CCT_1$ | Without HVDC | 0.989 | 0.974 | 0.978 |
| $CCT_2$ | With HVDC | 1.218 | 1.272 | 1.319 |
| $S_M(\%)$ | Stability Margin | 18.801 | 23.428 | 25.853 |

## 3.5 Observation

- Based on the simulation result in Table 3.1 above, it can be observed that, among the faults that occurred at various locations, the disturbances at Bus 2 have the quickest clearing times. Bus 2 has the shortest Critical Clearing Time (CCT) because its transmission connections are weaker than those of other buses. Specifically:
  - **Fewer parallel power lines**: Less redundancy, so faults cause bigger disruptions.
  - **Poorer voltage support**: Voltage drops faster during a fault, increasing instability risk.

  - **Lower inertia or higher impedance**: The system responds more slowly to disturbances, making it harder to recover.
    * A smaller CCT means the system is more sensitive to a fault at that location and must be cleared faster to avoid instability.

- The result in Table 3.2 shows that the HVDC link between the two country improves the transient stability of the Ethiopian grid. The performance of the improvement is indicated by the stability margin of the selected fault location. Bus 1 is the best fault location without HVDC (tolerates fault longest) but benefits least from HVDC. Bus 5 is the worst without HVDC (needs fast fault clearing), but becomes the most stable with HVDC.

- Without HVDC system, the system's critical clearing time of 0.989 seconds indicates a limited stability margin; if the fault is not cleared within this timeframe, the system may experience instability, resulting in oscillations or loss of synchronism. The rotor angle response shows significant deviations, highlighting the system's struggle to regain stability after the fault is cleared.

- The inclusion of HVDC extends the critical clearing time to 1.218 seconds, resulting in a greater stability margin that provides the system with additional time to respond to disturbances before instability occurs. This enhanced stability margin facilitates better damping of oscillations, allowing for a quicker recovery of both rotor angle and active power levels.

- As shown in Figures 3.6, 3.7, and 3.8, the rotor angle with HVDC was shifted to negative and below zero. This is because the LCC HVDC absorbed too much reactive power and required more power from the generators to operate.

- The best implication of the stability margin in transient rotor angle stability is indicated as follow.
  - Increased Time for Recovery: The longer critical clearing time (CCT) with HVDC provides the system with more time to react to disturbances, which is essential for maintaining stability during faults. This additional time enhances the effectiveness of protective relays and control systems, ensuring a more reliable response to faults.
  - Damping and Oscillation Control: The HVDC system plays a crucial role in damping oscillations and improving the overall dynamic response of the power system. A larger stability margin minimizes the risk of prolonged oscillations or instability following a disturbance, contributing to smoother system operation.

  - Reliability: Systems with improved stability margins are generally more reliable, as they can withstand disturbances without leading to cascading failures. This reliability is particularly vital for interconnected grids, where the stability of one part of the system can significantly impact the overall network.

- As shown in Figures 3.9, 3.10, and 3.11, the rotor angle with HVDC was shifted to negative and below zero. This is because the LCC HVDC absorbed too much reactive power and required more power from the generators to operate.

## 3.6 Summary

This study presents a comprehensive modeling of the Ethiopia-Kenya LCC HVDC system, utilizing DIgSILENT for analysis. The model is rigorously validated through RMS and EMT time-domain simulations, which enable a thorough examination of the fundamental impacts of HVDC links on the transient stability of the power grid.

The findings from the simulations indicate a significant enhancement in the transient stability of the Ethiopian power grid when an HVDC link is installed between Ethiopia and Kenya. This improvement is primarily evidenced by an increase in the CCT when compared to scenarios without HVDC connections. The CCT is a crucial parameter, as it determines the maximum duration that the system can remain stable following a disturbance before it risks becoming unstable. Moreover, the stability margin is a key indicator of transient stability and also reflects a positive trend with the integration of the HVDC link. Higher stability margins signify that the system can withstand disturbances more effectively, thereby confirming that the presence of the HVDC link contributes to a more resilient power grid. In summary, the results demonstrate that the implementation of the LCC HVDC system not only enhances the transient stability of the Ethiopian power grid but also provides a robust solution for managing power flow and ensuring reliability in the face of potential disturbances. The study underscores the importance of HVDC technology in modernizing and strengthening power grid infrastructures in the region.

# 4 Damping of Power Oscillation Using FACT Devices

## 4.1 Background

The transition towards renewable energy sources is a pivotal aspect of modern power system development, driven by the need for sustainable and environmentally friendly electricity generation. Among the various renewable technologies, LSP systems have gained prominence due to their potential to significantly contribute to the energy mix, especially in regions with abundant solar resources. In Ethiopia, where the demand for electricity is rapidly increasing, integrating LSP systems into the existing power grid presents both opportunities and challenges [50]. Challenges in integrating PV systems into the existing grid include output fluctuations from sunlight dependence, the absence of inertia from SGs, and the need for advanced inverters, all of which complicate operations and heighten the risk of frequency oscillations. Furthermore, successful integration of PV systems necessitates compatibility with the current infrastructure, which often requires significant upgrades to accommodate the new technology [51], [52], [53]. While PV integration presents challenges, it also offers significant opportunities, including carbon-free electricity, enhanced sustainability, and faster renewable integration. PV systems promote decentralization, reduce transmission losses, and improve grid resilience through advanced inverters and storage. With decreasing costs, they can lower electricity prices and decrease fossil fuel dependence, while also allowing for easy scaling to manage peak demand and supply fluctuations [54].

Numerous research studies have been conducted on solar PV arrays concerning the steady-state and transient stability aspects of grid-connected systems. Transient stability, defined as the ability of a power system to maintain synchronism under transient disturbances, is a critical aspect of grid reliability [17], [55]. The presence of SGs has traditionally provided the necessary inertia and reactive power support to enhance system stability. However, as the penetration of LSP systems rises, particularly in the context of replacing SGs, it becomes essential to evaluate the impacts on rotor angle stability and overall system dynamics [56]. Furthermore, the introduction of LCC HVDC links adds another layer of complexity, as these systems can both stabilize and destabilize AC networks depending on their operational conditions [57]. Replacing SGs with PV systems in a grid-connected to an LCC HVDC link can pose challenges to transient stability, particularly in terms of inertia, reactive power support, and commutation reliability. Implementing robust control strategies and additional support mechanisms is crucial to mitigate these effects [58].

The integration of large-scale PV plants reduces system inertia, increasing the risk of transient instability due to poorly damped electromechanical oscillations. In this context, the implementation of POD and Control CLF strategies using FACTS devices becomes crucial. These supplementary controls mitigate the adverse effects of inertia depletion by enhancing damping performance and stabilizing rotor angle dynamics during transients. STATCOM-based POD controllers, for instance, improve transient stability by modulating reactive power to suppress oscillations, thereby accelerating post-fault recovery [59]. In addition, CLF-based strategies offer a robust nonlinear control framework, optimizing the dynamic response by ensuring that Lyapunov stability criteria are met under large disturbances [60]. This assertion is reinforced by the mathematical framework (shown under 4.2.6) of Lyapunov theory, which provides conditions for stability in the presence of significant disturbances. For PV-integrated grids, FACTS devices equipped with advanced damping features (STATCOM with POD and STATCOM with CLF) are particularly effective. These systems improve stability by dynamically regulating voltage and reactive power, which is critical during sudden load changes or faults [61]. Studies show that STATCOM-POD improves damping ratios by up to 30% in low-inertia systems [62], while CLF-based methods provide superior transient stability margins by adaptively tuning control parameters [15]. Such approaches are indispensable for maintaining grid resilience, especially near critical infrastructure like HVDC links, where rapid voltage fluctuations can propagate instability [63].

This study aims to investigate the transient stability of the Ethiopian power grid in scenarios featuring increased penetration of LSPs and replacement of synchronous generators. Using the DIgSILENT PowerFactory program, a solid three-phase fault is simulated on the rectifier side of a grid linked to an LCC HVDC connection with Kenya. The focus is on assessing the effects of varying levels of LSP integration on rotor angle dynamics, active power output, and bus voltage fluctuations near the rectifier terminal bus post-fault, while also evaluating the effectiveness of FACTS-based supplementary controllers. The findings will provide valuable information on the role of renewable energy in modern power systems, particularly about fault conditions and system stability.

## 4.2 Power System Model

To study the high levels of PV integration, an analysis of the Ethiopian power system is performed, which operates at voltages of 15 kV, 33 kV, 45 kV, 66 kV, 132 kV, 230 kV, and 400 kV. The Ethiopian network connects to the Kenyan grid through a new LCC HVDC system with a capacity of 2000 MW, linking the Wolayta/Sodo 400 kV AC substation in Ethiopia to the Suswa 400 kV AC substation in Kenya. The ±500 kV bipolar HVDC converter has a rated capacity of 2x1000 MW and spans approximately 1045 km, with the Ethiopian grid connected

to its rectifier side [64]. In the Ethiopia-Kenya interconnection model, the Kenyan system is represented by an equivalent Thevenin voltage source and its associated Thevenin reactance. The generalized system setup of the Ethiopian and Kenyan grid is shown in Figure 4.1 which is the slight modification of Figure 3.1. Synchronous generators are modeled together with exciter systems and governor-turbine systems. The generators' exciters, governors, and other controllers in the Ethiopia system are modeled by DSL, and their representative values used for the models are obtained from Ethiopia Electric Power (EEP).

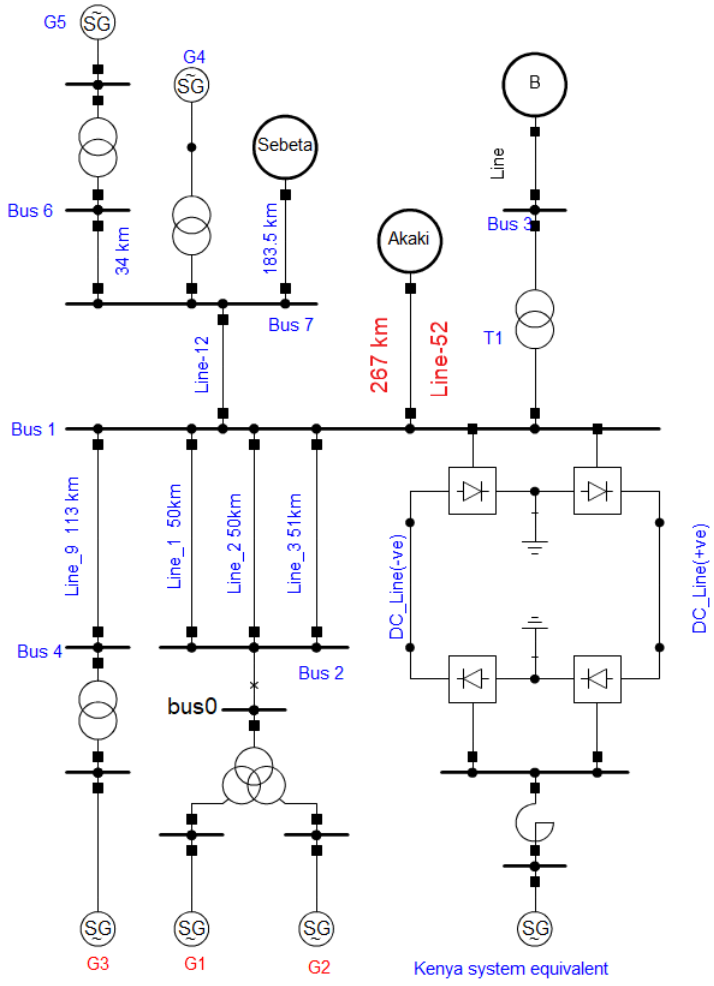


**Figure 4.1:** Overall Ethiopian grid with LCC HVDC

### 4.2.1 Transient Stability in a Multimachine Power System

In a multimachine power system, transient stability analysis involves modeling the electromechanical dynamics of all synchronous generators, their control systems, and the network interactions. The system is described by a set of differential-algebraic equations (DAEs) that capture:

1. Machine dynamics (rotor angle, speed, and internal voltages).
2. Network power flow constraints (nodal power balance).
3. Control systems (excitation, governors, PSS, HVDC/FACTS if present).

The general equations that describe a set of differential-algebraic equations is given by Equation 3.5 and 3.6. PowerFactory solves transient stability problems using a combination of dynamic models (for machines, controls, and loads) and network equations.

### 4.2.2 Load modeling

Load modeling involves the mathematical representation of the relationship between power and voltage on a load bus. To simplify this process, an aggregate load model is employed, which can be expressed as:

$$\overline{S}_L = n\overline{S}_{st} + (1-n)\overline{S}_{dyn} \tag{4.1}$$

Where $\overline{S}_{st}$ is the static apparent power consumed by the load and $\overline{S}_{dyn}$ is the dynamic apparent power consumed by the load. In this research wor,k only static loads are considered, setting n to one, giving the load as:

$$\overline{S}_L = P_{st} + jQ_{st} = P_L + jQ_L \tag{4.2}$$

This allows the modeling of the load as

$$\begin{cases} P_L = P_{LO}\left(\frac{U_L}{U_{LO}}\right)^{kp} \\ \\ Q_L = Q_{LO}\left(\frac{U_L}{U_{LO}}\right)^{kq} \end{cases} \tag{4.3}$$

where $U_L$ is the current bus voltage, $U_{L0}$ is the initial bus voltage, $P_L$ and $Q_L$ are the current active and reactive power consumption and $P_{L0}$ and $Q_{L0}$ are the initial active and reactive power consumption. The voltage exponents kp and kq therefore represent the parameters of the given load with the following characteristics:

- kp = kq = 0 represent constant power
- kp = kq = 1 represent constant current
- kp = kq =2 represent constant impedance

subsectionPV system modelling for transient stability analysis To model the PV system for transient stability analysis of the Ethiopian grid interconnected with Kenya, the PV system

will replace some synchronous generators, injecting active power into the grid. PV system is connected to the electrical grid through a voltage source converter (VSC) that matches the frequency and voltage of the electrical grid [65]. To examine the impact of incorporating PV generation, a negative constant load will substitute for synchronously generated energy in varying amounts, defined as:

$$\begin{cases} P_{VSC} = -P_{VSC0} \\ Q_{VSC} = -Q_{VSC0} \end{cases} \tag{4.4}$$

This corresponds to setting kp = kq = 0 in (4.3) to ensure that the load consistently injects power into the grid, as indicated by the negative sign. Here, $P_{VSC0}$ and $Q_{VSC0}$ represent the active and reactive power injected by the VSC into the system. Modeling renewable energy as a constant negative load is justified by the rapid response of the power inverter's system regulation, which will be confirmed through simulations.

### 4.2.3 Steady-State Stability Assessment

A steady-state analysis is conducted on the previously described system, focusing on the penetration of large-scale photovoltaics. Different PV generation levels are examined for power flow studies within the studied area. The percentages of PV penetration are calculated using the following equation:

$$PVPenetration(\%) = \frac{PVt}{PGt}100\% \tag{4.5}$$

Where PVt is total PV (MW) of individual cases and PGt is total generation of the grid. The total generation of the grid is 3027 MW and total PV is the summation of the PV that replaced synchronous generators in each cases.

### 4.2.4 Modelling and Control Approaches for STATCOM

STATCOM is a shunt connected device that includes a VSC that generates or absorbs reactive power to control the magnitude and angle of the voltage $\overline{U}_{pcc}\angle\theta$ of bus 1 shown in figure 4.2(A), where STATCOM is connected. The STATCOM continuously monitors the system voltage through sensors and adjusts the VSC output voltage to match the desired setpoint. PWM techniques are employed to synthesize the desired sinusoidal output voltage waveform by varying the width and timing of voltage pulses [17].

By taking into account the voltage at the PCC as $V_{pcc}\angle\theta$, and that of the STATCOM is $V_{st}\angle\alpha$ the mathematical expressions for the active and reactive power exchange between the

STATCOM and the electrical grid can be formulated as follows [66]:

$$P = 3\left(\frac{V_{pcc}V_{st}}{X_{tr}}\right)\sin(\theta - \alpha) \tag{4.6}$$

$$Q = 3\left(\left(\frac{V_{pcc}V_{st}}{X_{tr}}\right)\cos(\theta - \alpha) - \frac{V_{pcc}^2}{X_{tr}}\right) \tag{4.7}$$

Where, P and Q are the active and reactive power at the common coupling respectively, $V_{pcc}$ is voltage at point of common coupling, $V_{st}$ is terminal voltage of the STATCOM, and $X_{tr}$ is the reactance of the coupling transformer. It is important to note that, in reactive power compensation, the angles of the STATCOM terminal voltage and the PCC voltage are closely aligned with each other.

It can be seen that the active power flow is dominated by the change of phase angle between the STATCOM voltage and the grid voltage $(\theta - \alpha)$, while the STATCOM reactive power depends on the difference between the STATCOM voltage and grid voltage. It is also clear from Eq. (4.7) that when grid voltage sag occurs and the pcc bus voltage $V_{pcc}$ becomes less than the STATCOM voltage $V_{st}$, the STATCOM acts as a capacitor injecting reactive power to the grid. In contrast, when $V_{pcc}$ is greater than the STATCOM voltage, the STATCOM operates as an inductor that absorbs reactive power from the grid [67]. I utilized a STATCOM rated at 2x120 MVA in this thesis work for a transient stability study.

### 4.2.5 Supplementary Controller for STATCOM

The Power Oscillation Damping with FACTS is a control method used to damp low-frequency oscillations in power systems caused by various disturbances. The POD with FACTS approach is a linear control method that modulates FACTS devices to provide damping for these low-frequency oscillations. The POD signal can be inserted at different positions in the regulator and designed as shown in Figure 2D [68]. The residue method is used to obtain the POD signal by tuning the lead-lag filters of the linearized system given in Equations 3.5 and 3.6. The POD consists of a washout filter (Tw) that passes only the high signals where oscillations occur, Lead-lag filters for phase compensation and a gain block (KPOD) to keep the signal within limits. The input to the POD can be various signals, such as generator rotor angle deviation, generation speed deviation, power flow, current, or signals derived using Lyapunov theory [69]. In this paper, the input of the POD is the speed deviation of the remote generators ($\omega_i$=$\omega_{SIME}$). The right choice of input signal, along with appropriate POD gain and tuned filter parameters, can provide sufficient damping to the electromechanical oscillations, leading to improved system stability.

The controller modeling and design for STACOM, based on the DSL of the PowerFactory simulation environment, was very crucial for this thesis work. As can be seen in Appendix

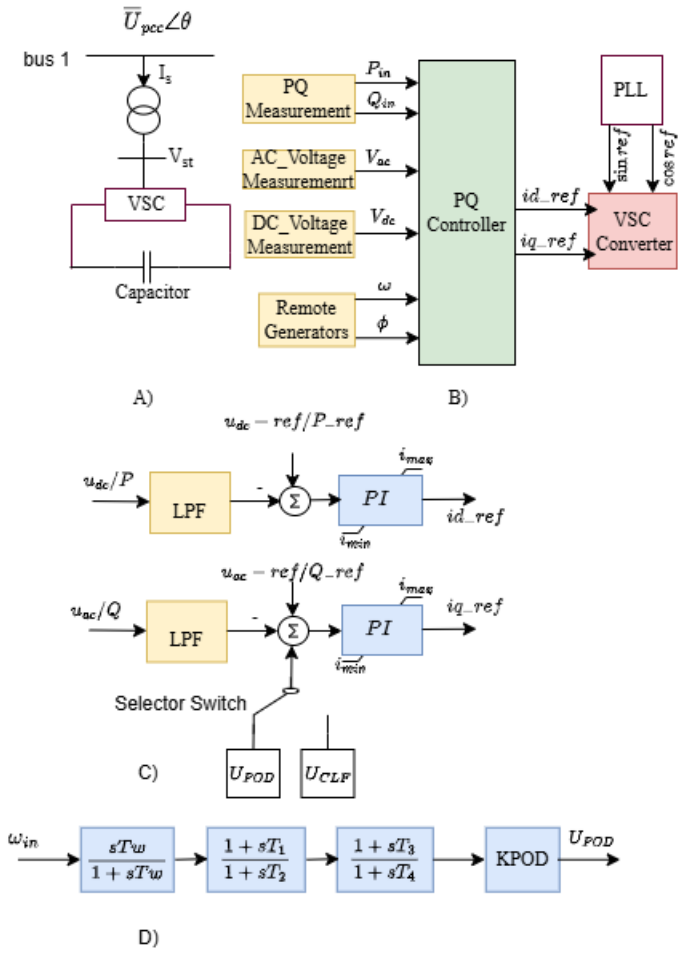


**Figure 4.2:** A) Equivalent circuit of the STATCOM, B) STATCOM Power factory frame, C) STATCOM Controller, and D) Regulator of a linear POD

7.3, Figure 7.4, the AC voltage and reactive power control mechanisms in the STATCOM controller are structured to ensure effective regulation. The AC voltage control begins by using a low-pass filter to generate a smooth AC voltage output, denoted as $du_{ac}$. This smoothed AC voltage is then compared with the reference AC voltage ($u_{ac-ref}$) to produce the deviation $du_{ac}$. Simultaneously, the reactive power input undergoes a similar process. It is filtered through a low-pass filter to generate a smoothed reactive output, labeled $Q_d$. This output is then compared with the reference reactive power $Q_{ref}$, resulting in the deviation $d_q$. Both $d_q$ and $du_{ac}$ serve as inputs to separate Proportional-Integral (PI) controllers. The PI controller for the reactive power generates the output $i_{qq}$, while the AC voltage controller produces $i_{qv}$. Finally, these two outputs, $i_{qq}$ and $i_{qv}$, are fed into a mode selector, which determines the controlled $i_q$-axis current based on the selected inputs. This structured approach allows for precise regulation of both voltage and reactive power, enhancing the overall performance of the STATCOM system.

In the block diagram of Figure B.3, the id-axis current control starts with the power

reference $P_{in}$, which is processed through a low-pass filter to produce a smoothed output. A gain block then scales this filtered output to generate the voltage $e_1$. Following this, the output of the low-pass filter is compared with the reference, resulting in the deviation $d_p$. Additionally, the voltage $e_2$, obtained from the DC voltage control, is considered before both outputs are directed into a Min block. This block selects the minimum value between $e_1$ and $e_2$, ensuring that the control system functions effectively within its operational limits. The references for the id and iq axes, denoted as $id_{ref}$ and $iq_{ref}$ are generated after the mode selector selects the id component and Min block generates the id-axis component.

In multi-machine power systems, the SIME can be applied to the CLF-based control laws in the SIME system by substituting the state variables $\delta$ and $\omega$ with $\delta_{SIME}$ and $\omega_{SIME}$, respectively, as noted by [70]. In the SIME method, we identify which generators act as critical and non-critical machines at the oscillatory mode. Critical and non-critical machine groups can be identified through oscillatory mode analysis, either via mode-shape compass plots or by observing rotor angle deviations ($\Delta\delta$) during dynamic simulations. In this study, AWASH II is identified as the critical generator. For a multi-machine system with $m$ critical SGs ($\mathbf{i} \in \{1, 2, \ldots, m\}$) and $n$ non-critical SGs ($\mathbf{j} \in \{1, 2, \ldots, n\}$), where the total SGs in the grid are defined as $m + n$, the SIME variables ($\delta_{SIME}$, $\omega_{SIME}$) are defined as the weighted difference between the aggregated critical and non-critical machines. This theory was formulated using the Center-of-Inertia (COI) formulation [70].

## COI for Critical Machines

For a group of $m$ critical machines:

$$\delta_{C_i} = \frac{\sum_{i=1}^{m} H_i \delta_i}{\sum_{i=1}^{m} H_i}, \quad \omega_{C_i} = \frac{\sum_{i=1}^{m} H_i \omega_i}{\sum_{i=1}^{m} H_i} \tag{4.8}$$

where:

- $H_i$: Inertia constant of the $i$-th critical machine
- $\delta_i, \omega_i$: Rotor angle and speed deviation of the $i$-th critical machine

## COI for Non-Critical Machines

For a group of $n$ non-critical machines:

$$\delta_{NC_i} = \frac{\sum_{j=1}^{n} H_j \delta_j}{\sum_{j=1}^{n} H_j}, \quad \omega_{NC_i} = \frac{\sum_{j=1}^{n} H_j \omega_j}{\sum_{j=1}^{n} H_j} \tag{4.9}$$

where:

- $H_j$: Inertia constant of the $j$-th non-critical machine
- $\delta_j, \omega_j$: Rotor angle and speed deviation of the $j$-th non-critical machine

The SIME signals ($\delta_{SIME}$, $\omega_{SIME}$) are defined as the deviation between state variable of the critical ($\delta_C$ , $\omega_C$) and non-critical machines ($\delta_{NC}$, $\omega_{NC}$), which can be described using the following general form,

$$\delta_{SIME} = \delta_{C_i} - \delta_{NC_i} \tag{4.10}$$

$$\omega_{SIME} = \omega_{C_i} - \omega_{NC_i} \tag{4.11}$$

For the STATCOM-based CLF strategy, the feedback control law is derived using the formulation in Equation (12). As illustrated in Fig. 4.2(C), the STATCOM regulates the converter's output voltage magnitude, which serves as the input to a PI voltage regulator. This PI controller adjusts the $q\_axis$ current to modulate reactive power, which is subsequently fed into the VSC-PWM system. In this study, the STATCOM operates exclusively in reactive power compensation mode, with active power set to zero to prioritize voltage stability. The CLF-based control law used for the STATCOM was as follows:

$$U_{CLF} = K \sin(\delta_{SIME})\omega_{SIME} \tag{4.12}$$

This approach is grounded in the study of Control Lyapunov Functions (CLF), an extension of Lyapunov theory that traditionally applies only to systems without inputs. The value of constant gain K was obtained by a trial and error approach for this work.

A transient stability analysis is best explained using modal analysis. Modal analysis identifies oscillatory mode (frequency and damping) in power systems by solving the eigenvalues of the linearized system matrix of Equation 3.5 and 3.6 using DIgSILENT simulation tools. The eigenvalues characterize the oscillatory mode (frequency $\omega$, damping $\sigma$), and the damping ratio quantifies how quickly oscillations decay [17]. Complex eigenvalues occur as conjugate pairs, expressed in the form

$$\lambda_k = \sigma_k \pm j\omega_k \tag{4.13}$$

In the context where $\sigma_k$ and $\omega_k$ represent the real and imaginary components, these components correspond to specific oscillatory modes. Conversely, real eigenvalues do not produce oscillatory behavior.

The frequency of the oscillations for the $k\_th$ mode is then given by

$$f_k = \frac{\omega_k}{2\pi} \tag{4.14}$$

To measure how quickly oscillations are damped, a damping ratio $\zeta_k$

$$\zeta_k = \frac{-\sigma_k}{|\lambda_k|} \tag{4.15}$$

is used, where a large positive damping ratio yields fast attenuation of oscillations and a negative result indicates an unstable equilibrium point [19].

## Assessment of Lyapunov stability using Lyapunov definitions

To assess Lyapunov stability using the specified function of Equation 4.12, the author proposes and follow the following most important theory to evaluate whether the Lyapunov stability criteria are satisfied for the system using the specified Lyapunov function $U_{CLF}$ or not:

1. **Definition of Variables:**
   - From Equation 4.12, $K$ is defined as a positive constant to scale the Lyapunov function.
   - The rotor speed of the equivalent machine, denoted as $\omega_{SIME}$, is specified.
   - The rotor angle is represented by $\delta$.
2. **Positive Definiteness Check:**
   - It is proposed that $U_{CLF} > 0$ for all $\delta \neq 0$ and $U_{CLF} = 0$ when $\delta = 0$ to confirm the positive definiteness of the function.
3. **Time Derivative Computation:**
   - The research work clearly propose calculating the time derivative $\dot{U}_{CLF}$ as follows:

     $$\dot{U}_{CLF} = K \cdot \left(\dot{\omega}_{SIME} \cdot \sin(\delta) + \omega_{SIME} \cdot \cos(\delta) \cdot \dot{\delta}\right),$$

     where $\dot{\omega}_{SIME}$ and $\dot{\delta}$ are the time derivatives of the rotor speed and angle, respectively.
4. **Derivative Analysis:**
   - The authors suggest assessing $\dot{U}_{CLF}$ to determine stability:
     - If $\dot{U}_{CLF} < 0$ for all $\delta \neq 0$, the system is considered asymptotically stable.
     - If $\dot{U}_{CLF} = 0$ and does not increase, the system is classified as stable.
     - If $\dot{U}_{CLF} > 0$ for some states, the system is deemed unstable.

5. **Robustness Evaluation:**
    - The authors emphasize verifying that the stability conditions hold under various operational scenarios and disturbances.
6. **Simulation Validation:**
    - It is proposed that numerical simulations be conducted to validate the theoretical findings, enabling the observation of the system's dynamic behavior in response to disturbances.

By following these proposed steps, the authors aim to evaluate whether the Lyapunov stability criteria are satisfied for the system using the specified Lyapunov function $U_{clf}$.

## 4.3 simulation results

The effectiveness of the proposed controllers was evaluated through simulations in an Ethiopian power system. The simulation results for the design are shown in Figures 4.3 to 4.10. A solid three-phase fault was applied to bus 1 at 1 second and cleared after 200 ms. The original system was restored once the fault was resolved. Based on the given fault condition, the cases are structured as follows and are clearly shown in Table I:

- **Case 1**: Base case with 0% PV.
- **Case 2**: PV plants generate 30% of the total grid power, with synchronous generators contributing 70%
- **Case 3**: grid power is equally shared between PV plants and synchronous generators, each supplying 50%

In the first case, the transient stability of the grid is analyzed without the integration of a PV system. Figure 4.3 shows the rotor angles of all generators following a three-phase fault on bus 1 with 0% PV. This illustrates the transient stability challenges of the Ethiopian grid. Significant oscillations in certain generators result from the duration of the fault. Notably, Awash II, experiences the largest peak oscillations from the grid.

### 4.3.1 Simulation Results of the three cases without Proposed controller

The simulation result illustrated in Figure 4.4 shows the deviation of the rotor angle ($\Delta\delta$) of the critical generator over time, reflecting different levels of PV penetration. At 0% PV or Base-case, the deviation of the rotor angle exhibits stable behavior with smaller oscillation

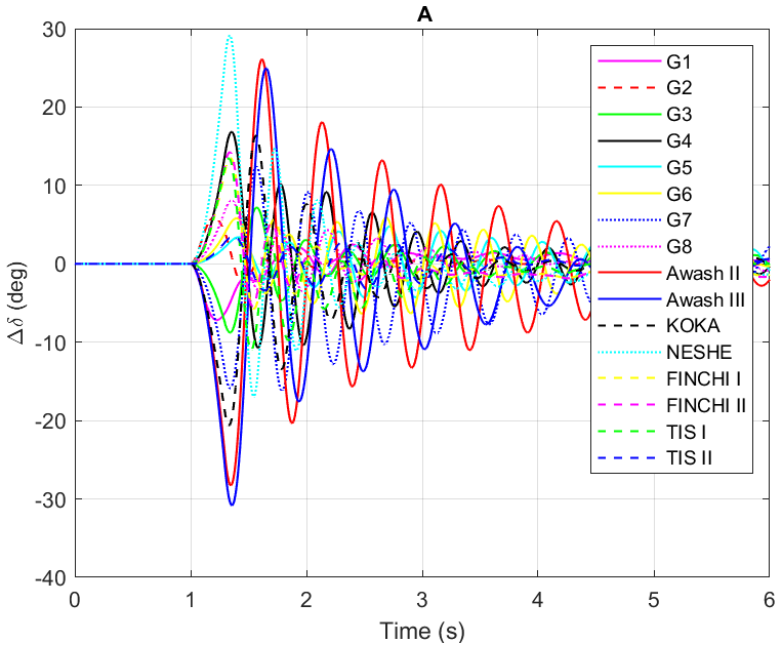


**Figure 4.3:**
A) Rotor angle deviation of SGs without PV penetration.

amplitudes and more damped oscillations, indicating good stability. As the penetration of PV increases to 30%, the amplitude of the oscillations increases, showing that the introduction of the PV system starts to affect the dynamic response of the system while still maintaining some degree of stability. However, at 50% PV penetration, the oscillation amplitude becomes more pronounced and less damped. This suggests that high levels of PV penetration can contribute to rotor angle instability, posing challenges for overall system stability.

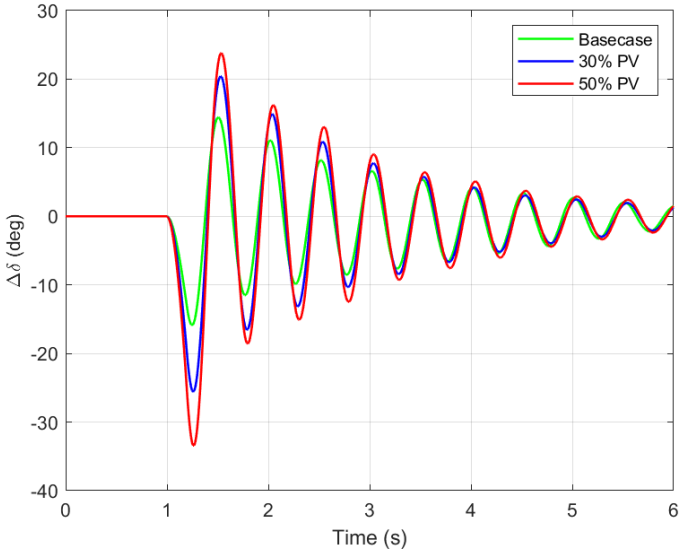


**Figure 4.4:** Rotor Angles of AWASH II with and without PV levels.

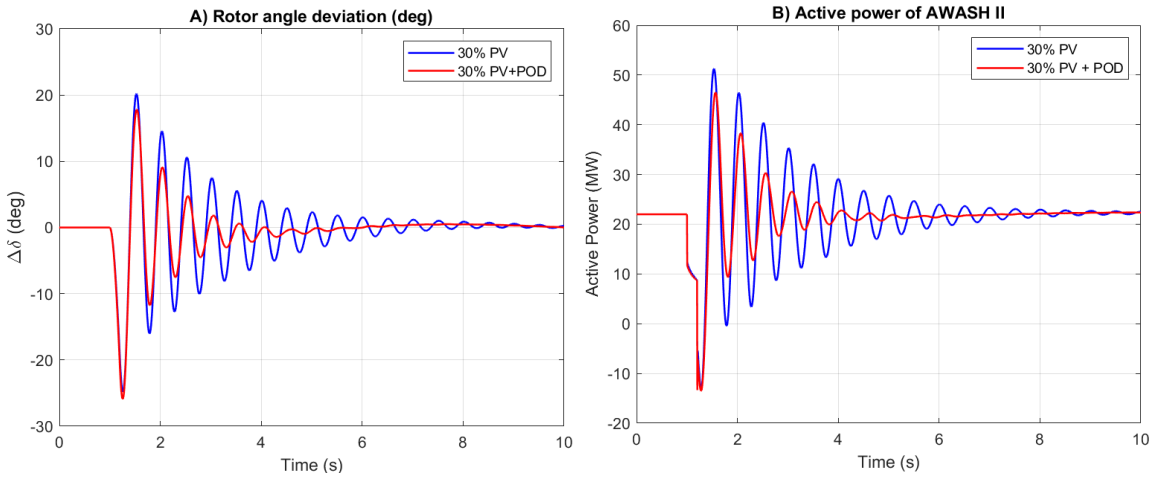


**Figure 4.5:** (A) Rotor angle deviation and (B) Active power of the critical generator for case 2

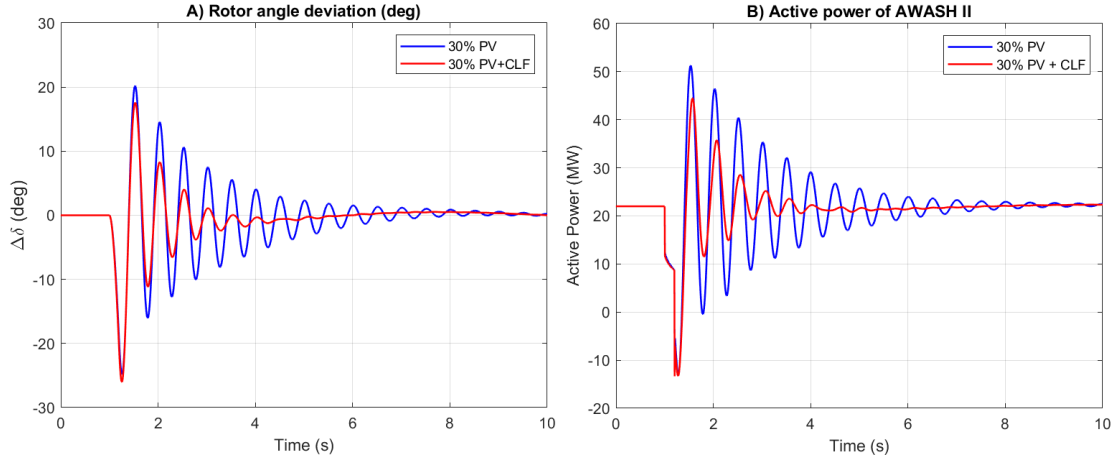


**Figure 4.6:** (A) Rotor angle deviation and (B) active power of the critical generator for case 2

### 4.3.2 Simulation Results of 30% and 50% PV with and without Proposed controllers

In Case 2, PV plants contribute 30% of the total generation of the grid, providing 947 MW, while SGs supply 2080 MW. The integration of PV systems has reduced the inertia constant, negatively impacting the stability of the rotor angle and increasing the oscillations with lower damping. Although a STATCOM was added, it did not significantly improve stability. To enhance performance, a POD or CLF controller was implemented along with STATCOM, as shown in Figure 4.2. When we consider the simulation of the three cases, the model's dynamics without any FACTS device is simulated without any disturbance. The eigenvalues and mode of interest were identified using the built-in modal analysis of the Power Factory software. From this, we determined the lowest damping ratio in the base-case scenario and other cases and indicated it in Table 4.2. Without POD, the angle of the rotor and the active power show considerable oscillations, indicating insufficient damping and instability.

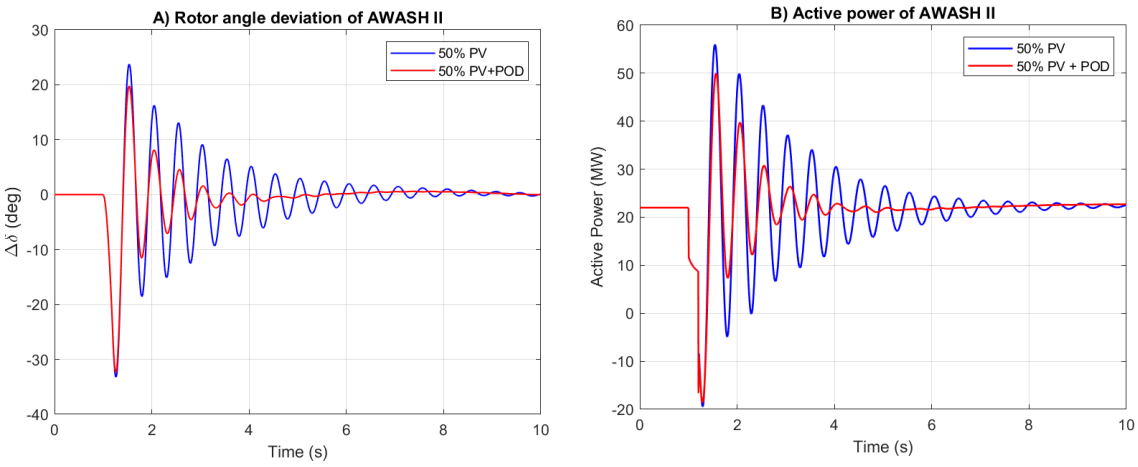


**Figure 4.7:** (A) Rotor angle deviation and (B) active power of the critical generator for case 3.

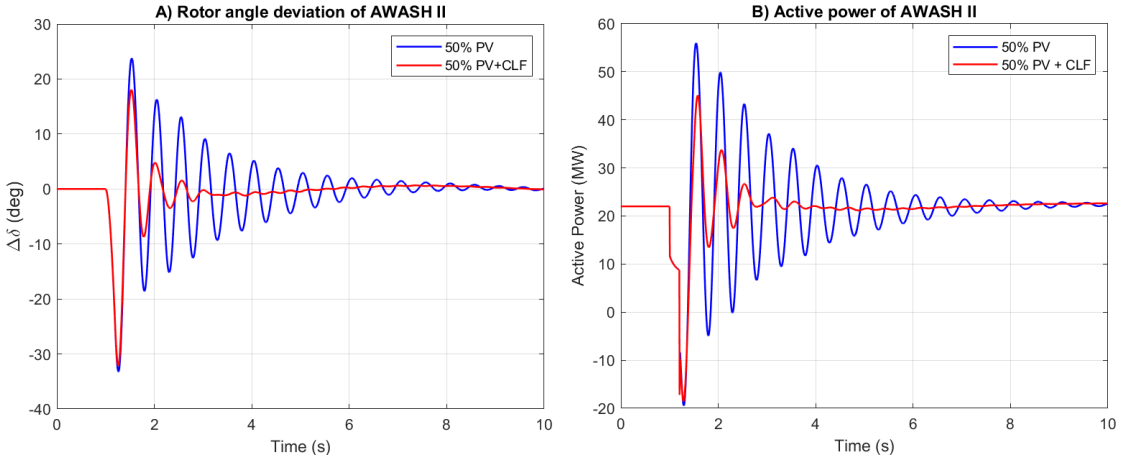


**Figure 4.8:** (A) Rotor angle deviation and (B) active power of the critical generator for case 3.

In the case of 30% PV, the performance of STATCOM with POD and CLF controller is indicated in Figures 4.5 and 4.6, respectively, and Table 4.2.

- The combination of STATCOM and POD demonstrates a significant improvement in transient stability when integrating 30% PV.
- The damping ratio is improved with 30% PV when compared with the basecase scenario, improving stability, but still leaves room for enhancement.
- When with STATCOM + POD, the damping ratio is improved greatly and this increase in damping ratio indicates much better transient stability, allowing the system to recover quickly from disturbances. To sum up, the introduction of the POD controller effectively enhances the system's ability to dampen oscillations, leading to quicker stabilization in rotor angle and active power.

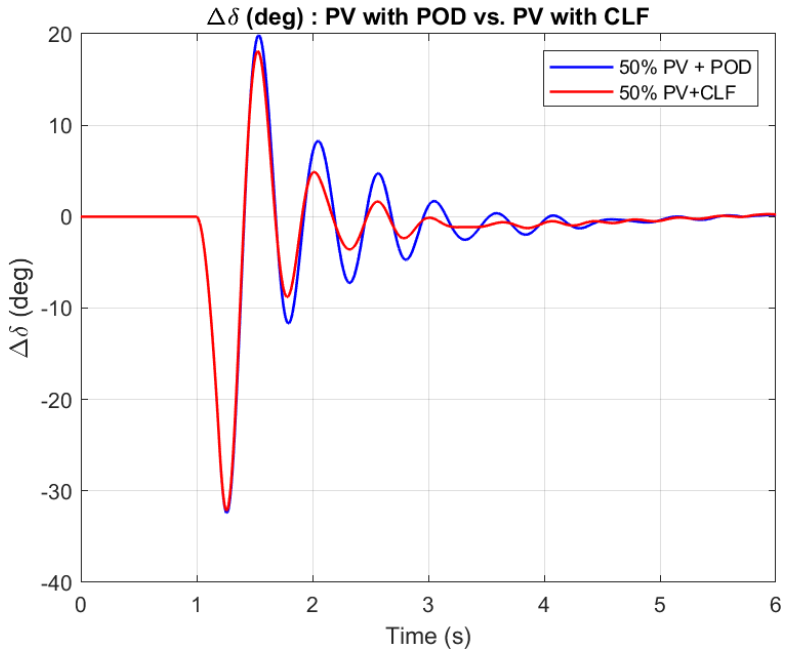


**Figure 4.9:** Performance of CLF and POD controllers

**Table 4.1:** The amount of PV power in percent for each generator Terminal($T_G$) and case

| Cases | Case 1 | Case 2 | Case 3 |
|---|---|---|---|
| $T_{G1}$ | 0 | 8 | 13 |
| $T_{G2}$ | 0 | 8 | 13 |
| $T_{G3}$ | 0 | 0 | 5 |
| $T_{G4}$ | 0 | 5 | 5 |
| $T_{G5}$ | 0 | 0 | 3 |
| $T_{G6}$ | 0 | 5 | 7 |
| $T_{G7}$ | 0 | 4 | 4 |
| Total PV [%] | 0 | 30 | 50 |

- The performance of CLF, when combined with STATCOM, also yields improvements in transient stability.
- The results from Figure 4.6 and Table 4.2 indicate that the addition of CLF effectively reduces oscillation amplitudes in rotor angle and active power, thereby enhancing system stability.
- The damping ratio also improved and is indicated by relative damping in percentage. This shows the effectiveness of the POD as well as the CLF controller in stabilizing rotor movements.
- Similar to the POD, the CLF provides robust damping, ensuring that the system responds quickly to disturbances while maintaining stability.

- Both POD and CLF demonstrate substantial benefits in enhancing the stability of power systems with high levels of PV integration. The choice between the two may depend on specific system requirements, control objectives, and implementation considerations. The results clearly illustrate the importance of supplementary control mechanisms to maintain stability in modern power grids.

In Case 3, the grid power is equally distributed between PV plants and synchronous generators (SGs), each contributing 50%. Comparative analysis of rotor angle deviation and active power between Case 2 (lower PV penetration) and Case 3 reveals that:

- Rotor Angle Deviation and Active Power in Case 3 (50%PV): Exhibits larger oscillations and more frequent instability due to reduced system inertia from higher PV share, exacerbating rotor angle instability.

- POD Controller: Enhances stability in both scenarios; the 50% PV with POD configuration shows marked stabilization and substantial reduction in rotor angle deviation and active power oscillations compared to the scenario without PV (Figure 4.7). These results highlight the POD controller's efficacy in counteracting instability induced by elevated PV penetration, effectively mitigating power fluctuations and improving dynamic performance.

- Notably, the POD parameters (KPOD gain and lead-lag filter time constants) remain consistent across both 30% PV + POD and 50% PV + POD cases with small variation in KPOD as indicated in Table 4.2. Despite identical settings, transient stability improves more prominently in the 50% PV + POD case, as quantified by the damping ratio. The relative damping ratio for the 50% PV + POD configuration surpasses that of the 30% PV + POD case, underscoring enhanced stability with higher PV integration when paired with POD control.

The performance of the CLF controller in the case of 50% PV is explicitly represented by the simulation result shown in Figure 4.8 and Table 4.2.

- CLF: Accelerates oscillation damping and strengthens stability; its improvement is highly sensitive to the gain (K) in Equation 4.12, where smaller (K) results in limited amplitude reduction and larger (K) leads to pronounced stabilization, as illustrated by the rotor angle and active power responses in Figure 4.8.

- Transient Stability Enhancement: Table 4.2 quantifies relative damping metrics, showing that the transition from 30% PV + CLF to 50 % PV + CLF results in a greater increase in both absolute and relative damping ratios, demonstrating that CLF-enabled systems achieve higher stability margins with larger PV shares.

- Transient stability of rotor angle deviation at 50% PV integration shows substantial improvements in the CLF case compared to the POD case at higher PV integration levels, given appropriate gain K values. These findings collectively emphasize that while increased PV penetration reduces inherent system inertia, advanced control strategies like POD and CLF effectively mitigate instability, with their performance contingent on parameter tuning and control gain selection.

This research also analyzes how DC power is transferred from the Ethiopian grid through a rectifier converter to the equivalent system in Kenya. The result shown in Figures 4.10 and 4.11 examines the effects of a solid three-phase fault that occurs at 1 second on the rectifier side bus (bus 1), with the fault clearing after 200 milliseconds. Figure 4.10 clearly shows the effect of the AC fault on the rectifier and inverter DC voltage, while Figure 4.11 shows the effect of the fault on bus voltage magnitude and its corresponding angle.

- Fault impact on Rectifier DC Power
  - At the moment the fault occurs (1 second), there's a significant drop in the rectifier power output. This is due to the fault causing a voltage dip at the rectifier terminal (see Figure 4.10), which affects its ability to supply power to the inverter.
- Inverter DC power Behavior:
  - The inverter DC power experiences a sharp decrease during the fault period. This drop indicates that the inverter is receiving less power from the rectifier, which is a direct consequence of the voltage reduction following the fault.
  - This behavior is critical as it demonstrates how faults can disrupt the power flow in HVDC systems, particularly when reliant on renewable sources like PV.

As can be seen in Figure 4.10, initially both cases show normal operating conditions before the fault occurs.

- With 50% PV, drops sharply to zero, indicating complete voltage collapse in this scenario.
- With 30% PV, experiences a decline but does not reach zero, falling below 0.5 p.u.
- Reactive Power Support:
  - The voltage collapse in the 50%PV scenario is attributed to reduced reactive power support from synchronous generators as they are replaced by PV systems.
  - This indicates that the system with 50% PV integration is more susceptible to phase angle instability during the fault.
- Rectifier Voltage Magnitude:

  - As can be seen in Figure 4.11, at 30% PV, the magnitude of the rectifier voltage experiences a noticeable drop during the fault, indicating reduced power delivery capability; at 50% PV, the drop is more pronounced, reflecting the increased sensitivity of the system to faults with a higher penetration of PV.

- Rectifier Voltage Angle:
  - At 30% PV, the rectifier voltage angle shows a significant change during the fault, indicating instability in system operation; at 50% PV, a larger angle shift is observed, suggesting that higher integration of the PV exacerbates the instability of the phase angle caused by the fault.

- Recovery Post-Fault:
  - After the fault is cleared, the voltage and also the angle are recovered, but the recovery time is fast with 30%

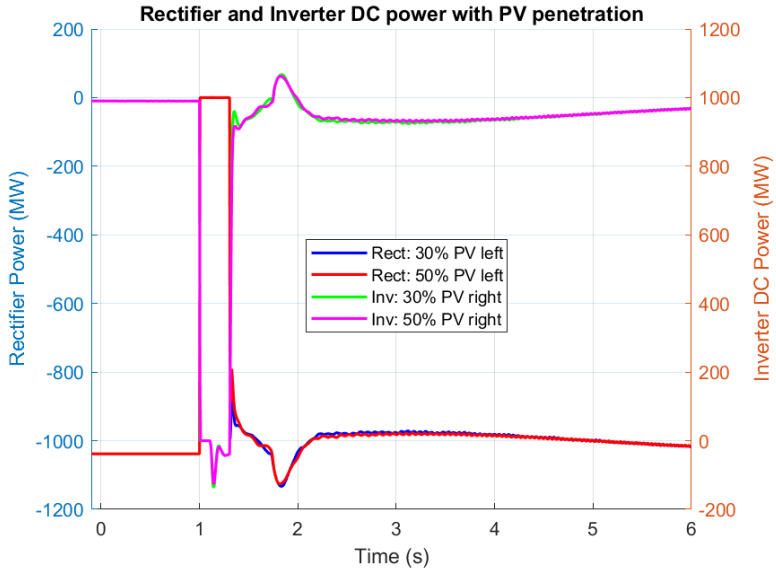


**Figure 4.10:** Rectifier and Inverter DC Power.

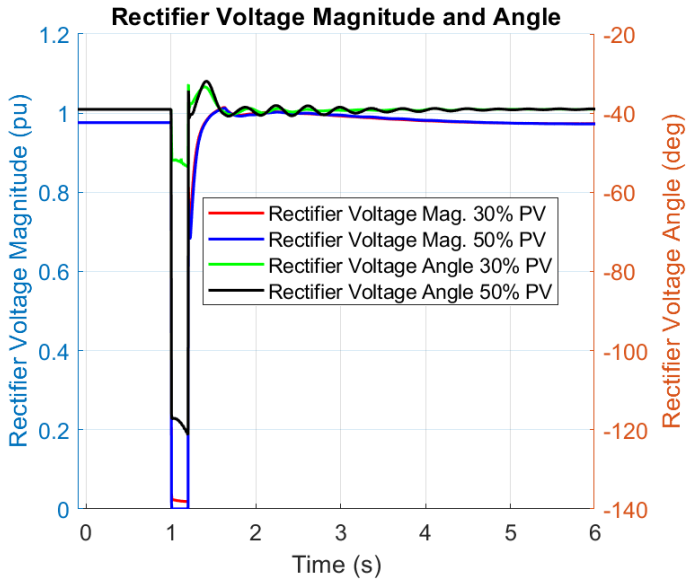


**Figure 4.11:** Rectifier AC voltage magnitude and voltage angle.

**Table 4.2:** Frequency and damping ratio of the mode of interest for different PV penetration and base-case scenario

| Cases | $\zeta_k(\%)$ | $f_k(Hz)$ | $T_1$ | $T_2$ | $T_3$ | $T_4$ | KPOD | Relative damping(%) |
|---|---|---|---|---|---|---|---|---|
| Basecase | 2.94 | 2.26 | - | - | - | - | - | - |
| 30% | 4.47 | 2 | - | - | - | - | - | - |
| 50% | 4.5 | 1.994 | - | - | - | - | - | - |
| 30% + POD | 7.82 | 1.87 | 1.15 | 0.56 | 1.15 | 0.62 | 40 | 75 |
| 30% + CLF | 7.8 | 1.87 | - | - | - | - | K=350 | 74.5 |
| 50% + POD | 10.69 | 2.1 | 1.15 | 0.56 | 1.15 | 0.62 | 32 | 138 |
| 50% + CLF | 10.98 | 2.05 | - | - | - | - | K=350 | 144 |

## 4.4 Summary

In this research, the transient stability of the Ethiopia-Kenya LCC HVDC power system was evaluated with a significant percentage of conventional generation replaced by PV generation, focusing on critical disturbances near the HVDC link. The findings indicate a negative impact on system stability, particularly in degrading the damping capacities of electromechanical oscillations.

1. The key findings of this research work are:
    - The introduction of the Power Oscillation Damping (POD) controller significantly enhanced system performance for both 30% and 50% PV integration scenarios. After fault clearance, the POD controller effectively mitigated instability, especially in the 50% PV case.
    - Simulations demonstrated that the integration of supplementary controllers, specifically STATCOM-based POD and CLF, is essential for enhancing transient stability as PV systems replace synchronous generators.
2. Simulation results
    - In the 30% PV scenario, PV plants contributed 947 MW, while synchronous generators supplied 2080 MW. The lower inertia due to PV integration negatively impacted rotor angle stability and increased oscillations.
    - The implementation of POD and CLF controllers led to a marked reduction in oscillation amplitudes, enhancing both rotor angle stability and active power delivery.
    - The damping ratio improved significantly in both cases, with POD increasing to 7.82% and CLF to 7.8%, indicating effective damping and stability improvement.
3. Comparative analysis
    - The 50% PV case exhibited larger oscillations and greater instability due to further reduced system inertia. However, the POD or CLF controller effectively stabilized this scenario, demonstrating a notable reduction in rotor angle and active power oscillations compared to cases without control.
    - The CLF controller offers a slightly higher damping ratio (10.98%) compared to the POD (10.69%) with more relative damping. This suggests that CLF may provide marginally better performance in damping oscillations with increased PV penetration.
    - Transient stability of rotor angle deviation at 50% PV integration shows substantial improvements in the CLF case compared to the POD case at higher PV integration

levels, given appropriate gain K values. These findings collectively emphasize that while increased PV penetration reduces inherent system inertia, advanced control strategies like POD and CLF effectively mitigate instability, with their performance contingent on parameter tuning and control gain selection.

This study emphasizes the necessity of thorough transient stability analyses in power systems transitioning to higher levels of converter-based generation. The findings underscore the considerable damping potential of utility-scale PV systems when equipped with advanced control strategies like POD and CLF, ultimately contributing to improved grid stability and performance.

# 5 Frequency Control of Ethiopian Grid

## 5.1 Background

The frequency of the power system serves as an effective measure of the active power balance within it, remaining constant when the electrical power produced matches the consumption by loads, including system losses. When this balance is disrupted, frequency fluctuations occur. Specifically, frequency decreases when an increase in load or a loss of generation is not compensated by a corresponding increase in turbine power from connected generators. This power deficit slows down the generator rotors, leading to a reduction in frequency. Significant drops in frequency can activate protection systems, potentially resulting in system separation, loss of load, and outages for customers, as many devices in a power system, such as power supply systems, cannot withstand excessively low frequencies [19].

Frequency stability analysis can be performed using local measurements, as the frequency serves as a global parameter reflecting the overall state of the power system. By monitoring frequency, operators can assess the balance of generation and load, enabling timely interventions to maintain stability. Frequency controllers play a crucial role in achieving specified frequency targets and are integrated into the electricity market through various control schemes. Although generator governors are the most common type of frequency controller, other devices, such as loads, HVDC links, batteries, and renewable energy sources connected via power electronics, can also contribute to frequency control in multiple ways. These diverse tools improve the system's ability to maintain frequency stability and respond effectively to changes in power demand and generation [18].

Ethiopia focuses on the generation of electricity from clean and renewable sources, particularly hydroelectric, wind, and solar power. With a hydropower potential of 45 GW and wind potential of 1.35 GW, both are economically viable. Currently, hydropower accounts for 94% of installed capacity, while the remainder comes from wind, solar, geothermal, and diesel sources [71]. Increasing electricity demand and concerns about global warming have driven significant growth in renewable energy use. To combat high greenhouse gas emissions from coal-fired plants, utility companies are integrating renewable sources like wind and solar into their energy portfolios. This strategy aims to reduce carbon emissions and highlights the sustainability and economic benefits of renewable energy [72], [73].

The integration of RESs, such as PV systems and wind turbine generators, has significantly increased in power system networks, contributing to global energy exchange [74]. However,

the intermittent nature of RESs poses challenges to grid stability. The asynchronous connection of RESs through power electronic devices limits their ability to provide inertia response support, which can lead to reduced system inertia and inadequate frequency support [75].

The incorporation of PV systems can exacerbate issues in power system control, leading to increased oscillations and frequency deviations [5]. Inverter-based RESs may indirectly connect to the power network, further reducing system inertia and complicating frequency stability. High PV penetration in microgrids can negatively affect frequency response during disturbances [76]. To address these challenges, solutions such as energy storage systems, advanced power electronics, and comprehensive grid planning are essential for the stable integration of RESs. Various frequency response devices, including primary frequency control, frequency FCR, and BESS, are utilized in auxiliary services to stabilize grid frequency during emergencies [77]. BESS is particularly effective in low-inertia power systems, providing rapid response capabilities to manage frequency deviations caused by sudden load changes or generator failures [78].

Research has highlighted the frequency challenges associated with high PV integration. Analyses demonstrate a correlation between decreasing system inertia and increasing frequency oscillations, with higher PV penetration potentially leading to oscillations that exceed operational standards [79]. To mitigate these effects, control strategies such as power oscillation dampers [80], synchronous power controllers [81], and adaptive control methods [82] have been proposed to enhance system damping. BESS offers considerable advantages for frequency regulation due to its fast response time and sophisticated control capabilities [83]. However, existing control strategies often use fixed coefficients, which can limit the effectiveness of frequency regulation [8]. Some studies propose hierarchical control strategies based on the SOC, but these may lead to overcharging [84]. Alternative approaches suggest using SOC as a feedback variable to refine control coefficients, though they may not fully exploit BESS capabilities during severe disturbances [85].

This study aims to propose a droop-type control for BESS, designed to mitigate the effects of high PV penetration under various disturbances. The performance of the proposed BESS will be evaluated through simulations of combined generation from large and small-scale distributed PVs at different penetration levels, alongside transient frequency simulations to compare outcomes with and without BESS. Furthermore, the study acknowledges limitations in energy storage capacity and variable photovoltaic output, which may hinder the ability of BESS to provide effective frequency control, especially in the context of the Ethiopian grid [86]. The findings of this research could serve as a reference for future power system operations, particularly for the HVDC interconnection between Ethiopia and Kenya.

## 5.2 Overview of the Ethiopian Power Grid and Study Framework

The power system being examined includes the complete Ethiopian power grid, as illustrated in Figure 3.7. The connection of both PV and BESS is on bus 3. This grid includes a 2000 MW DC power connection to the Kenyan grid through an LCC HVDC link, which serves as the first high-voltage DC power pool in eastern Africa. The Kenyan networks are modeled using Thevenin voltage source and reactance equivalents [38]. The SGs with the highest generation capacity in the grid are linked to the rectifier bus via a tie-line. Figure 3.7 represents a compact and generalized portion of the Ethiopian grid, including the interconnection with the HVDC through the SEBETA II and AKAKI II substations. The Ethiopian power grid comprises a total of 24 power plants, including 18 SGs, 3 wind turbines, 1 geothermal plant, and several diesel power plants, resulting in 572 bus bar systems. The grid is connected to the rectifier side, while the inverter side is connected to the Kenyan substation. The LCC HVDC link operates at a voltage level of 400 kV line-to-line on both sides of the grids. The selected power system is modeled using DIgSILENT simulation software, which incorporates the modeling of SGs, exciter systems, governor-turbine systems, and other controllers. The generators' exciters, governors, and relevant controls, including the LCC HVDC standard controls, are represented using the DSL.

Ethiopia's national power grid, managed by the state-owned Ethiopian Electric Power (EEP), currently focuses on HVDC interconnection with neighboring counties and renewable energy, primarily hydropower. It is expanding its capacity to meet the growing electricity demand. This integration of renewable energy sources introduces variability, posing challenges for maintaining frequency stability. The grid features an extensive network of transmission lines, allowing efficient electricity transfer across the country, and is interconnected, allowing regional cooperation, such as the 500kV DC transmission line to Kenya. As independent power producers contribute to the grid, addressing potential load and generation contingencies such as unexpected changes in electricity demand or sudden generation shortfalls has become increasingly critical. Despite ongoing challenges like energy shortages and load shedding, significant progress has been made since the formulation of the Eastern Ethiopia Electricity Grid Reinforcement Project in 2023. Currently, this project is pivotal in reinforcing the transmission system and enhancing access to electricity, both essential for effective frequency control. Current upgrades to control systems and substations are also underway, further supporting the grid's ability to balance load and generation. These efforts are crucial for ensuring a stable frequency as renewable energy sources are increasingly utilized.

**Key focus on frequency stability and contingency management**

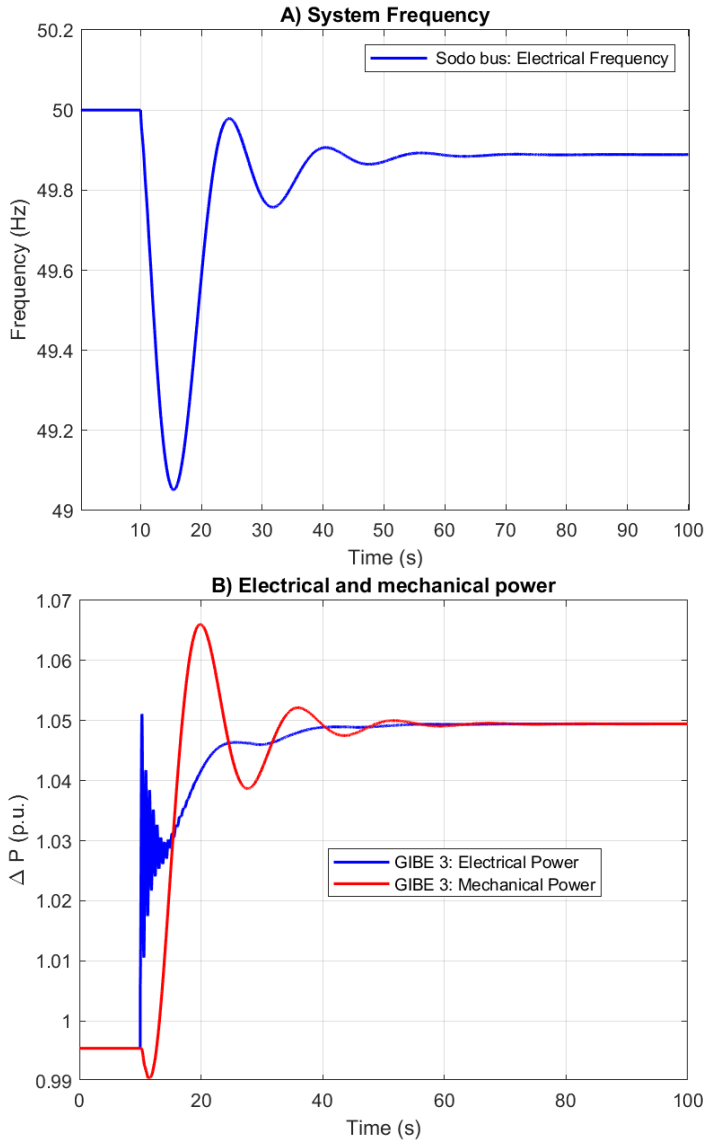


**Figure 5.1:** Variation of frequency and change in power with Load disturbance

Frequency stability in Ethiopia's grid depends on rapid response mechanisms to counteract imbalances caused by:

- **Sudden load increases**, which cause frequency drops as demand temporarily outstrips supply.
- **Generation contingencies**, such as hydropower fluctuations or unexpected outages, leading to under-frequency events.
- **Renewable Intermittency** – Solar and wind variability introduce generation unpredictability, demanding fast-frequency response (FFR) from battery storage (BESS) or flexible generation.
- **HVDC Integration Effects** – While HVDC links (e.g., Ethiopia-Kenya line) enhance

power exchange, they lack inherent frequency support. Fast control schemes (like virtual inertia or FFR) are needed to mitigate frequency instability during disturbances.

Ethiopia's electrical grid effectively maintains frequency stability in response to load or generator disturbances. The plots shown in Figure 5.1 illustrate how the system frequency and generator power output react to changes in demand. To enhance clarity, a 10% load variation is introduced at 10 seconds. The simulation results are generated using MATLAB, with data exported from Power-Factory software.

1. Before the load increase ($t < 10s$)
   - **Load = Generation:** The system is in steady-state equilibrium
     - Generator electrical power output ($P_e$) = turbine mechanical power input ($P_m$).
     - Frequency (f) is constant at the nominal value (50 Hz).
     - No net acceleration or deceleration of the generator rotors.
2. Immediately After Load Increase (t = 10 s)
   - **Sudden 10% Load Increase:**
     - The electrical power demand ($P_e$) rises instantaneously because load is supplied by the kinetic energy of rotating generators.
     - Frequency Drops: Since $P_e > P_m$, generators lose kinetic energy, slowing the rotor speed, and reducing the frequency of the grid.
     - Mechanical Power ($P_m$) Lags: Turbines (governed by slower mechanical systems) cannot adjust instantly. ($P_m$) initially remains unchanged, creating a power deficit.
3. Short-Term Response (t > 10 s)
   - Governor Action:
     - The speed governors detect the frequency drop and increase mechanical power $P_m$ by opening turbine valves.
     - $P_m$ rises gradually to match the new load demand
   - Frequency Stabilization:
     - As $P_m$ increases, the gap between $P_m$ and $P_e$ narrows, reducing rotor deceleration.
     - Frequency stops dropping and settles at a new, lower steady-state value (due to droop control in governors).

## 5.3 Potential Challenges of Frequency Stability in the Ethiopian Power System Due to PV Penetration

One of the significant challenges facing the Ethiopian power system is related to frequency stability, particularly in light of the increasing penetration of PV generation. This challenge arises due to the intermittent nature of PV power and its impact on system dynamics. PV penetration refers to the proportion of PV generation capacity in relation to the overall power system capacity. As PV penetration increases, more solar power is integrated into the grid, which can lead to fluctuations in power supply. The intermittent nature of PV generation, influenced by factors such as weather conditions and daylight availability, introduces variability in the power system. These fluctuations can affect the frequency of the system, potentially compromising its stability [87].

The percentage of PV solar energy capacity that has been incorporated into an existing grid or power system is referred to as the PV penetration level. It is a measurement of the amount of power produced by solar panels about the overall demand for or production of electricity in a certain region or system. The PV penetration levels can be calculated by dividing the installed PV capacity by the total power generation of the system and then multiplying the result by 100 to indicate the PV penetration level as a percentage.

As PV penetration increases, frequency stability becomes a concern. Variability of photovoltaic generation can lead to frequency deviations from the desired value, resulting in imbalances between power supply and demand. Frequency deviations outside the acceptable range can have a negative impact on the performance and reliability of the power system, potentially causing disruptions or blackouts [29].

To ensure the reliable and efficient operation of a power system, it is essential to keep various parameters within acceptable limits. Among these crucial variables, stable frequency holds significant importance. Maintaining the system's frequency within acceptable bounds is vital to prevent issues such as the entire generation capacity attempting to balance the total load. However, owing to dynamic fluctuations in both generation and demand, temporary imbalances can occur between the total generation and total demand, resulting in frequency deviations [88].

Frequency serves as a common parameter for all components of a synchronous electric power system and is an accepted indicator of the system's ability to balance resources and demand, as well as manage disturbances. Under normal operation, the frequency of the East African Power Pool (EAPP) Interconnected Transmission System is typically maintained at 50 Hz (±1%) and controlled within the range of 49.5 Hz to 50.5 Hz. In the event of a system disturbance, such as a load variation in the Ethiopian grid, the frequency band may be extended to 49.0 Hz to 51.0 Hz (±2%). If a major generating unit or transmission element fails,

or large loads are abruptly disconnected, the maximum frequency band expands to 48.75 Hz to 51.25 Hz (±2.5%). In extreme scenarios where multiple contingencies occur simultaneously, the frequency can drop below 47.5 Hz or exceed 51.5 Hz (±5%) for up to 20 seconds, requiring immediate actions to restore system stability. The frequency limits mentioned are based on the Ethiopian National Electricity Transmission Grid Code Draft report, as shown in Table 1. Following a power imbalance brought on by a contingency event, there are several stages of frequency response: the inertial reaction to control the RoCoF (uncontrolled response), PFC, secondary frequency control, and tertiary frequency control. SGs linked to the network altered their speed in response to various disruptions [89].

**Table 5.1:** Frequency Standards in Ethiopian power system

| Frequency Excursions (Hz) | | | |
|---|---|---|---|
| Description | Ethiopia | Kenya | Integrated System |
| Normal operating conditions | 49.95 - 50.05 | - | 49.50-50.50 |
| System disturbance conditions | 49.00 - 51.50 | - | 49.00-51.00 |
| Maximum band under disturbance | 49.00 - 49.50 | - | 48.75 - 51.25 |
| Extreme fault conditions | > 48.50 < 52.50 | - | > 47.50 < 51.50 |

### 5.3.1 Conventional Frequency Control in Power Grid

Conventional frequency control is a power system technique that regulates the frequency of electrical power to maintain a balance between power generation and demand on the grid. It achieves this by adjusting the stored energy associated with the rotational mass of all operational SGs. These adjustments allow the SGs to supply or absorb excess or deficient power, thereby ensuring system stability [90]. When there is a variation in frequency or generator speed, SGs with PFC capabilities initiate action by adjusting their input reference based on the frequency deviation. PFC then gradually adjusts the frequency over a period of time, typically ranging from 0 to 30 seconds, to establish a new steady state [17]. It highlights that the conventional frequency control technique involves adjusting the stored energy associated with the rotational mass of synchronous generators to supply or absorb surplus or shortage of power, thereby achieving system balance.

The RoCoF can be derived from the swing equation [17], which describes the dynamic behavior of synchronous generators.

$$RoCoF = \frac{f_0}{2H_{sys}S_{base}}(\Delta P_m - \Delta P_e) \tag{5.1}$$

Where $f_0$ is the nominal frequency of the system, $\Delta P_m$ and $\Delta P_e$ are the mechanical inputs and electrical power outputs, respectively, and $S_{base}$ is the base electrical power of the system.

$H_{sys}$ represents the aggregate inertia constant. This inertia constant in a power system containing n generating units is obtained from:

$$H_{sys} = \frac{\sum_{k=1}^{n} H_k \times S_k}{S_{sys}} \tag{5.2}$$

As shown in Equation 5.1, the relationship between RoCoF and system inertia is inverse. This suggests that the frequency will deviate more quickly if an unexpected change occurs in a system with lower inertia (higher RoCoF). Large frequency deviations, potentially resulting in generator tripping and load shedding, may be caused by a greater initial RoCoF [91]. When renewable energy sources are integrated into the power system, equation 5.1 shows that the system's inertia decreases, increasing frequency deviation. However, by introducing synthetic inertia through the use of BESS, the frequency deviation can be reduced. Speed-droop or speed-governor characteristics refer to changes in a generator's power output in response to variations in system frequency. The droop control, represented by the coefficient $R_m$, is a well-known technique for regulating the frequency. This coefficient determines the steady-state relationship between generator speed and load characteristics. It can also describe the connection between changes in generator output and frequency deviation ($\Delta f$), as expressed in Equation 5.3 [17].

$$R_m = \frac{\Delta f}{f_0} \frac{S_m}{\Delta P_m} \tag{5.3}$$

Equation (5.3) calculates $R_m$, which represents the power frequency characteristic at the system level. It reflects the steady state frequency error after the power system is restored to balance through PFC [17]. It also indicates how much the frequency changes in response to changes in power. Power system disturbances create imbalances between generation and load, which is a critical concern in maintaining system stability. When these disturbances occur—due to factors such as sudden changes in demand or generation—there is a mismatch between the electricity produced and consumed. This imbalance can lead to frequency deviations in the power system, making it essential to understand how these fluctuations affect overall performance. Higher droop coefficients amplify frequency deviations, increasing the risk of frequency instability. In the case of the Ethiopian power grid, the load is composed of diverse components that exhibit varying static and dynamic characteristics, further complicating the response to disturbances. To effectively model the static behavior of this load and its voltage dependence, the ZIP model is employed (see Table 5.2). This model incorporates constant impedance, current, and power characteristics, allowing for a more accurate representation of how different load types respond to changes in frequency.

**Table 5.2:** Proposed Composite Model

| Ethiopia power system | | |
|---|---|---|
| Composition | Active Power [%] | Reactive Power [%] |
| Constant Power | 20 | 20 |
| Constant Current | 70 | 10 |
| Constant Impedance | 10 | 70 |

## 5.4 HVDC Modeling and Control

The Ethiopia AC network's converter transformer, convertor, filter bank, DC side system, and rectifier and inverter management system were all taken into account when creating the HVDC system model for this study. In this paper, HVDC modeling and control are required just to transfer 2000 MW of DC power from Ethiopia and Kenya. This is ensured by controlling the DC power using constant current control on the rectifier side and constant voltage control on the inverter side. As clearly shown in Figure 3.1, the CIGRE benchmark, which was simulated using the DIgSILENT Power-factory simulation environment, served as the basis for the HVDC system employed in this study. As described in paper I, Independent control strategies and coordinate control strategies are two terms used to describe control strategies for LCC HVDC. The coordinate control method can regulate both the active and reactive power of a single converter station, in contrast to the independent control strategy employed in this research, which can only manage a single variable, such as DC current or DC voltage. The control algorithm used in this study essentially controls a constant DC voltage for the inverter and a constant DC current for the rectifier converter.

## 5.5 Battery Energy Storage System

A BESS is a crucial technology for efficient electrical energy storage and utilization. It consists of two components: an energy storage unit for storing and restoring energy, and a rectifier/inverter for converting between DC voltage from the storage unit and the required AC voltage for the grid. The wide range of battery technologies and their variations pose a challenge in developing a simple, reliable model that applies universally. Nonetheless, previous studies have attempted to create simplified battery response models with fewer parameters [92]. The main challenges in battery modeling are striking a balance between realism and complexity and obtaining accurate parameters from manufacturers for optimal performance.

### 5.5.1 Fast Frequency Control Using BESS

Fast frequency control using BESS stabilizes the electrical grid by promptly addressing imbalances between power generation and consumption. During low-demand periods, BESS stores excess power in its batteries, and during high-demand or power shortage scenarios, it releases stored energy back into the grid. This rapid response and power adjustment from BESS minimizes frequency fluctuations, ensuring reliable grid operation and maintaining supply-demand equilibrium. When the nominal system frequency $f_0$ and the locally measured frequency $f_{meas}$ vary ($\Delta f = f_0 - f_{meas}$), fast frequency response reserves react. Therefore, a battery reacts to positive frequency variations by discharging and to negative frequency deviations by charging. To maintain the nominal system frequency, the generator should continually match the load demand by adjusting for any power imbalances using the stored kinetic energy of the generator. As a result, the following equation describes the frequency response of the governor for n number of generator [74].

$$\frac{\Delta f}{\Delta t} = \frac{f_0}{2} \frac{\Delta P_d}{\sum H_n} \tag{5.4}$$

Where, $\Delta P_d = P_G - P_L$ is the change in power demand, $P_G$ is generated power, $P_L$ is load power demand, $\sum H_n$ is the sum of system inertia constant of all rotating machines and $f_0$ is the nominal frequency. With a rise in load demand or a generator failure, the total inertia of the power grid decreases. When the zero inertial penetration of photovoltaic energy increases in the power grid, the overall inertia decreases. As a result, if alternative mechanisms do not increase system inertia, conventional governor-regulated frequency mechanisms may be unable to adequately rectify power imbalances caused by disturbance events such as generation contingency, fluctuating PV output, or load contingency. As a result, in this work a new droop control is presented to manage the lower frequency caused by the decrease in the inertia constant of the system that helped with fast frequency control and to reduce the negative effects of photovoltaic penetration into the grid [93]. As shown in Equation 5.4, when BESS is introduced in the system, the denominator is further increased by the inertia constant, $H_{BESS}$ of the battery ($2 \sum H_n + H_{BESS}$) and reduced frequency deviation.

### 5.5.2 Modeling of BESS Controller

The BESS controller (clearly described and detailed in Appendix 7.2) is a power system control technique used to ensure that the power output of BESS is distributed in proportion to the available power demand, thereby stabilizing the grid frequency. It employs a standard PI control algorithm to model the BESS controller's response to changes in grid frequency. The PI control algorithm calculates the difference between the desired frequency and the actual frequency, adjusting the BESS power output accordingly. For a BESS with an IGBT-based

converter, there are two parameters to regulate: one for real power (d-axis) and another for reactive power (q-axis). This allows for control over both active power production and the management of AC voltage using reactive power.

The PQ control block depicted in Figure 5.2 highlights the importance of the BESS control approach in this investigation. It consists of two key components: the reactive power controller (Q controller) and the BESS's active power controller (P controller). The signals for active power and reactive power are both fed into the respective loops of the P and Q controllers. In the event of power grid disruptions, fluctuations in both active and reactive power, as well as variations in voltage and frequency, can occur. Therefore, achieving a balance between supply and demand through the regulation of the BESS control can help minimize such variations.

The battery connection point's location is vital for designing a battery energy storage system used in frequency control. Proximity to the fault location enables quick detection and response to frequency changes. Being far away can cause delays and reduced effectiveness. Factors affecting access point selection in distributed generation grid-connected systems include proximity to energy sources, grid congestion, stability, and capacity requirements.

- Distance and Loss: Proximity of the BESS connection point to the energy source directly impacts transmission losses and system efficiency.
- Grid Congestion: Place BESS access points in congested areas of the grid system to address voltage stability, transient stability, and power factor correction.
- Grid Stability: Choose access points with grid stability in mind, considering the BESS size and position. Factors like peak load periods and voltage level variations should influence access point placement decisions.
- Capacity: Ensure selected access points can handle the demand in the area effectively.

The battery was connected to the rectifier bus, which is operated at a voltage level of 400kV AC. This bus was critical for the grid and was selected for two reasons. Firstly, it had several high-capacity generators connected to it. Secondly, it served as the PCC for Ethiopia's grid and rectifier converter. In this research, the battery's DC/AC terminal voltage was set at 0.9/0.4 kV, respectively. To enable connection at different network voltages, a 0.4/400kV step-up transformer was used to link the BESS AC to the grid.

#### 5.5.2.1 Frequency Controller

The frequency controller, shown in Figure 5.3 (a), plays a crucial role in the design of the BESS controller. Its primary objective is to reduce the frequency deviation; for this purpose, a simple P controller is sufficient. The difference between the measured frequency and the

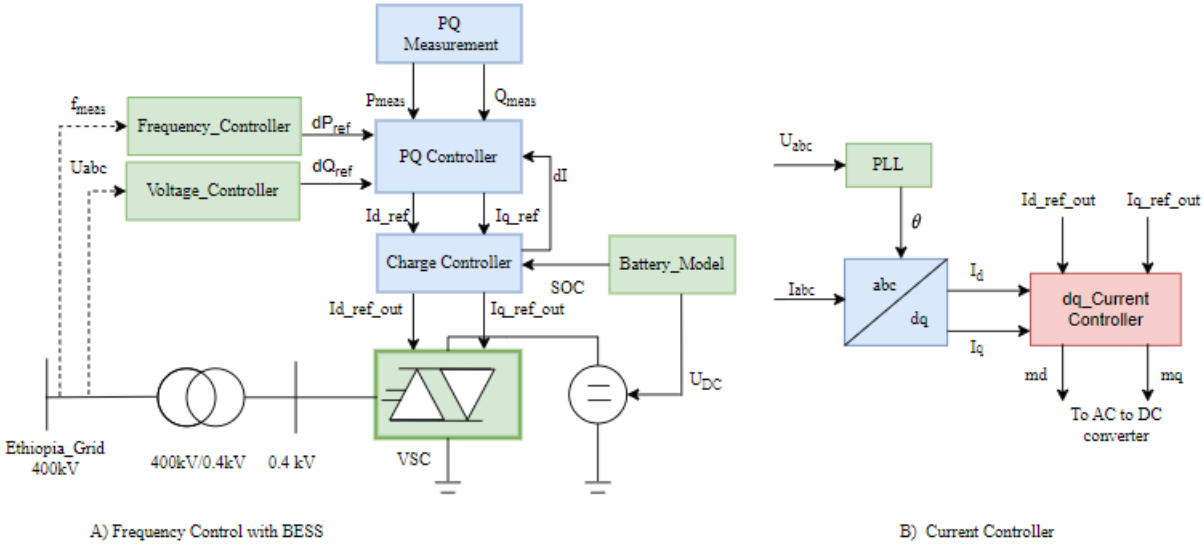


**Figure 5.2:** Block diagram of BESS and dq-Current controller

nominal frequency is processed through a dead-band signal. This signal, combined with the droop controller gain, determines the reference active power. To prevent the BESS from operating within the non-operating frequency range defined by the grid, a small dead band is introduced. The droop control establishes the amount of active power that the BESS will inject or absorb in response to any deviation in the grid frequency. This will only act on deviation outside the nominal range of operations for the integrated system of Ethiopia-Kenya ( 49.00 Hz $\leq f_0 \leq$ 51.00 Hz), where, $f_0$ is the nominal frequency in Hz. The authors propose that this frequency band would be ideal for a future link between Kenya and Ethiopia, even be used for other neighboring countries. With less system inertia, the power frequency droop is dramatically affected, which has a considerable impact on the stability of the power system [94], and its droop characteristics can be given in Equation (5.5).

$$dP_{ref} = \frac{1}{K_{BESS}}(f_0 - f_{meas}) \tag{5.5}$$

Where $f_{meas}$ is the measured frequency, $dP_{ref}$ is the active power reference based on the power-frequency droop controller, $K_{BESS}$ is the droop parameter. In the instance of fast frequency control, the maximum permitted frequency variation is used to determine the gain of the droop controller in terms of pu. Based on the frequency excursion in Table 5.1, it can be clarified that the value of 0.01 pu is a deviation of 49.5 Hz from 50 Hz. In Equation 5.6, 0.01 pu is the maximum frequency deviation allowed, at which point the full BESS should be fully committed.

$$\begin{cases} IFD_{max} = \frac{50-49.5}{50} = 0.01pu. \\ Droop - gain = \frac{1}{0.01} = 100. \end{cases} \tag{5.6}$$

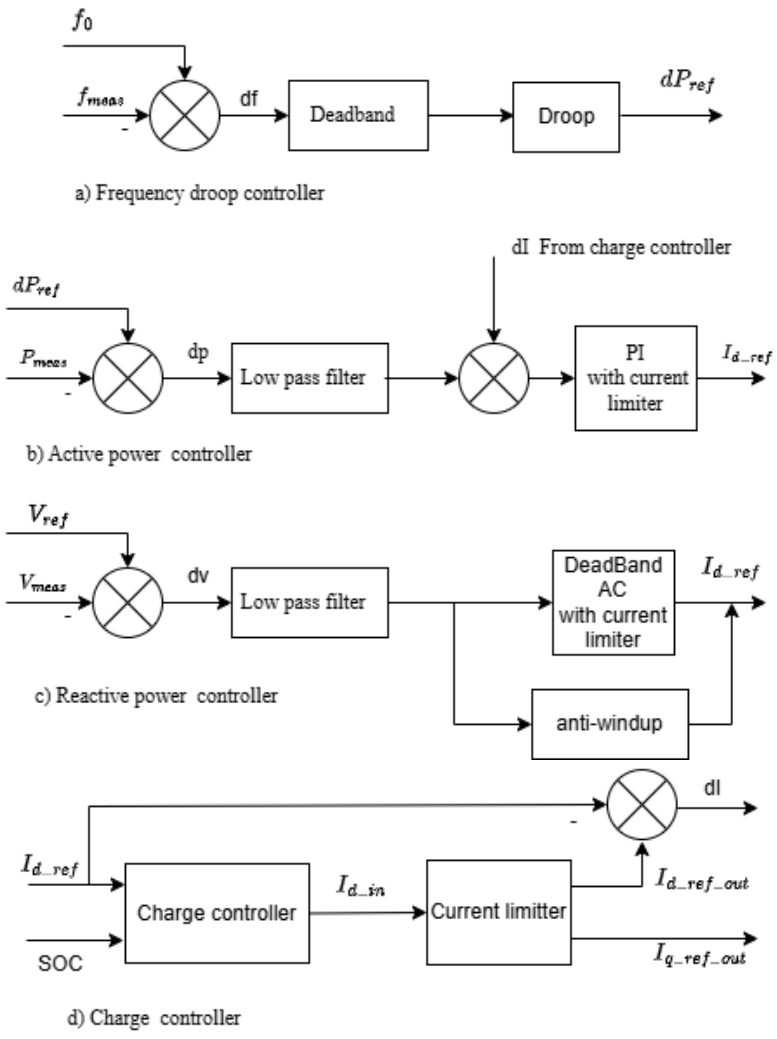


**Figure 5.3:** Generalized PQ-Controller

### 5.5.2.2 Voltage Controller

The voltage droop controller, as seen in Figure 5.3 (c), operates on a similar concept to the frequency droop controller and is given in Equation (5.7).

$$dQ_{ref} = \frac{1}{K_{BESS-vac}}(V_{ref} - V_{meas}) \tag{5.7}$$

where $V_{ref}$ is the reference voltage (steady state voltage in pu), $dQ_{ref}$ is the reactive power reference, and $K_{BESS-vac}$ is the voltage droop parameter. As shown in Fig. 5.3 (c), BESS injects and absorbs reactive power for positive and negative values of dv, respectively. The proposed BESS in the Ethiopian grid is connected to the Wolayta Sodo bus, the connection point of the rectifier converter, and voltage measurement has been taken from this bus for the AC voltage controller. As seen in Figure 5.2 (a), the input signals to generate and control the

active and reactive power of BESS are chosen from the local measurement of voltage and frequency at the BESS connection point (Sodo bus).

#### 5.5.2.3 Active/Reactive (PQ) Controller

BESS typically uses Active-Reactive (PQ) controllers to regulate the power output of the battery in response to changes in the grid. The PQ controller is responsible for maintaining stable voltage and frequency in the grid by adjusting the active (P) and reactive (Q) power output of the battery. The goal of frequency and P controllers is to provide active power control signals, whereas voltage and Q controllers start reactive power signals. The detail of the modeling of PQ is based on the dead band with the Anti-Windup controller given in [7]. The reference signals are generated by the frequency ($dP_{ref}$) and voltage controllers ($dQ_{ref}$), and then the PQ controller processes them further. A first-order low-pass filter is used to pass through the difference between the power reference produced by the frequency controller and the power output at the BESS AC terminal. To monitor the output at the BESS terminal and to modify the reference, the charge controller feedback current is employed. Active/Reactive power is controlled by adding the charge controller output in d-axis/q-axis, dId/dIq to the active/reactive current reference to regulate active/reactive power output, respectively. The current from the charge controller ($dI$) has two components, $dI_d$ and $dI_q$, and are designed as follows in 5.8:

$$\begin{cases} dI_d = i_{dref-out} - i_{dref} \\ dI_q = i_{qref-out} - i_{qref} \end{cases} \tag{5.8}$$

**Table 5.3:** Lithium-ion Battery parameters

| Name | Parameter value |
|---|---|
| Initial SOC (pu) | 0.8 |
| Battery Capacity/cell (Ah) | 120 |
| Number of parallel cells | 60 |
| Nominal voltage (kV) | 0.9 |
| $SOC_{min}$ | 0.2 |
| $SOC_{max}$ | 1 |
| $u_{max}$ voltage of full cell (V) | 13.85 |
| $u_{min}$ voltage of full cell (V) | 12.05 |
| Battery Internal resistance | 0.0001 |
| Battery power rating (MVA) | 120 |

#### 5.5.2.4 Battery Charge Controller

The battery charge controller is a device that is responsible for regulating and controlling the charging process of a battery. Its main purpose is to ensure that the battery is charged safely and efficiently while maximizing its lifespan. Typically, the controller is connected between the battery and the charging source, such as a solar panel or power supply. It continuously monitors the voltage and current of the battery and adjusts the charging process accordingly. This prevents overcharging, which can be detrimental to the battery's health, and ensures that the battery reaches its full charge without wasting energy [95]. In this study, a lithium-ion battery is used, which is currently the most widely adopted type of grid-connected battery. Lithium-ion batteries excel in terms of their effectiveness, energy and power capacity, as well as their energy density, outperforming other battery technologies [96].

BESS output (charging/discharging) is controlled by the battery charge controller based on the value and polarity of the d-axis reference as well as the accessible battery SOC. If the SOC capacity stays within the prescribed operational bounds, BESS injects or absorbs active power. In Equation (5.9), the operational areas of the SOC are described. To prevent BESS overload, the current limiter controls and limits current flow. BESS injects or absorbs active power if the SOC capacity remains within the specified operating constraints. So, we can write the droop-type charging/discharging strategy as shown in Equation (5.9), and its parameter is given in Table 5.3 [97]:

$$i_{d-in} = \begin{cases} i_{dref} & SOC \geq SOC_{min} \\ -i_{dref} & SOC \leq SOC_{max} \\ 0 & otherwise \end{cases} \tag{5.9}$$

The above condition states that a battery can use energy (charge) if $SOC \leq SOC_{max}$, and provide energy when it is more than or equal to $SOC_{min}$. If SOC is outside of these maximum and minimum limitations, the battery cannot be charged or drained. As can be seen in Table 5.3, 1 indicates the upper limit of the battery's charge capacity and 0.8 is a design choice based on system requirements and performance considerations.

### 5.5.3 PWM Converter Control in BESS

The VSC with pulse width modulation (PWM) is a 2-level converter that serves as the standard foundation for the rectifier/inverter. The PWM converter control signal is obtained by controlling the current on the d and q axes of the charge controller. The reference of the current controller on the d and q axes ($Id\_ref\_out$ and $Iq\_ref\_out$) is obtained from the BESS damping controller, and the measured current signal of the AC converter axes d and q are the inputs to the current controller. PLL technology is used to modify the pulse width

modulation md and mq output on the current controller to provide a reference phase angle and the same reference to control the DC/AC converter.

## 5.6 Simulation Results With BESS-Based FFC

To obtain the simulation results, various operating scenarios were developed and summarized in Table 5.4. Additionally, Table 5.5 presents important base case data for the Ethiopian grid. Through conducting numerous dynamic simulations, the study examined how the system behaves in different scenarios, with a specific focus on evaluating the response of the BESS to frequency decrease resulting from load fluctuations and generation contingencies. The study primarily concentrated on the Ethiopia-Kenya interconnected power grid, incorporating an LCC HVDC link. Four operational scenarios were considered, including the base case, scenarios involving BESS implementation, and scenarios with varying levels of PV penetration. These scenarios aimed to comprehensively understand different aspects of frequency stability influenced by various disturbances.

**Table 5.4:** Generation and Load Contingency for different operational strategy

| Disturbance and PV penetration levels | | |
|---|---|---|
| operational strategy | PV penetration [%] | Load contingency [MW] |
| Case 1 w/out BESS | 15 | 213.12 |
| | 30 | 213.12 |
| | 45 | 213.12 |
| Case 2 with BESS | 15 | 213.12 |
| | 30 | 213.12 |
| | 45 | 213.12 |
| operational strategy | PV penetration [%] | Gen contingency [MW] |
| Case 3 w/out BESS | 15 | 200 |
| | 30 | 200 |
| | 45 | 200 |
| Case 4 with BESS | 15 | 200 |
| | 30 | 200 |
| | 45 | 200 |

**Table 5.5:** Base case system data from load flow calculation

| | | |
|---|---|---|
| Generation | Total Generation | 4074.24 MW |
| Load | Total Load | 1937.47 MW |
| | Grid Losses | 264.01 MW |
| HVDC | External In feed | -1871.00 MW |
| HVDC | Inter Grid Flow | -2113.68 MW |

### 5.6.1 Case 1: PV Penetration Levels and Load Disturbance

This section investigates the impact of PV penetration levels on frequency deviation in the absence of compensation from the BESS during a load disturbance of 213.12 MW at t = 10 s. Figure 5.4 illustrates the frequency response of the Ethiopian grid at different levels of penetration of PV. The blue line represents the frequency response of the Ethiopian SGs under base-case conditions, with a 213.12 MW (11%) step-load increase. Without PV penetration, the system frequency, IFD, SSFD, and rate of RoCoF are 49.04 Hz, -0.9461 Hz, -0.1125 Hz and -0.2258 Hz / sec, respectively. With 15% PV penetration (indicated in red), the simulation results change to 48.75 Hz, -1.235 Hz, -0.1033 Hz, and -0.2303 Hz / sec, respectively. The addition of PV to the grid immediately reduces the overall system inertia provided by SGs, resulting in an increase in IFD and RoCoF after disturbance. Further increasing the penetration level to 30% and 45% leads to rapid increases in IFD and RoCoF.

As indicated in Table 5.6, higher levels of photovoltaic penetration result in a significant increase in the dynamic frequency deviation. The frequency excursion exceeds the frequency disturbance range of the system ($49.00 \leq f_0 \leq 51.00$ Hz) for all three levels of PV penetration. This occurs because the SGs are unable to maintain the frequency within the specified ±2% boundary of the nominal magnitude of the load disturbance. Notably, in the case of 45% PV penetration, the frequency excursion reaches 48.36 Hz, which is beyond the maximum allowable frequency range under fault conditions. Consequently, the system becomes unstable and enters a state of blackout. To address these challenges, the authors employ a design frequency control technique to ensure that the frequency remains within the prescribed range.

**Table 5.6:** Simulation results for 11% Load variation in the Ethiopian grid with different PV penetration levels

| Operational scenario | Frequency excursion (Hz) | IFD (Hz) | SSFD (Hz) | RoCoF (Hz/sec) |
|---|---|---|---|---|
| Base-case | 49.04 | -0.9461 | -0.1125 | -0.2258 |
| 15% PV | 48.75 | -1.235 | -0.1033 | -0.2303 |
| 30% PV | 48.55 | -1.443 | -0.1129 | -0.2947 |
| 45% PV | 48.36 | -1.626 | -0.1131 | -0.3245 |
| 15% PV & 120 MW BESS | 49.64 | -0.3603 | -0.09197 | -0.1659 |
| 30% PV & 120 MW BESS | 49.29 | -0.7052 | -0.08852 | -0.1954 |
| 45% PV & 120 MW BESS | 49.02 | -0.96 | -0.08762 | -0.1956 |

### 5.6.2 Case 2: PV Penetration Levels and Load Disturbance with BESS compensation

To assess the performance of the BESS in handling a rapid increase in PV penetration and sudden load variation, an 11% load increase was considered for the Ethiopia-Kenya system.

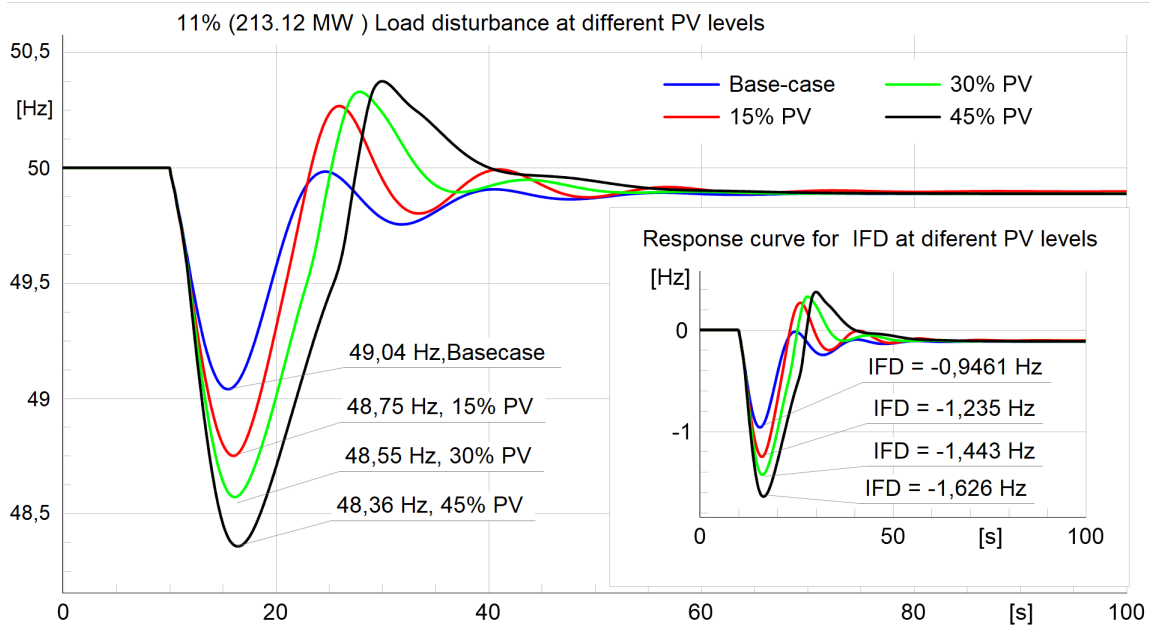


**Figure 5.4:** Result of Case 1: The frequency response curve of the Ethiopian grid at various PV penetration levels and load disturbance.

The performance of the system was evaluated both with and without the BESS. The simulation results presented in Figure 5.5 and Table 5.6 provide insight into improved performance in terms of IFD, SSFD, and RoCoF.

Table 5.6 demonstrates that the presence of the BESS alters and improves frequency excursion, IFD, SSFD, and RoCoF at different PV penetration levels. The BESS compensates for active power mismatches by generating the necessary amount of active power. Figure 5.5(A) illustrates how frequency deviation sharply increases with higher PV penetration levels. At 45% PV penetration, the frequency drops to 48.36 Hz, falling below the major failure scenario listed in Table 5.1 and leading to a blackout. Therefore, modeling and managing the BESS are crucial for the success of this research.

When BESS is integrated into the system, it positively impacts the frequency. For example, at 15% PV penetration, the frequency increases from 48.75 Hz to 49.64 Hz; at 30% PV penetration, it changes from 48.55 Hz to 49.29 Hz, and at 45% PV penetration, it rises from 48.36 Hz to 49.02 Hz. These findings highlight that the integration of a BESS effectively mitigates frequency deviations and enhances the system stability as the penetration levels of photovoltaics increase.

Figure 5.5(B) demonstrates the relationship between the BESS's output and frequency variations. When the frequency decreases from 49.78 Hz to 49.02 Hz, the BESS actively injects a constant power to compensate for the frequency drop. Similarly, as the frequency starts to increase from 49.02 Hz to 49.78 Hz, the constant power injected by the BESS supports the frequency, effectively stabilizing it. As the frequency further increases from 49.78 Hz to 50

Hz, the output power of the BESS is reduced, and the BESS initiates the charging process to store active power.

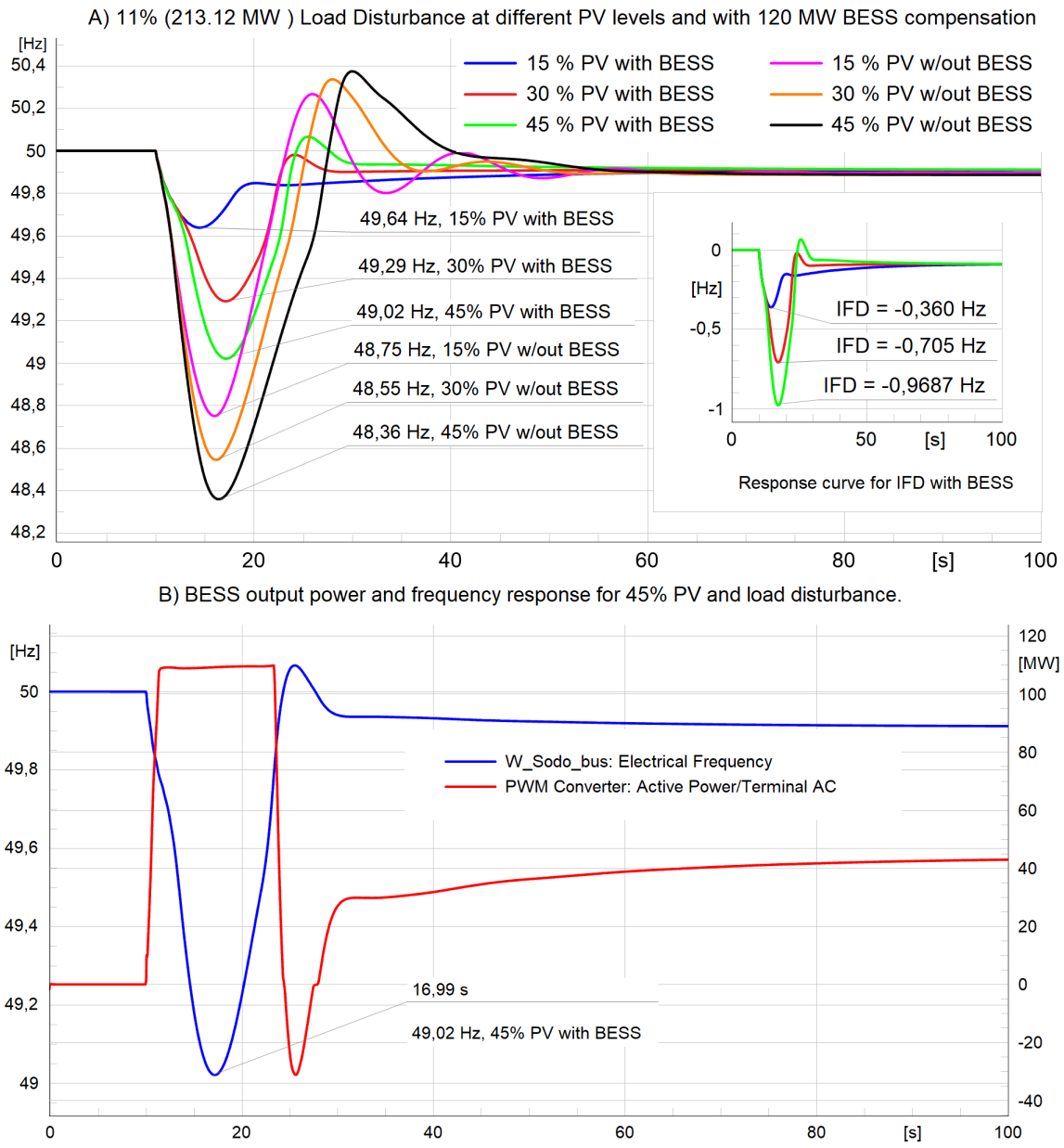


**Figure 5.5:** Results of Case 2: A) System frequency response with different PV penetration, B) Right, BESS output power and Left, the Frequency response for 45% PV penetration respectively

### 5.6.3 Case 3: PV Penetration Levels and Generator Contingency

This section explores the impact of PV penetration levels on frequency deviation in the absence of BESS compensation during a generator trip contingency. At t = 10 sec, a generation contingency is introduced to simulate the effects under various PV penetration levels.

Figure 5.6 illustrates the frequency response of the Ethiopian grid and the corresponding

IFD response curve at different PV penetration levels. Without PV penetration, the frequency excursion, IFD, and RoCoF are 48.94 Hz, -1.063 Hz, and -0.2926 Hz/sec, respectively, as shown in Table 5.7. The frequency dip resulting from the 200 MW generator trip exceeds the limits specified in Table 5.1, indicating that the generators are unable to maintain the grid-defined frequency limit of ±2% of the nominal value during this disturbance event at t = 10 sec.

However, as the penetration level of photovoltaics increases, the frequency deviation is significantly affected, leading to system instability. To address this issue, a 120 MW BESS is installed on bus 3 (as depicted in Figure 3.7). The BESS provides additional damping and effectively reduces frequency deviation, mitigating the adverse effects caused by the generator trip contingency.

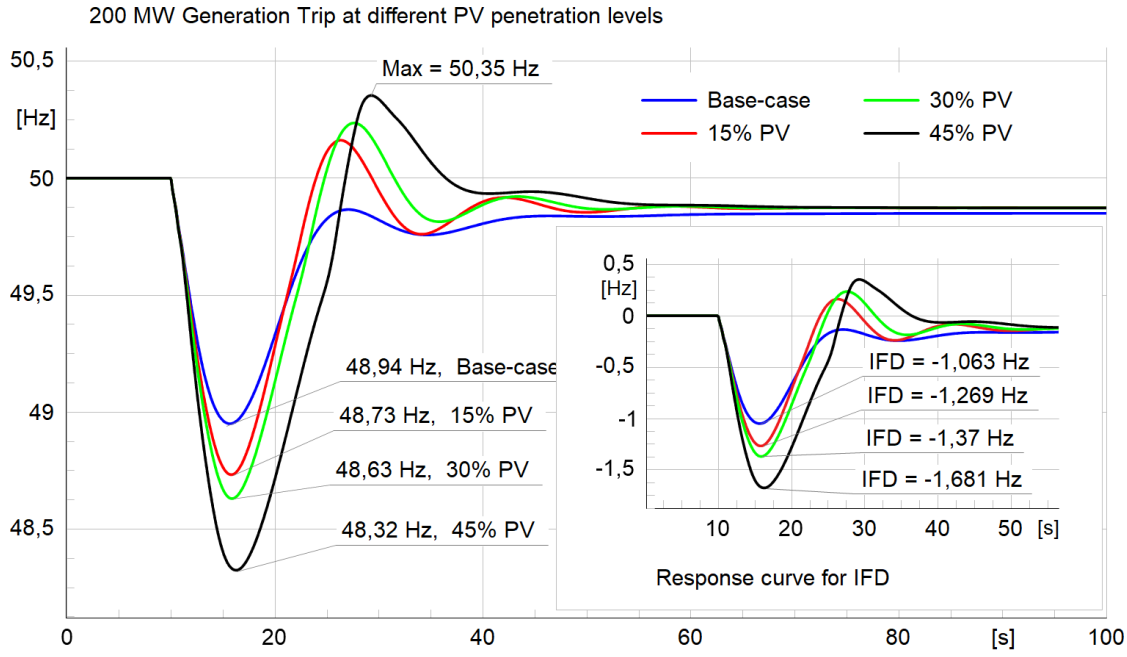


**Figure 5.6:** Result of Case 3: The frequency response curve of the Ethiopian grid at various PV penetration levels and generation contingency.

**Table 5.7:** Simulation results for 200 MW Generator trip in the Ethiopian grid with different PV penetration levels, with and without BESS

| Operational scenario | Frequency excursion (Hz) | IFD (Hz) | SSFD (Hz) | RoCoF (Hz/sec) |
|---|---|---|---|---|
| Base-case | 48.94 | -1.063 | -0.1415 | -0.2926 |
| 15% PV | 48.73 | -1.269 | -0.1307 | -0.3103 |
| 30% PV | 48.63 | -1.37 | -0.1311 | -0.3229 |
| 45% PV | 48.32 | -1.681 | -0.1311 | -0.3593 |
| 15% PV & 120 MW BESS | 49.45 | -0.5439 | -0.0656 | -0.1157 |
| 30% PV & 120 MW BESS | 49.34 | -0.6651 | -0.05973 | -0.1211 |
| 45% PV & 120 MW BESS | 49.08 | -0.9163 | -0.04791 | -0.1542 |

### 5.6.4 Case 4: PV Penetration Levels and Generator Contingency with BESS Compensation

This study investigated the impact of a generator trip on the frequency of the Ethiopian grid at different levels of PV penetration. It also examined how a BESS could compensate for the power loss caused by this disruption and help stabilize the frequency. Simulation results for Case 4, considering various PV penetration levels and a 200 MW generator trip, were presented in Figure 5.8 and Table 5.7.

The results showed that as PV penetration increased from 15% to 45%, both the frequency deviation and RoCoF increased significantly. However, the frequency excursion decreased notably. Specifically, at a 15% PV penetration level, the proposed 120 MW BESS scheme achieved a frequency excursion of 49.45 Hz, an IFD of -0.5439 Hz, and a RoCoF of -0.1157 Hz/sec. The integration of the BESS increased the frequency from 48.73 to 49.45 Hz, which fell within the frequency excursion range of the standard operating mode specified by the TSO in Table 5.1. This demonstrated how the BESS improved frequency excursion and IFD at the 15% PV penetration level.

At a 30% PV penetration level, the frequency increased from 48.63 Hz to 49.34 Hz. However, compared to the 15% PV penetration level with BESS, the frequency improvement was lower due to increased PV penetration and generator overload. At a 45% PV penetration level, the frequency dropped to 48.32 Hz, causing a blackout. But with the presence of the BESS, the frequency improved to 49.08 Hz by injecting power from the battery into the grid using a power converter. The converter converted DC power from the battery into synchronized AC power, matching the grid's frequency and voltage.

The simulation results depicted in Figure 5.7 show the BESS output power and battery charging status. In Figure 5.7(A), it is observed that with increasing PV penetration, the frequency decreases rapidly. When the frequency falls below 49.9 Hz, the BESS injects active power into the grid to raise the frequency. During frequency drops and insufficient generated power, the stored energy in the BESS is discharged to supplement the electrical energy. As the frequency stabilizes, the BESS charges and reaches a steady state. The power converter reduces the BESS's output to maintain a constant value. Figure 5.7(B) shows that when the frequency drops due to a generator trip and PV penetration, the battery's SOC decreases as it discharges stored energy to support the grid.

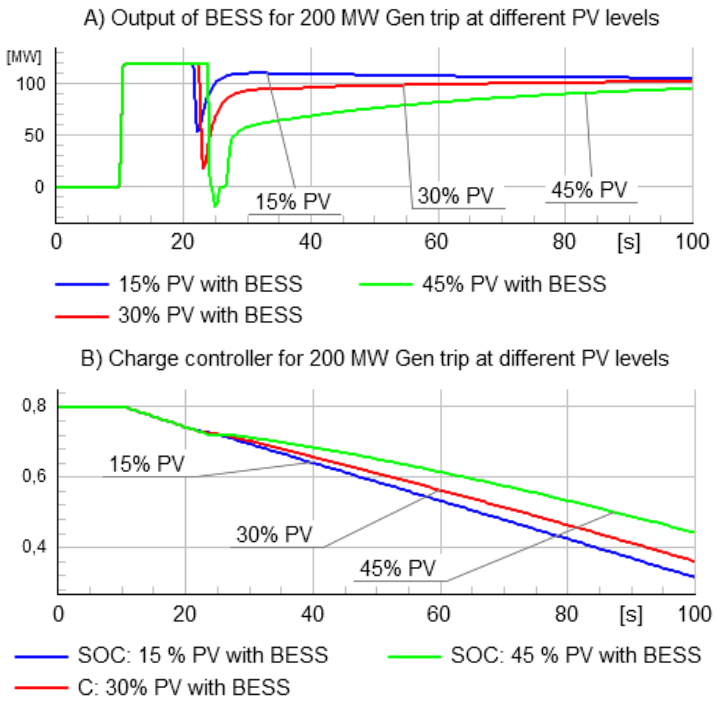


**Figure 5.7:** Results of Case 4: A) BESS output power, B) State of Charge (SOC) Controller, for different PV penetration levels.

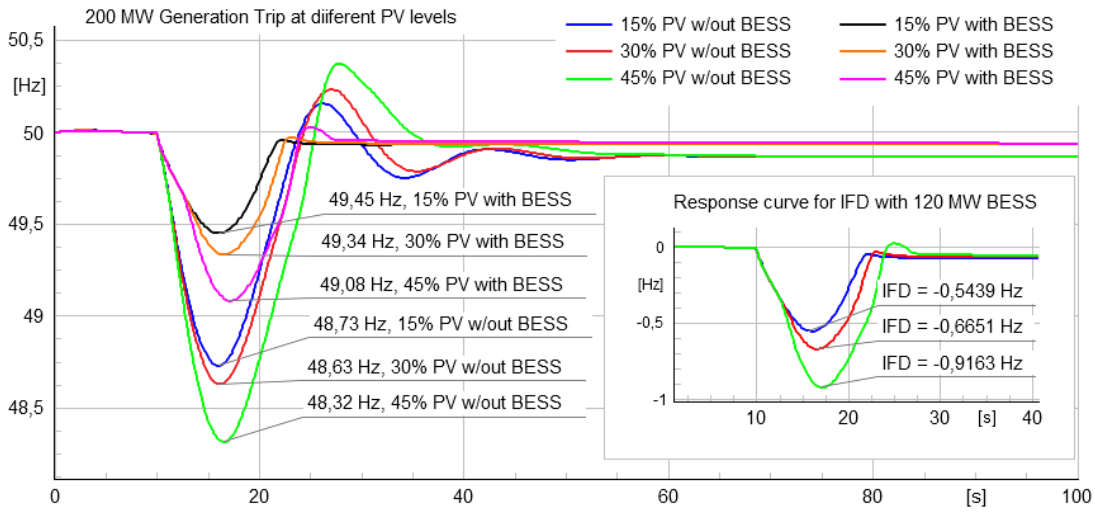


**Figure 5.8:** Case 4: The frequency response curve of the Ethiopian grid at various PV penetration levels and 120 MW BESS compensation.

**Table 5.8:** Comparison of all cases

| Parameters | Case 1 | Case 2 | Case 3 | Case 4 |
|---|---|---|---|---|
| Frequency excursion after disturbance(Hz) | 48.75 | 49.64 | 48,73 | 49.45 |
| | 48.55 | 49,29 | 48,63 | 49,34 |
| | 48.36 | 49,02 | 48,32 | 49.08 |
| Instantaneous Frequency Deviation (Hz) | -1,235 | -0,3603 | -1,269 | -0,5439 |
| | -1,443 | -0,7052 | -1,37 | -0,6651 |
| | -1,626 | -0.96 | -1,681 | -0,9163 |
| Rate-of-Change-of-Frequency (Hz/sec) | -0,2303 | -0,1659 | -0,3103 | -0,1157 |
| | -0.2947 | -0.1954 | 0.3229 | -0.1211 |
| | -0.3245 | -0.1956 | -0.3593 | -0.1542 |

As summarized in Table 5.8, the analysis of frequency stability under various operational strategies reveals significant insights across four cases involving load and generation contingencies. In Case 1, a sudden load increase of 213 MW without BESS results in notable frequency drops, particularly exacerbated by higher levels of PV penetration (15%, 30%, and 45%). Conversely, in Case 2, the integration of BESS during the same load contingency mitigates these fluctuations by providing stored energy, thereby enhancing frequency stability across all PV penetration levels. Similarly, Case 3, which examines a 200 MW generator trip without BESS, also experiences significant frequency instability due to the loss of generation, further intensified with increased PV penetration. However, Case 4 demonstrates that integrating BESS in response to the generator trip allows for a rapid response to maintain frequency stability, showcasing the benefits of energy storage solutions. In general, the findings underscore the critical role of BESS in improving the resilience and stability of the system, particularly as the penetration of photovoltaic energy increases.

## 5.7 Summary

This research work introduces an efficient method for enhancing system stability and frequency control in BESS. The approach involves implementing droop control with frequency deviation input in the BESS controller. The performance of this frequency control strategy is evaluated using DIgSILENT simulation software, considering different disturbance sizes and levels of PV penetration. The simulations convincingly demonstrate that the proposed BESS frequency control scheme effectively reduces the maximum frequency deviation and suppresses significant frequency excursions under various disturbance and PV penetration conditions.

Simulation results demonstrate that the frequency excursion in a power system rapidly decreases during periods of increasing photovoltaic PV levels and abrupt changes in power demand or generation. However, this drop in frequency increases IFD and makes the system more vulnerable to failure. The overall simulations highlight the effectiveness of the suggested FFC system using BESS. The BESS control method successfully reduces instantaneous frequency deviation and RoCoF while suppressing frequency excursions under various disturbance and PV penetration levels. Additionally, integrating BESS into the grid significantly improves the system's SSFD. Furthermore, due to the selected BESS capacity of BESS limitation, the simulations reveal that when PV penetration exceeds 45%, the frequency excursion exceeds the acceptable level, causing cascading generation failure. These findings emphasize the criticality of addressing the

# 6 Conclusions & Outlook

## 6.1 Conclusion

The rise of the non-synchronous generation poses a risk to system frequency stability due to a decrease in overall inertia. Specifically, the transition from conventional generators to renewable energy sources results in a reduction of the system's kinetic energy, making it increasingly susceptible to significant disturbances. The studies demonstrate that implementing HVDC links, advanced control mechanisms, and BESS significantly improve transient stability and frequency control across various grid conditions. The findings show that HVDC connections between Ethiopia and Kenya enhance transient stability by increasing critical clearing times, while the integration of LSP plants necessitates sophisticated control strategies to mitigate reduced system inertia and associated risks of transient instability. Specifically, POD and CLF strategies have proven effective in stabilizing rotor dynamics and enhancing damping performance in the presence of high PV penetration, with CLF controllers outperforming POD in certain scenarios. Furthermore, the use of droop control in BESS has shown promise in managing frequency deviations and suppressing significant fluctuations during disturbances, although challenges arise when PV penetration exceeds 45%, leading to potential cascading failures.

Overall, these insights underscore the necessity of robust control mechanisms and system enhancements to ensure reliable and stable power systems as renewable energy continues to evolve.

## 6.2 Future work

1. This article does not cover the frequency control and stability specific to Kenya due to insufficient system data. The future work will simulate a comprehensive power network and examine the impact of increased PV penetration in each operational region of the Ethiopia-Kenya HVDC interconnection.

2. Field Testing and Validation: Implementing field tests to validate theoretical models and simulations in real-world scenarios, ensuring the reliability of proposed solutions.

3. Practical Implementation Considerations: Address practical considerations such as cost optimization, maintenance strategies, and scalability of BESS systems. Explore

the economic feasibility and scalability of deploying BESS on a larger scale to support high PV penetration levels in the Ethiopian power grid.

4. Parameter Sensitivity Analysis: Conduct a sensitivity analysis to identify critical parameters that affect the performance of STATCOM + POD and STATCOM + CLF, providing information on optimal tuning for diverse operating conditions.

5. Long-Term Stability Assessment: Analyze the long-term impacts of improvements in transient rotor angle stability on overall system reliability and performance, considering the integration of significant renewable resources.

6. Extended Controller Variants: Investigate the performance of additional control strategies beyond POD and CLF, such as model predictive control (MPC) or adaptive control techniques, to further enhance system stability in varying operating conditions.

# 7 Appendix

## 7.1 Grid Data

**Table 7.1:** Parameters of SGs in Ethiopia's Grid.

| Parameters | Units (n) | H | PG (MW) | MVA | MVA*n | MVA*n*H | Area |
|---|---|---|---|---|---|---|---|
| Gibe I | 3 | 3.02 | 147 | 73 | 219 | 661 | South West |
| Gibe II | 4 | 3.04 | 300 | 125 | 500 | 1520 | South West |
| Gibe III - 1 | 5 | 3,27 | 655 | 220 | 1100 | 7194 | South |
| Gibe III - 2 | 5 | 3,27 | 655 | 220 | 1100 | 7194 | South |
| Genale III | 4 | 3 | 280 | 125 | 500 | 1500 | South |
| Tekeze | 4 | 4.26 | 218 | 86.7 | 346.8 | 1477 | North |
| Fincha I | 3 | 2.64 | 76 | 40.2 | 120.6 | 318 | West |
| Fincha II | 2 | 2.64 | 51 | 40.2 | 80.4 | 212 | West |
| Neshe | 2 | 2.65 | 67 | 53 | 106 | 281 | West |
| Awash II | 2 | 2.56 | 22 | 20 | 40 | 102 | Central |
| Awash III | 2 | 2.56 | 22 | 20 | 40 | 102 | Central |
| Melka Wakena | 4 | 3.16 | 107 | 45 | 180 | 569 | Central |
| Aluto Langa | 2 | 1.16 | 8 | 4.5 | 9 | 10.44 | Central |
| Koka | 3 | 2.26 | 30 | 18 | 54 | 122 | Central |
| Beles | 4 | 3.14 | 328 | 133 | 532 | 1670 | North West |
| Tis Abay 2 | 2 | 3 | 50 | 40 | 80 | 4240 | North West |
| Tis Abay 1 | 3 | 2.01 | 8 | 4.8 | 14.4 | 29 | North West |
| Aba Samuel | 4 | 3 | 3 | 1.44 | 5.76 | 17 | Addis Ababa |

Where:

- H-Inertia constant of synchronous generators
- n- number of parallel connected generators
- PG (MW) total active power injected by the generators

$$\sum_{i=1}^{18} PG_i = 3027 \quad [\text{MW}]$$

- MVA - is the rating of a single unit of a generator

- MVA*n-Total MVA connected
- MVA*n*H-Total Stored Kinetic Energy

The synchronous generator control system consists of several key components:

- The Power System Stabilizer (PSS), which enhances damping of power system oscillations by adjusting excitation voltage;
- The Automatic Voltage Regulator (AVR), which maintains the generator's output voltage by regulating excitation current based on voltage feedback and ;
- the Governor (GOV), which controls the mechanical power input to the generator to maintain frequency stability by adjusting fuel supply in response to load changes.

The Generator Element (Gen) converts mechanical energy into electrical energy, while signal blocks facilitate communication between these components, ensuring cohesive operation. This interconnected system ensures the generator operates efficiently and stably in response to varying load demands and system dynamics.

General Flow

- The Governor adjusts the mechanical input to change generator power based on system demand.
- The AVR manages the output voltage and reacts to any changes in load or generator performance.
- The PSS monitors system stability and makes adjustments to enhance damping.

**Table 7.2:** Synchronous Generators with Exciter and Governor Types

| Generator | Exciter Type | Governor Type |
|---|---|---|
| Gibe I | EXST1 | HYGOV |
| Gibe II | EXST1 | HYGOV |
| Gibe III | EXST1 | HYGOV |
| Genale III | EXST1 | HYGOV |
| Tekeze | EXST1 | HYGOV |
| Fincha I | SCRX | HYGOV |
| Fincha II | SCRX | HYGOV |
| Neshe | SCRX | HYGOV |
| Awash II | SCRX | HYGOV |
| Awash III | SCRX | HYGOV |
| Melka Wakena | SCRX | HYGOV |
| Aluto Langa | SEXS | TGOV1 |
| Koka | SCRX | HYGOV |
| Tis Abay II | EXST1 | HYGOV |
| Tis Abay I | EXST1 | HYGOV |
| Aba Samuel | SEXS | TGOV1 |

**Table 7.3:** EXST1 Parameters

| Parameter | Value |
|---|---|
| Tr - Measurement Delay [s] | 0.01 |
| Tb - Filter Delay Time [s] | 0.4 |
| Tc - Filter Derivative Time Constant | 0.04 |
| Ka - Controller Gain | 60 |
| Ta - Controller Time Constant | 0.02 |
| Kc - Exciter Current Compensation Factor | 0 |
| Kf - Stabilization Path Gain (pu) | 0.03 |
| Tf - Stabilization Path Delay Time [s] | 1 |
| Vimin - Controller Minimum Input [pu] | -0.3 |
| Vrmin - Controller Minimum Output [pu] | -5 |
| Vimax - Controller Maximum Input [pu] | 0.2 |
| Vrmax - Controller Maximum Output [pu] | 5 |

**Table 7.4:** SCRX Parameters

| Parameter | Value |
|---|---|
| Tb - Filter Delay Time [s] | 10 |
| Ta - Filter Derivative Time Constant [s] | 0.1 |
| K - Controller Gain | 100 |
| Te - Exciter Time Constant | 0.1 |
| rc_rfd Crowbar resistor factor [pu] | 0 |
| Cswitch Cswitch [0,1] | 0 |
| Emin - Controller Minimum Output [pu] | 0 |
| Emax - Controller Maximum Output [pu] | 5 |

**Table 7.5:** SEXS Parameters

| Parameter | Value |
|---|---|
| Tb - Filter Delay Time [s] | 0.1 |
| Ta - Filter Derivative Time Constant [s] | 0.1 |
| K - Controller Gain [p.u.] | 100 |
| Te - Exciter Time Constant [s] | 0.1 |
| Emin - Controller Minimum Output [p.u.] | 0 |
| Emax - Controller Maximum Output [p.u.] | 3 |

**Table 7.6:** HYGOV Parameters

| Parameter | Value |
|---|---|
| r - Temporary Droop [pu] | 0.5 |
| Tg - Governor Time Constant [s] | 6 |
| Tf - Filter Time Constant [s] | 0.05 |
| Tg - Servo Time Constant [s] | 0.1 |
| Tw - Water Starting Time [s] | 1 |
| At - Turbine Gain [p.u.] | 1.2 |
| Dtrb - Frictional Losses Factor pu [pu] | 0 |
| qnl - No Load Flow [pu] | 0 |
| R - Permanent Droop [pu] | 0 |
| PN - Turbine Rated Power (0 > PN = Pg) [MW] | 0 |
| Gmin - Minimum Gate Velocity Limit [pu] | 0.167 |
| Gmax - Maximum Gate Limit [pu] | 1 |

**Table 7.7:** TGOV1 Parameters

| Parameter | Value |
|---|---|
| T3 - Turbine Delay Time Constant [pu] | 3 |
| T2 - Turbine Derivative Time Constant [pu] | 1 |
| Dt - Turbine Power Coefficient [pu] | 1 |
| Fl - Frictional Losses Factor [pu] | 0 |
| R - Controller Droop [pu] | 0.05 |
| Tm - Governor Time Constant [s] | 0.4 |
| PN - Turbine Rated Power (0 > PN = Pg) [MW] | 0 |
| Vmin - Minimum Gate Limit [pu] | 0 |
| Vmax - Maximum Gate Limit [pu] | 1 |

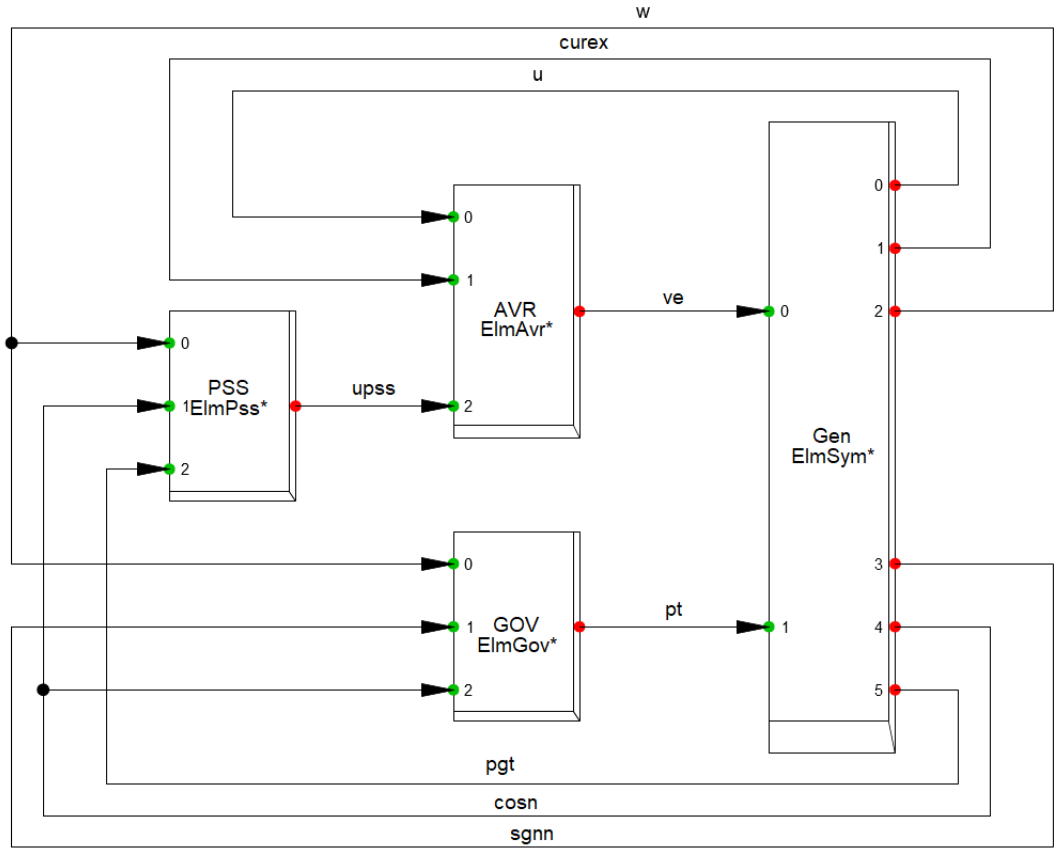


**Figure 7.1:** Synchronous generators composite model block diagram

## 7.2 Detailed modeling of BESS

The BESS model typically includes a three-phase bi-directional DC/AC converter, a battery bank, and a three-phase step-up transformer connecting BESS into the system. The key components of the design of BESS are :

1. Frequency Controller
2. Active/Reactive power controller
3. Voltage Controller
4. Battery charge controller
5. d-q Current controller

The general block diagram or the BESS frame used in power factory software is shown as follows:

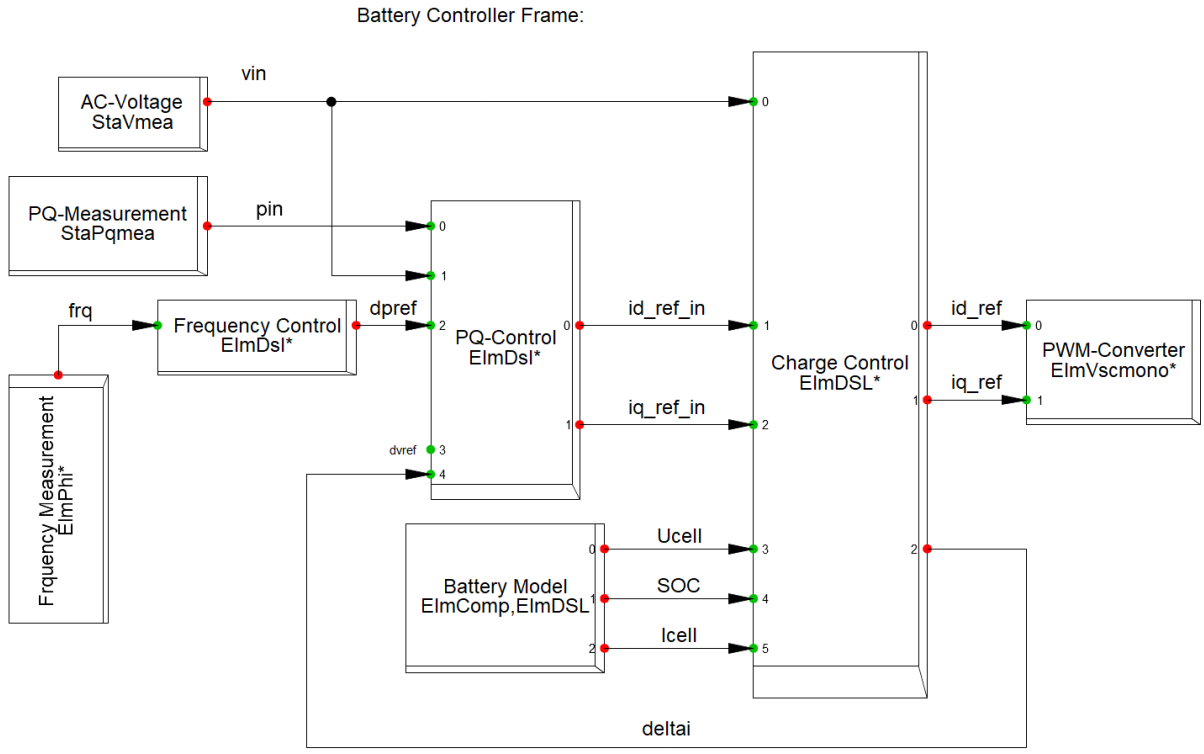


**Figure 7.2:** BESS DIgSILENT frame

- The main purpose of the frequency measurement block in a BESS system is to continuously monitor the frequency of the electrical signal. The output of the frequency measurement block is $\Delta P_{ref}$, and a drop in frequency typically indicates that demand is exceeding supply. Conversely, an increase in frequency suggests that supply exceeds

demand. The frequency measurement helps calculate how much power needs to be adjusted. This adjustment is represented as $\Delta P_{ref}$

- $\Delta P_{ref}$ indicates how much power should be either supplied to or absorbed from the grid to restore frequency to its nominal value. This is crucial for maintaining grid stability.
- $\Delta P_{ref}$ informs the battery management system on how to adjust its charging or discharging strategy. For instance, if $\Delta P_{ref}$ is positive, the system may need to discharge power; if negative, it may need to charge.
- The outputs of PQ measurements work in conjunction with $\Delta P_{ref}$ to ensure effective frequency control and grid stability. Considering control signal generation, the calculated $\Delta P_{ref}$ is then used to generate control signals for the BESS system:
  - Discharge Power: If $\Delta P_{ref}$ is positive, the system discharges power to the grid to help restore frequency.
  - Charge Power: If $\Delta P_{ref}$ is negative, the system absorbs power from the grid to help reduce frequency.
- The Battery Model block in a Battery Energy Storage System (BESS) plays a crucial role in simulating and managing the behavior of the battery. Here's an overview of its functions and significance:
  1. State of Charge (SOC) Estimation:
     - The Battery Model continuously estimates the SOC, which indicates how much energy is stored in the battery relative to its full capacity. This is essential for understanding the available energy for discharge or the need for charging.
  2. Dynamic Behavior Simulation:
     - The block simulates the dynamic behavior of the battery under various conditions, including charging, discharging, and temperature variations. This helps predict how the battery will respond to different operational scenarios.
  3. Voltage and Current Relationships:
     - It models the relationships between voltage, current, and SOC. This includes understanding how the battery voltage changes with SOC and the effects of different load conditions on performance.

- The output currents from the Charge Controller block are derived from the inputs it receives, which include $i_{d_{\text{ref,in}}}$, $i_{q_{\text{ref,in}}}$, SOC, $U_{\text{cell}}$, and $I_{\text{cell}}$.

  1. Inputs to the Charge Controller

     - $i_{d_{\text{ref,in}}}$: This is the reference current for direct (active) control of the battery. It indicates how much power the battery should ideally discharge or charge based on the system's requirements.
     - $i_{q_{\text{ref,in}}}$: This is the reference current for reactive (supportive) control, used for managing the power factor and providing reactive power support to the grid.
     - State of Charge (SOC): The current state of charge indicates how much energy is stored in the battery. This helps the controller determine safe operating limits for charging and discharging.
     - $U_{\text{cell}}$: The voltage of the battery cell provides information about its current state and is essential for calculating power and efficiency.
     - $I_{\text{cell}}$: This is the actual current flowing through the battery cell, which is vital for monitoring performance and ensuring that the battery operates within specified limits

  2. Outputs from the Charge Controller

     - $\Delta i$: This output represents the change in current necessary to adjust the battery's charging or discharging based on the input references and current conditions.
     - $id_{ref}$: This is the adjusted direct reference current output for the battery, indicating how much direct current should be supplied or absorbed to achieve the desired operational state.
     - $iq_{ref}$: This current is used for reactive (supportive) control, managing the power factor, and providing reactive power support to the grid.

  3. PWM Conversion block:

     - In the context of a battery controller, the d-axis reference current $id_{ref}$ and the q-axis reference current $iq_{ref}$ are crucial inputs to the PWM converter.
     - The PWM converter takes the reference currents as inputs to modulate the output voltage and current to the battery or grid.
     - The d-axis reference current $id_{ref}$ is associated with active power control, while the q-axis reference current $iq_{ref}$ is tied to reactive power control.

  4. Control Strategy:

- The charge controller calculates the required duty cycle for the PWM signal based on these reference currents.
- The duty cycle determines the duration for which the switch in the PWM converter is on versus off, effectively controlling the average output voltage and current.

5. Output Regulation:
   - By adjusting the duty cycle according to $id_{ref}$ and $iq_{ref}$, the PWM converter can regulate the power flow to or from the battery, ensuring that it operates efficiently and meets the system demands.
   - This regulation helps maintain voltage levels, manage charging/discharging rates, and support grid stability.

## 7.3 Detailed modeling of STATCOM controller

Modeling of a STACOM-based supplementary controller for transient stability enhancement in DIgSILENT is accomplished through several key steps:

- First, a STACOM is Frane and controller are modeled.
- Next, the POD controller is implemented. It is designed to use generator speed or power output as feedback, and a control law is established that adjusts the STACOM output to dampen oscillations effectively. The controller's gain and time constants are tuned for optimal performance.
- For the CLF controller, the appropriate state variables are defined, and a suitable Lyapunov function is chosen. Based on this function, a control strategy is developed that adjusts the STACOM output to maintain system stability during transients.
- Simulations are set up to test various transient scenarios, focusing on fault conditions and load changes. The results are analyzed to evaluate the effectiveness of both the POD and CLF controllers in enhancing stability. Their parameters are fine-tuned based on the outcomes, and sensitivity analyses are conducted to assess the impact of different settings.

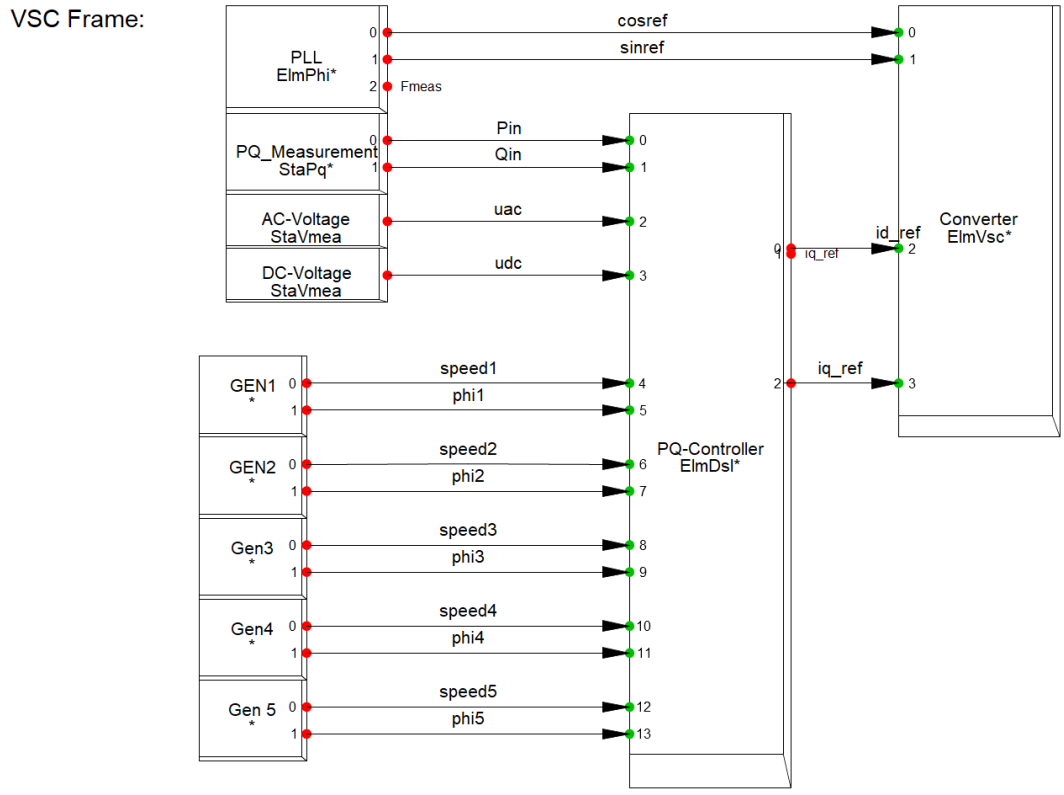


**Figure 7.3:** STATCOM frame

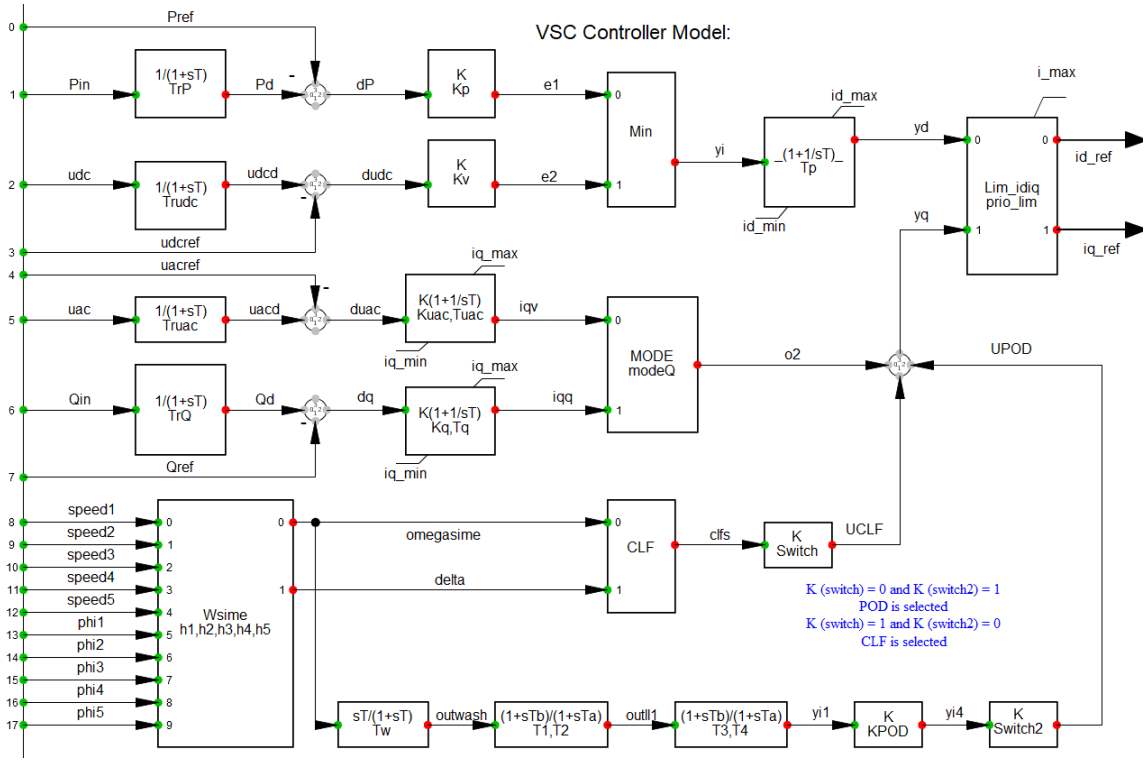


**Figure 7.4:** STATCOM with POD and CLF controller

## 7.4 HVDC model and important parameters

High Voltage Direct Current (HVDC) transmission systems are essential for long-distance power transmission, providing several advantages over traditional AC systems. The DIgSILENT software offers comprehensive modeling capabilities for HVDC systems, allowing for detailed analysis and simulation. Where:

**Table 7.8:** Data of DC transmission line of mono polar of LCC HVDC

| Line Name | $R_{OHL}$ $[\Omega]$ | $L_{OHL}[mH]$ | $V_{scheduled}$ [kV] | Rated power [MW] |
|---|---|---|---|---|
| $Line\_DC\_R$ | 12 | 1000 | 500 | 1000 |
| $Line\_DC\_I$ | 12 | 1000 | 500 | 1000 |

**Table 7.9:** Converter Data

| Name | Max $\alpha$ [deg] | Min $\alpha$ [deg] | Series Bridge | $U_{LL}$ | $X_C$ $[\Omega]$ | Max Tap | Min Tap | Cont-mode | Smoothing X $[mH/Pole]$ |
|---|---|---|---|---|---|---|---|---|---|
| Rectifier | 15 | 5 | 2 | 400 | 12.448 | 1.12 | 0.91 | DC current | 300 |
| Inverter | 20 | 20 | 2 | 400 | 12.448 | 1.12 | 0.91 | DC voltage | 300 |

**Table 7.10:** AC filter data for both rectifier and inverter

| Name | Volt [kV] | System type | Mvar Rating | Quality factor | parallel resistor $[\Omega]$ |
|---|---|---|---|---|---|
| HighFreq $Filter\_R\_P$ | 400 | AC | 339.07 | 0 | 83.32 |
| HighFreq $Filter\_R\_P1$ | 400 | AC | 339.07 | 0 | 83.32 |
| LowFreq $Filter\_R\_P$ | 400 | AC | 336.03 | 5.01 | 261.87 |
| HighFreq $Filter\_R\_N$ | 400 | AC | 339.07 | 0 | 83.32 |
| HighFreq $Filter\_R\_N1$ | 400 | AC | 339.07 | 0 | 83.32 |
| LowFreq $Filter\_R\_N$ | 400 | AC | 336.03 | 5.01 | 261.87 |
| HighFreq $Filter\_I\_P$ | 400 | AC | 762.9 | 0 | 37.03 |
| HighFreq $Filter\_I\_P1$ | 400 | AC | 762.9 | 0 | 37.03 |
| HighFreq $Filter\_I\_N$ | 400 | AC | 762.9 | 0 | 37.03 |
| HighFreq $Filter\_I\_N1$ | 400 | AC | 762.9 | 0 | 37.03 |

- $R_{OHL}$ is Resistance of the overhead line.
- $L_{OHL}$ is inductance of the overhead line.
- $Line\_DC\_R$ is DC transmission line in the Rectifier side.

- *Line_DC_I* is DC transmission line on the inverter side.
- $U_{LL}$ is the line-to-line AC voltage on both converters' AC side.
- $X_C$ is commutation reactance.
- Max Tap is a maximum tap changing transformer.
- Mix Tap is a minimum tap changing transformer.
- Smoothing X is the smoothing reactance of the converters.
- HighFreq *Filter_R_P* is the high-frequency filter for the positive rectifier pole.
- HighFreq *Filter_R_P*1 is the high-frequency filter for the positive rectifier pole.
- HighFreq *Filter_R_N* is the high-frequency filter for the negative rectifier pole.
- HighFreq *Filter_R_N*1 is the high-frequency filter for the negative rectifier pole.
- LowFreq *Filter_R_P* is the low-frequency filter for the positive rectifier pole.
- LowFreq *Filter_R_N* is the low frequency filter for the negative rectifier pole.
- HighFreq *Filter_I_P* is the high-frequency filter for the positive Inverter pole.
- HighFreq *Filter_I_P*1 is the high-frequency filter for the positive Inverter pole.
- HighFreq *Filter_I_N* is the high-frequency filter for the negative inverter pole.
- HighFreq *Filter_I_N*1 is the high-frequency filter for the negative inverter pole.

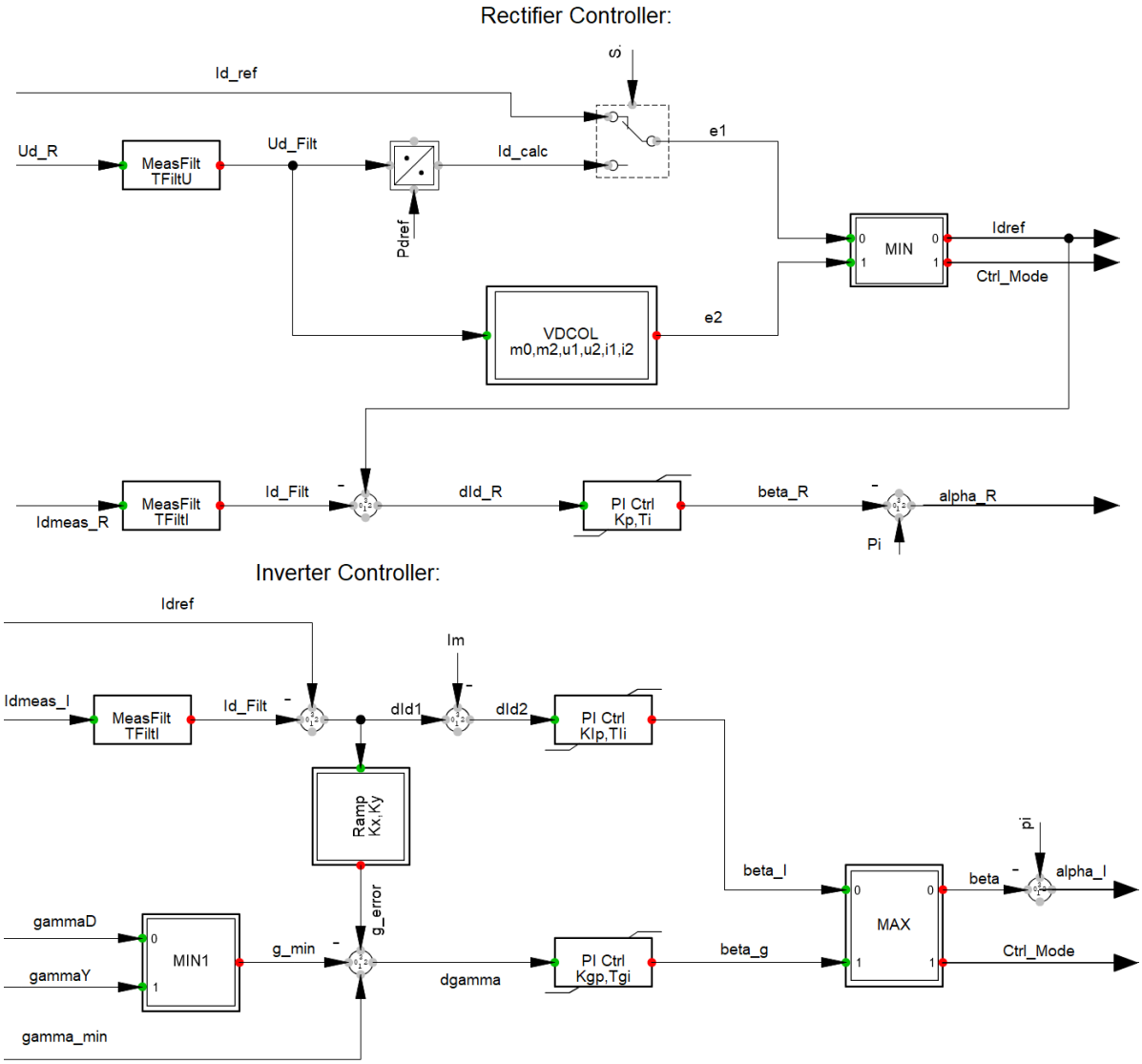


**Figure 7.5:** DSL of Rectifier and Inverter control of Monopolar LCC HVDC

## 7.5 Grid Modeling

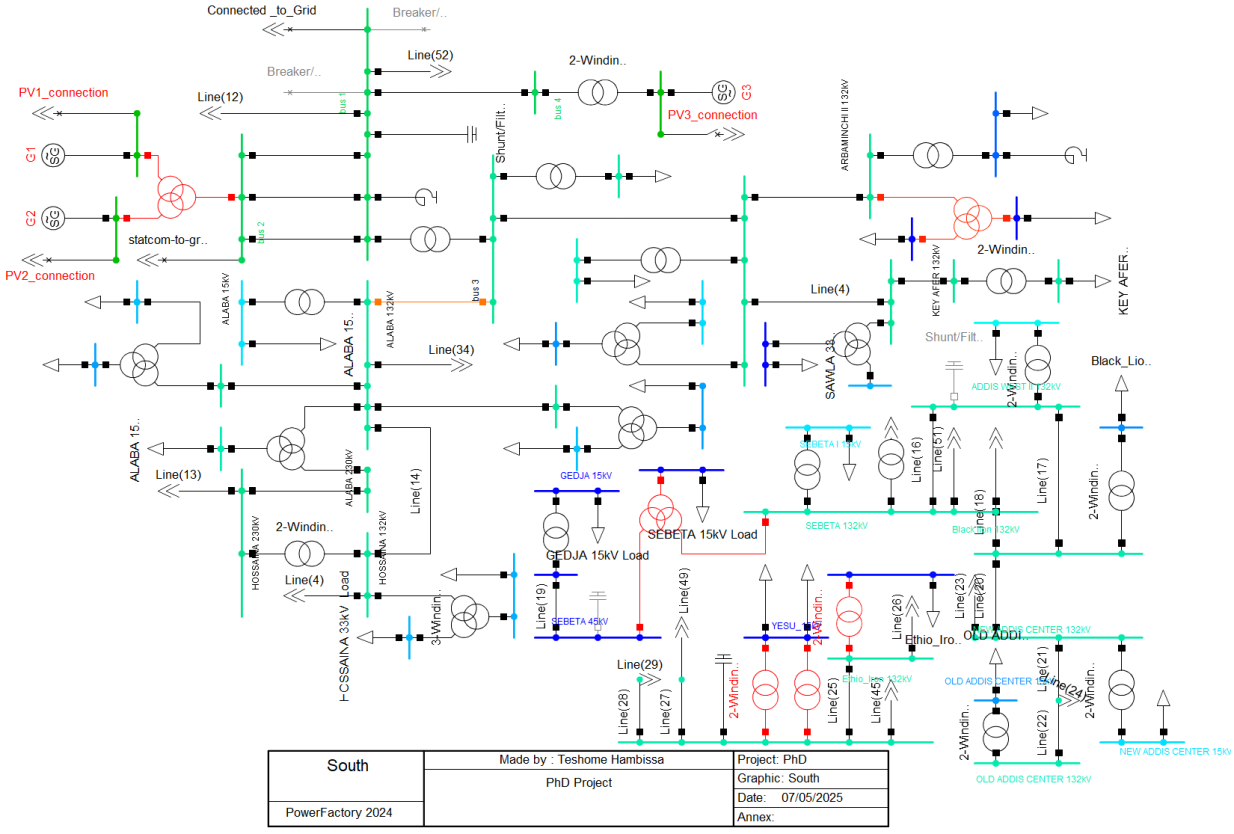


**Figure 7.6:** Area = South

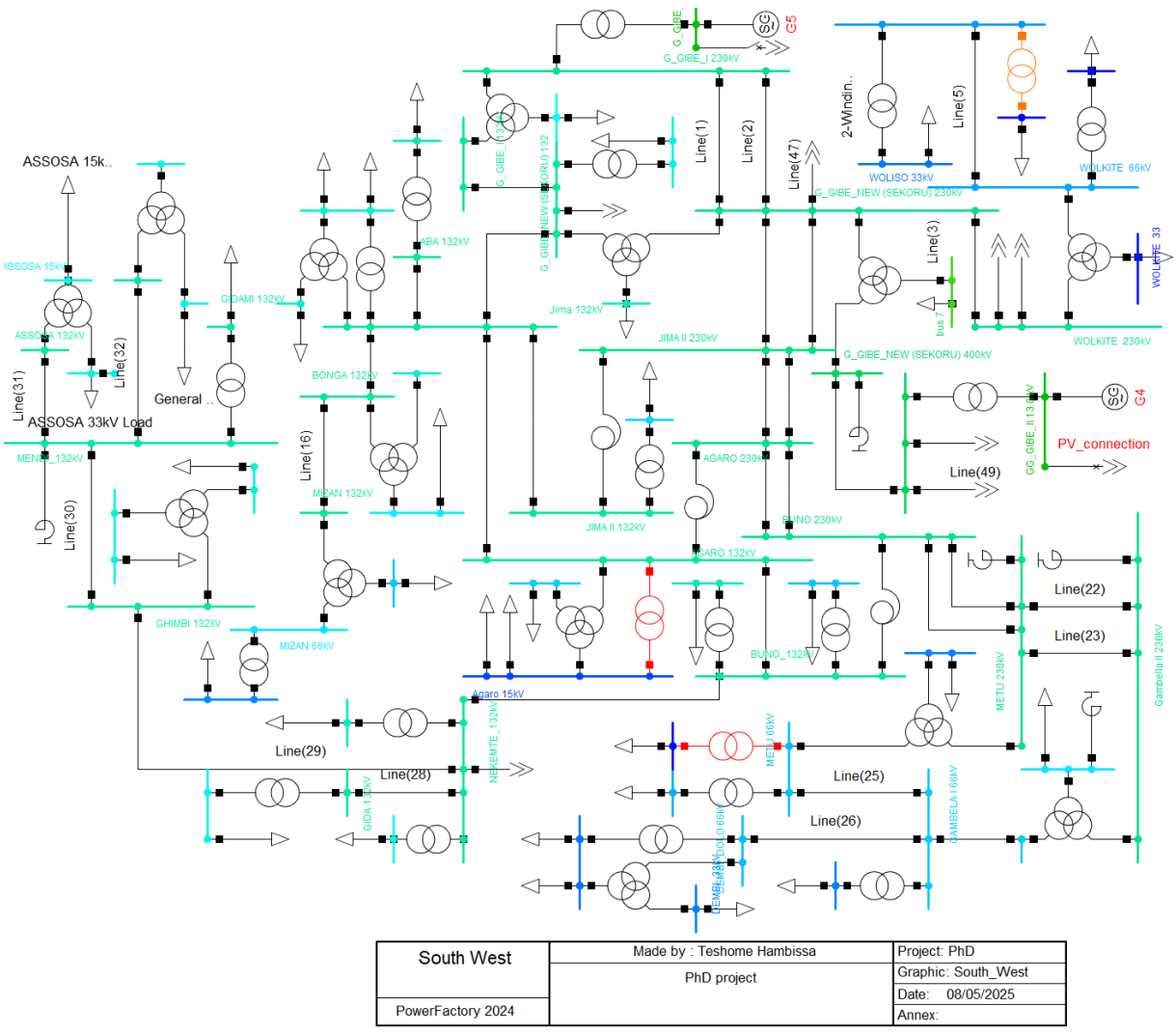


**Figure 7.7:** Area = South-West

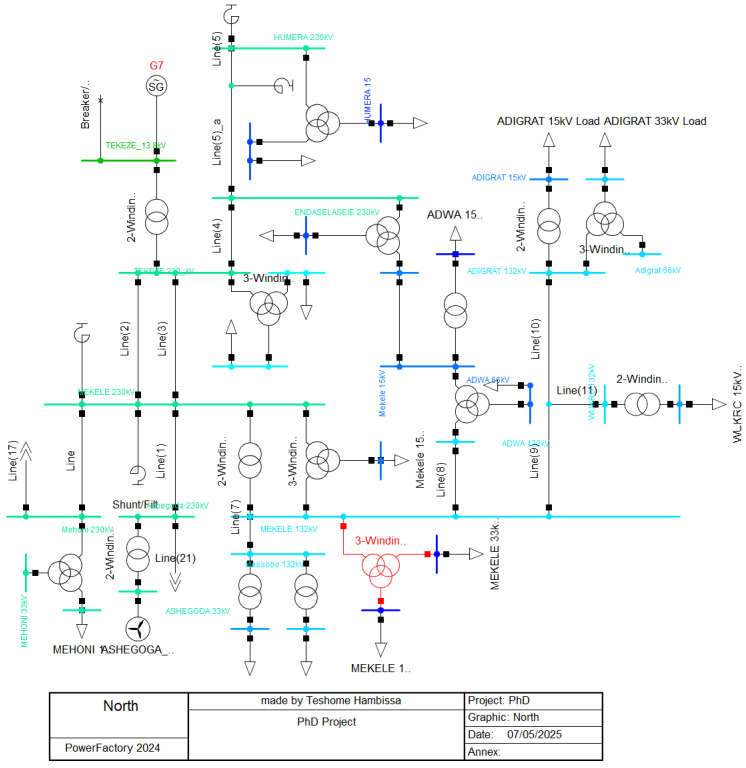


**Figure 7.8:** Area = North

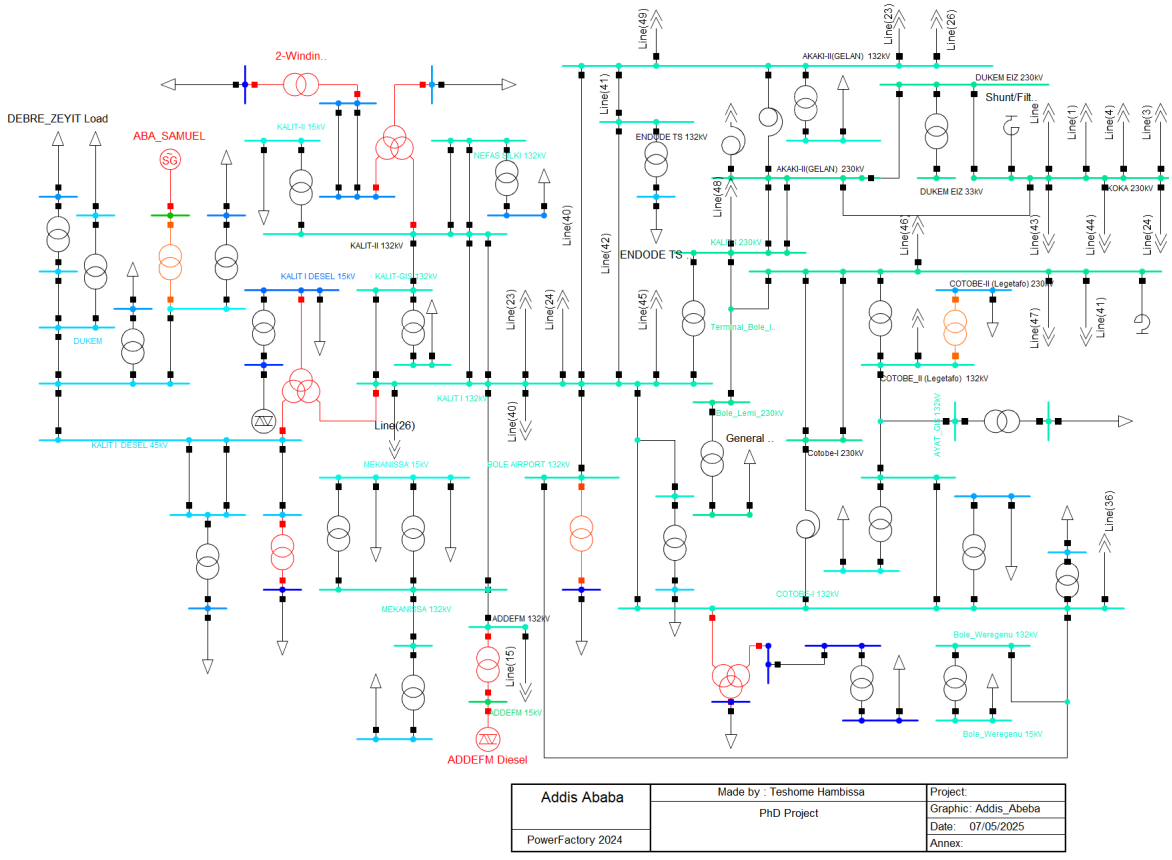


**Figure 7.9:** Area = Addis Ababa

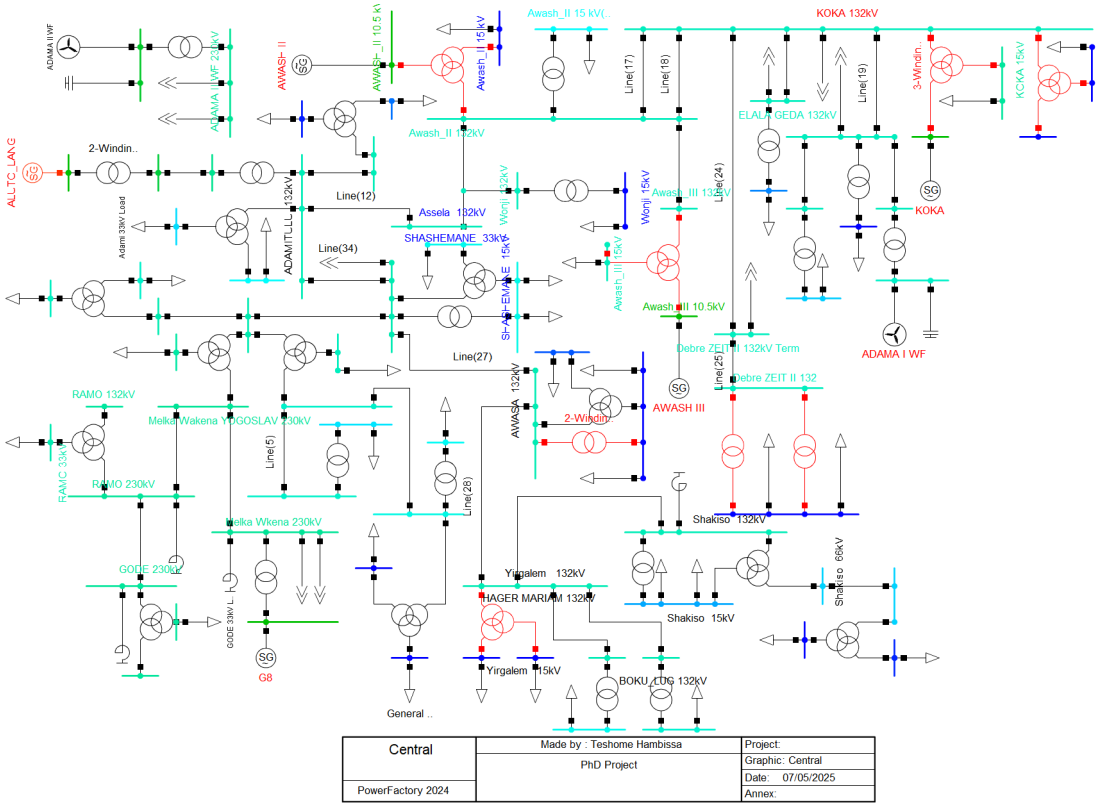


**Figure 7.10:** Area = Central

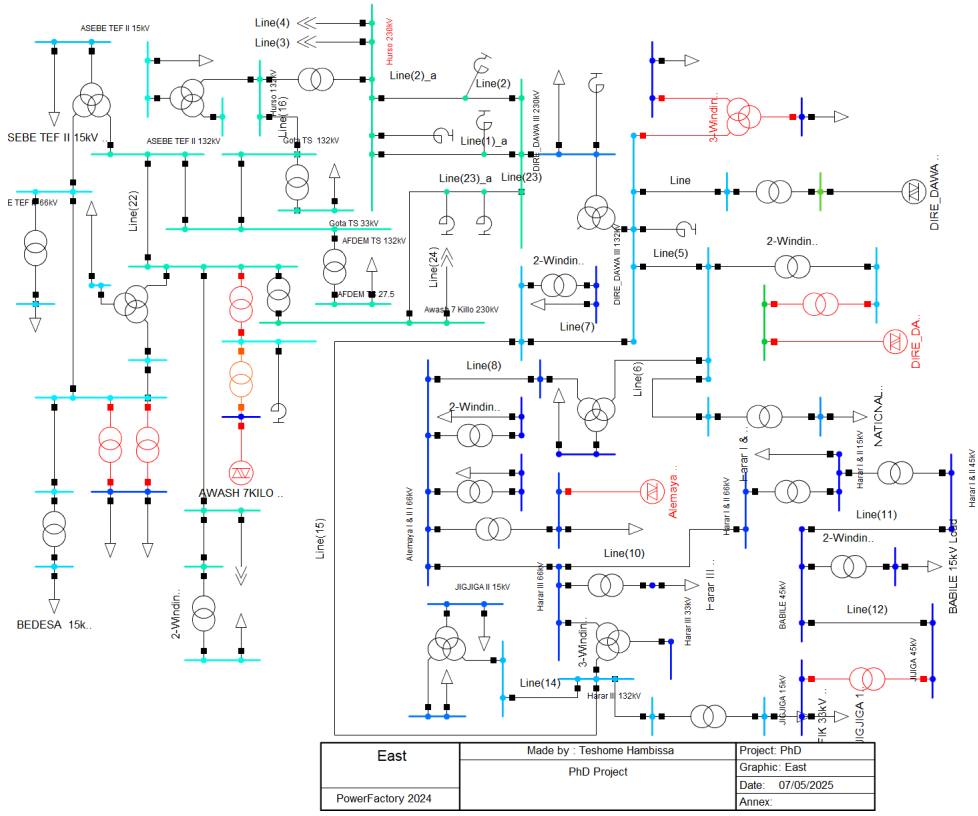


**Figure 7.11:** Area = East

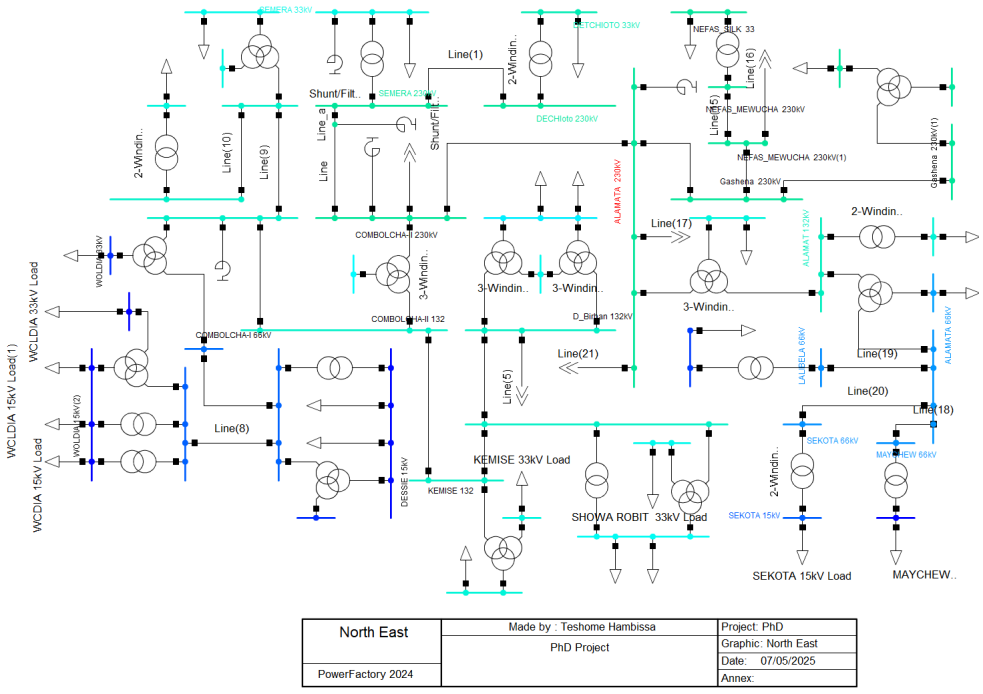


| North East | Made by : Teshome Hambissa | Project: PhD |
|---|---|---|
| | PhD Project | Graphic: North East |
| PowerFactory 2024 | | Date: 07/05/2025 |
| | | Annex: |

**Figure 7.12:** Area = North East

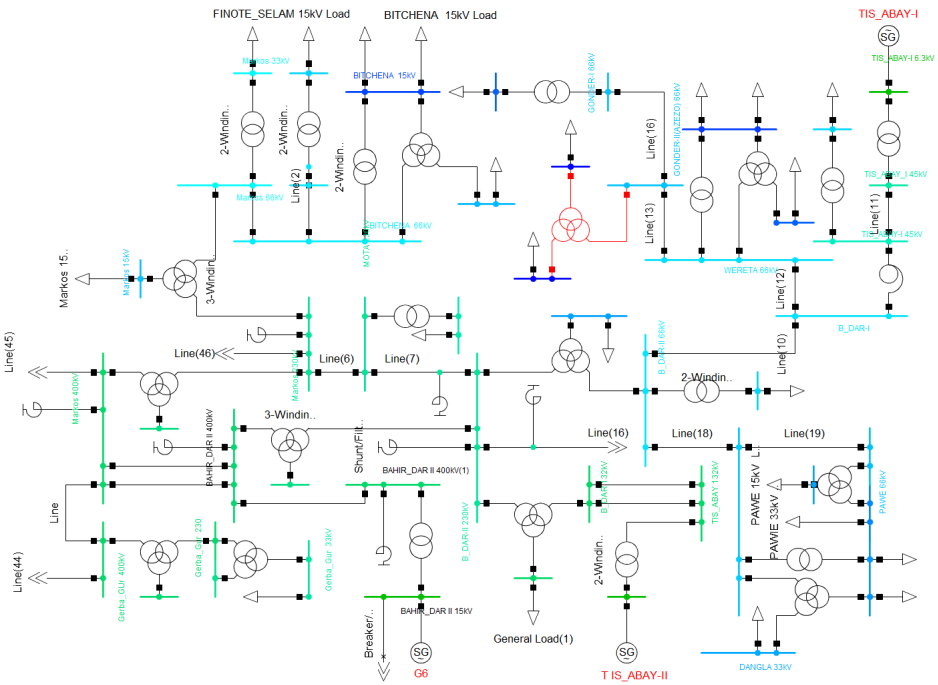


| North West | Made by Teshome Hambissa | Project: PHD |
|---|---|---|
| | PhD Project | Graphic: North_West |
| PowerFactory 2024 | | Date: 07/05/2025 |
| | | Annex: |

**Figure 7.13:** Area = North West

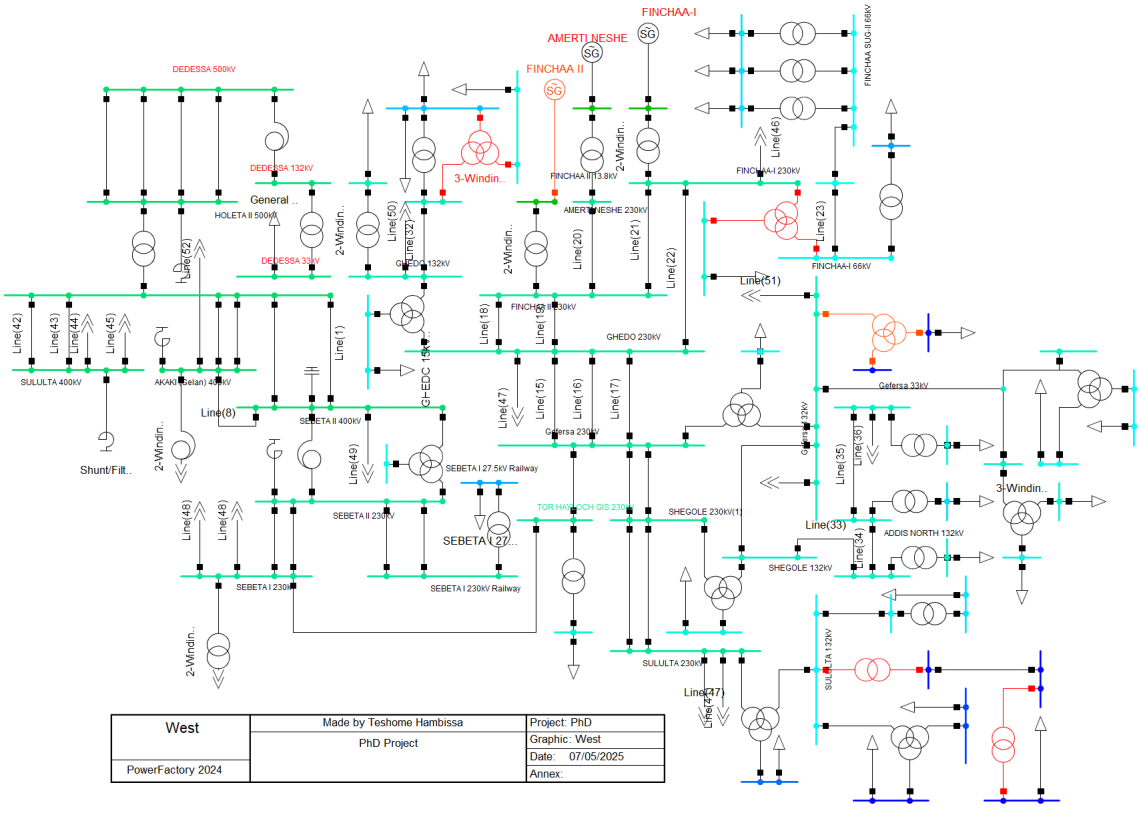


**Figure 7.14:** Area = West

# Bibliography


[1] E. Panos, M. Densing, and K. Volkart, **Access to electricity in the world energy council's global energy scenarios: An outlook for developing regions until 2030**, *Energy Strategy Reviews*, vol. 9, 28–49 (see page 1).

[2] H. Ritchie, P. Rosado, and M. Roser, **Access to energy**, *Our World in Data* (see page 1).

[3] G. E. Transformation, **Global energy transformation: A roadmap to 2050**, *IRENA: Abu Dhabi, United Arab Emirates* (see page 1).

[4] F. M. Gonzalez-Longatt and J. L. R. Torres, **Modelling and Simulation of Power Electronic Converter Dominated Power Systems in PowerFactory**. Springer Nature, 2020 (see page 2).

[5] P. Du and Y. Makarov, **Using disturbance data to monitor primary frequency response for power system interconnections**, *IEEE Transactions on Power Systems*, vol. 29:no. 3, 1431–1432 (see pages 2, 53).

[6] Y. Xue, Z. Zhang, N. Zhang, W. Hua, G. Wang, and Z. Xu, **Transient stability analysis and enhancement control strategies for interconnected ac systems with vsc-based generations**, *International Journal of Electrical Power & Energy Systems*, vol. 149, 109017 (see pages 2, 12).

[7] U. Datta, A. Kalam, and J. Shi, **Battery energy storage system control for mitigating pv penetration impact on primary frequency control and state-of-charge recovery**, *IEEE Transactions on Sustainable Energy*, vol. 11:no. 2, 746–757 (see pages 2, 9, 65).

[8] A. Oudalov, D. Chartouni, and C. Ohler, **Optimizing a battery energy storage system for primary frequency control**, *IEEE Transactions on power systems*, vol. 22:no. 3, 1259–1266 (see pages 2, 9, 53).

[9] C.-K. Kim, V. K. Sood, G.-S. Jang, S.-J. Lim, and S.-J. Lee, **HVDC transmission: power conversion applications in power systems**. John Wiley & Sons, 2009 (see page 3).

[10] C. Nguyen-Mau, K. Rudion, and Z. Styczynski, **Hvdc application for enhancing power system stability**, in *2011 EPU-CRIS International Conference on Science and Technology*, IEEE, 2011, 1–6 (see page 3).

[11] G. F. Reed, H. A. Al Hassan, M. J. Korytowski, P. T. Lewis, and B. M. Grainger, **Comparison of hvac and hvdc solutions for offshore wind farms with a procedure for system economic evaluation**, in *2013 IEEE energytech*, IEEE, 2013, 1–7 (see page 4).

[12] O. Peake, **The history of high voltage direct current transmission**, *Australian Journal of Multi-Disciplinary Engineering*, vol. 8:no. 1, 47–55 (see page 4).

[13] G. Asplund, C. Lennart, and O. Tollerz, **Years-part 1 abb-from pioneer to world leader**, *ABB Review*, 6–8 (see page 4).

[14] J. Arrillaga, **High voltage direct current transmission**. Iet, 1998 (see page 4).

[15] J. Arrillaga, Y. H. Liu, and N. R. Watson, **Flexible power transmission: the HVDC options**. John Wiley & Sons, 2007 (see page 5).

[16] M. Pai, K. Padiyar, and C. Radhakrishna, **Transient stability analysis of multi-machine ac/dc power systems via energy-function method**, *IEEE Transactions on Power Apparatus and Systems*: no. 12, 5027–5035 (see page 5).

[17] P. Kundur, **Power system stability**, *Power system stability and control*, vol. 10:no. 1, 7–1 (see pages 5–8, 12, 13, 32, 36, 40, 58, 59).

[18] D. Obradovic, **Coordinated frequency control between interconnected ac/dc systems**, Ph.D. dissertation, KTH Royal Institute of Technology, 2020 (see pages 5, 52).

[19] M. Ghandhari, **Stability of power systems**, *Electric Power Systems, Royal Institute of Technology, Stockholm, Sweden* (see pages 6–8, 41, 52).

[20] G. M. Njoka, L. Mogaka, and A. Wangai, **Impact of variable renewable energy sources on the power system frequency stability and system inertia**, *Energy Reports*, vol. 12, 4983–4997 (see page 8).

[21] S. Saha, M. Saleem, and T. Roy, **Impact of high penetration of renewable energy sources on grid frequency behaviour**, *International Journal of Electrical Power & Energy Systems*, vol. 145, 108701 (see page 8).

[22] J. Rezaei, M. E. H. Golshan, and H. H. Alhelou, **Impacts of integration of very large-scale photovoltaic power plants on rotor angle and frequency stability of power system**, *IET Renewable Power Generation*, vol. 16:no. 11, 2384–2401 (see page 8).

[23] L. Meegahapola, A. Sguarezi, J. S. Bryant, M. Gu, E. R. Conde D, and R. B. Cunha, **Power system stability with power-electronic converter interfaced renewable power generation: Present issues and future trends**, *Energies*, vol. 13:no. 13, 3441 (see page 9).

[24] N. G. Hingorani and L. Gyugyi, **Facts concept and general system considerations** (see page 9).

[25] A. H. Elkasem, M. Khamies, G. Magdy, I. B. Taha, and S. Kamel, **Frequency stability of ac/dc interconnected power systems with wind energy using arithmetic optimization algorithm-based fuzzy-pid controller**, *Sustainability*, vol. 13:no. 21, 12095 (see page 9).

[26] Y. Chen, **Stability Assessment of Power Systems with Multiple Voltage Source Converters: Bifurcation-Theory-Based Methods**. Springer Nature, 2024 (see page 9).

[27] M. Eidiani, "Modeling renewable energy resources using digsilent powerfactory software," in *Power systems operation with 100% renewable energy sources*, Elsevier, 2024, 165–202 (see page 11).

[28] Fichtner, *Ethiopia-kenya power systems interconnection project: Final feasibility study report*, 2009 (see page 11).

[29] G. Ludin, A. Nakadomari, A. Yona, S. Mikkili, S. S. Rangarajan, E. Collins, and T. Senjyu, **Technical and economic analysis of an hvdc transmission system for renewable energy connection in afghanistan**, *Sustainability*, vol. 14, 1468. DOI: 10.3390/su14031468 (see pages 12, 57).

[30] H. Huang, Z. Xu, W. Wang, and C. Wang, **Transient stability analysis of shanghai power grid with multiple hvdc links**, in *2010 International Conference on Power System Technology*, 2010, 1–6. DOI: 10.1109/POWERCON.2010.5666100 (see page 12).

[31] L. Sigrist, F. Echavarren, L. Rouco, and P. Panciatici, **A fundamental study on the impact of hvdc lines on transient stability of power systems**, in *2015 IEEE Eindhoven PowerTech*, 2015, 1–6 (see page 12).

[32] M. Ndreko, A. A. van der Meer, M. Gibescu, M. A. van der Meijden, J. A. Bos, and K. P. Jansen, **Transient stability analysis of an onshore power system with multi-terminal offshore vsc-hvdc transmission: A case study for the netherlands**, in *2013 IEEE Power & Energy Society General Meeting*, IEEE, 2013, 1–5 (see page 12).

[33] G. Sianipar and J. Naiborhu, **Determination of critical clearing time in transient stability analysis**, in *International Conference on Electrical Engineering and Computer Science (ICEECS), Indonesia*, 2018 (see page 12).

[34] O. E. Oni, A. G. Swanson, and R. P. Carpanen, **Impact of lcc–hvdc multiterminal on generator rotor angle stability**, *International Journal of Electrical and Computer Engineering*, vol. 10:no. 1, 22 (see page 12).

[35] L. Sundaresh, Z. Yuan, K. Sun, J. Pan, and Y. Liu, **Improving power grid transient stability and transfer capability using hvdc emergency power controls**, in *2020 IEEE/PES Transmission and Distribution Conference and Exposition (T& D)*, 2020, 1–5. DOI: 10.1109/TD39804.2020.9299660 (see page 12).

[36] T. Machida, **Improving transient stability of ac system by joint usage of dc system**, *IEEE Transactions on Power Apparatus and Systems*, vol. PAS-85:no. 3, 226–232. DOI: 10.1109/TPAS.1966.291661 (see page 12).

[37] J. Arrillaga and I. Elamin, **Transient stability performance of a 3-machine system including an hvdc link**, in *Proceedings of the Institution of Electrical Engineers*, vol. 123, 11, IET, 1976, 1239–1244 (see page 12).

[38] D. Jovcic, **High voltage direct current transmission: converters, systems and DC grids**. John Wiley & Sons, 2019 (see pages 12, 14, 54).

[39] G. Kalcon and A. Y. Abbas, **Performance evaluation of constant current hvdc transmission line** (see page 14).

[40] H. Li, K. Han, S. Liu, H. Chen, X. Zhang, and K. Zou, **A dynamic nonlinear vdcol control strategy based on the taylor expansion of dc voltages for suppressing the subsequent commutation failure in hvdc transmission**, *Energies*, vol. 16:no. 21, 7342 (see page 15).

[41] A. Ahmed, D. Khan, A. M. Khan, M. U. Mustafa, M. K. Panjwani, M. Hanan, E. B. Agyekum, S. E. Uhunamure, and J. N. Edokpayi, **Modeling of efficient control strategies for lcc-hvdc systems: A case study of matiari–lahore hvdc power transmission line**, *Sensors*, vol. 22:no. 7, 2793 (see page 16).

[42] M. Mankour and B. S. Sami, **Mitigation of commutation failure method in lcc converter based on hvdc systems by mean of modeling and simulation**, *Journal of Ambient Intelligence and Humanized Computing*, vol. 14:no. 5, 5837–5852 (see page 16).

[43] J. Rebled Lluch, **Modelling, control and simulation of lcc-hvdc systems for stability studies**, M.S. thesis, Universitat Politècnica de Catalunya, 2017 (see page 16).

[44] C. Zhao, J. Xia, C. Guo, and R. Zhan, **An improved control strategy for current source converter-based hvdc using fundamental frequency modulation**, *International Journal of Electrical Power & Energy Systems*, vol. 133, 107265 (see page 20).

[45] Y. H. Liu, N. R. Watson, K. L. Zhou, and B. F. Yang, **Converter system nonlinear modelling and control for transmission applications—part ii: Csc systems**, *IEEE Transactions on Power Delivery*, vol. 28:no. 3, 1391–1401 (see page 20).

[46] T. Smed, G. Andersson, G. Sheble, and L. Grigsby, **A new approach to ac/dc power flow**, *IEEE Transactions on Power Systems*, vol. 6:no. 3, 1238–1244 (see page 21).

[47] P. Ye, Y. Sui, Y. Yuan, X. Li, and J. Tao, **Dynamic behavior analysis of hu-liao hvdc and ac parallel transmission system**, in *2010 Asia-Pacific Power and Energy Engineering Conference*, IEEE, 2010, 1–5 (see page 22).

[48] X. Lei and D. Retzmann, **Static and dynamic approaches for analyzing voltage stability**, *European transactions on electrical power*, vol. 16:no. 3, 277–296 (see page 22).

[49] J. K. Robinson, **Power system stability-computation of critical clearing time and stability margin index.** (see page 26).

[50] G. Tiruye, A. Besha, Y. Mekonnen, N. Benti, G. Gebreslase, and R. Tufa, *Opportunities and challenges of renewable energy production in ethiopia. sustainability 2021, 13, 10381*, 2021 (see page 32).

[51] J. Bai, J. Wang, Y. Huang, Y. Li, and S. Zhang, **A renewable energy capacity allocation planning method considering the balance of renewable energy accommodation and system investment costs**, in *2021 China International Conference on Electricity Distribution (CICED)*, 2021, 1099–1104. DOI: 10.1109/CICED50259.2021.9556795 (see page 32).

[52] A. M. Mahfuz-Ur-Rahman, M. R. Islam, K. M. Muttaqi, and D. Sutanto, **An effective energy management with advanced converter and control for a pv-battery storage based microgrid to improve energy resiliency**, *IEEE Transactions on Industry Applications*, vol. 57:no. 6, 6659–6668. DOI: 10.1109/TIA.2021.3115085 (see page 32).

[53] O. O. Samuel, I. S. Sinneh, and J. O. Adasen, **Design and grid integration of mega (5mw) solar pv system**, in *2021 5th International Conference on Electrical, Electronics, Communication, Computer Technologies and Optimization Techniques (ICEECCOT)*, 2021, 100–105. DOI: 10.1109/ICEECCOT52851.2021.9708065 (see page 32).

[54] H. Nagpal, I.-I. Avramidis, F. Capitanescu, and A. G. Madureira, **Local energy communities in service of sustainability and grid flexibility provision: Hierarchical management of shared energy storage**, *IEEE Transactions on Sustainable Energy*, vol. 13:no. 3, 1523–1535. DOI: 10.1109/TSTE.2022.3157193 (see page 32).

[55] M. Pavella, **Power system transient stability assessment–traditional vs modern methods**, *Control Engineering Practice*, vol. 6:no. 10, 1233–1246 (see page 32).

[56] Y. Aisayev, K. Tergemes, A. Zhauyt, S. Sheryazov, and K. Bakenov, **The impact of replacing synchronous generators with renewable-energy technologies on the transient stability of the mangystau power system: An introduction to flexible automatic dosage of exposures**, *Energies*, vol. 17:no. 10, 2314 (see page 32).

[57] R. Radhika and K. S. Thampatty, **Impacts of renewable energy integration on power system stability**, in *2023 IEEE Technology & Engineering Management Conference-Asia Pacific (TEMSCON-ASPAC)*, IEEE, 2023, 1–6 (see page 32).

[58] A. Stan, S. Costinaș, and G. Ion, **Overview and assessment of hvdc current applications and future trends**, *Energies*, vol. 15:no. 3, 1193 (see page 32).

[59] M. Shafiee, M. Sajadinia, A.-A. Zamani, and M. Jafari, **Enhancing the transient stability of interconnected power systems by designing an adaptive fuzzy-based fractional order pid controller**, *Energy Reports*, vol. 11, 394–411 (see page 33).

[60] H. K. Khalil, **Lyapunov stability**, *Control systems, robotics and automation*, vol. 12, 115 (see page 33).

[61] M. Abido, **Power system stability enhancement using facts controllers: A review**, *The arabian journal for science and engineering*, vol. 34:no. 1B, 153–172 (see page 33).

[62] A. S. Mir, A. K. Singh, B. C. Pal, N. Senroy, and J. Tu, **Adequacy of lyapunov control of power systems considering modelling details and control indices**, *IEEE Transactions on Power Systems*, vol. 38:no. 3, 2275–2289. DOI: 10.1109/TPWRS.2022.3180397 (see page 33).

[63] A. Narula, M. Bongiorno, M. Beza, J. R. Svensson, X. Guillaud, and L. Harnefors, **Impact of steady-state grid-frequency deviations on the performance of grid-forming converter control strategies**, in *2020 22nd European Conference on Power Electronics and Applications (EPE'20 ECCE Europe)*, 2020, P.1–P.10. DOI: 10.23919/EPE20ECCEEurope43536.2020.9215947 (see page 33).

[64] T. Hambissa, M. Ghandhari, and G. Biru, **Modeling of ethiopia-kenya hvdc for power system stability study**, in *2023 IEEE AFRICON*, IEEE, 2023, 1–6 (see page 34).

[65] A. Ulbig, T. S. Borsche, and G. Andersson, **Impact of low rotational inertia on power system stability and operation**, *IFAC Proceedings Volumes*, vol. 47:no. 3, 7290–7297 (see page 36).

[66] O. Noureldeen and A. M. Ibrahim, **Performance analysis of grid connected pv/wind hybrid power system during variations of environmental conditions and load**, *International Journal of Renewable Energy Research*, vol. 8:no. 1, 208–220 (see page 37).

[67] B. Singh, R. Saha, A. Chandra, and K. Al-Haddad, **Static synchronous compensators (statcom): A review**, *IET power electronics*, vol. 2:no. 4, 297–324 (see page 37).

[68] A. S. Al-ahmed, **Performance of controlled facts and vsc-hvdc in a power system subject to inter-area oscillation** (see page 37).

[69] H. Latorre, M. Ghandhari, and L. Soder, **Multichoice control strategy for vsc-hvdc**, in *2007 iREP Symposium - Bulk Power System Dynamics and Control - VII. Revitalizing Operational Reliability*, 2007, 1–7. DOI: 10.1109/IREP.2007.4410511 (see page 37).

[70] M. Ghandhari, G. Andersson, M. Pavella, and D. Ernst, **A control strategy for controllable series capacitor in electric power systems**, *Automatica*, vol. 37:no. 10, 1575–1583 (see page 39).

[71] D. Derbew, **Ethiopia's renewable energy power potential and development opportunities**, *Ministry of Water and Energy: Abu Dhabi, UAE* (see page 52).

[72] Y. Wang, V. Silva, and M. Lopez-Botet-Zulueta, **Impact of high penetration of variable renewable generation on frequency dynamics in the continental europe interconnected system**, *IET Renewable Power Generation*, vol. 10:no. 1, 10–16 (see page 52).

[73] J. D. Watson, N. R. Watson, D. Santos-Martin, A. R. Wood, S. Lemon, and A. J. Miller, **Impact of solar photovoltaics on the low-voltage distribution network in new zealand**, *IET Generation, Transmission and Distribution*, vol. 10:no. 1, http://doi.org/10.1049/iet-gtd.2014.1076, 1–9 (see page 52).

[74] **A new approach for optimal sizing of battery energy storage system for primary frequency control of islanded microgrid**, *International Journal of Electrical Power & Energy Systems*, vol. 54, http://doi.org/j.ijepes.2013.07.005, 325–333, ISSN: 0142-0615 (see pages 52, 61).

[75] T. Ackermann, **Wind power in power systems**. John Wiley & Sons, 2012 (see page 53).

[76] A. Jawad and N.-A. Masood, **A systematic approach to estimate the frequency support from large-scale pv plants in a renewable integrated grid**, *Energy Reports*, vol. 8, http://doi.org/10.1016/j.egyr.2021.12.017, 940–954, ISSN: 2352-4847 (see page 53).

[77] D. Obradovic, M. Dijokas, T. Van Cutsem, R. Eriksson, M. Ghandhari, and A. Tosatto, **Assessment of hvdc frequency control methods in the nordic test system**, in *CIGRE 2020*, 2020 (see page 53).

[78] U. Datta, A. Kalam, and J. Shi, **Battery energy storage system control for mitigating PV penetration impact on primary frequency control and state-of-charge recovery**, *IEEE Transactions on Sustainable Energy*, vol. 11:no. 2, http://doi.org//10.1109/TSTE.2019.2904722, 746–757 (see page 53).

[79] S. You, G. Kou, Y. Liu, X. Zhang, Y. Cui, M. J. Till, W. Yao, and Y. Liu, **Impact of high pv penetration on the inter-area oscillations in the us eastern interconnection**, *IEEE Access*, vol. 5, http://doi.org/10.1109/ACCESS.2017.2682260, 4361–4369 (see page 53).

[80] R. Shah, N. Mithulananthan, and K. Y. Lee, **Large-scale pv plant with a robust controller considering power oscillation damping**, *IEEE Transactions on Energy Conversion*, vol. 28:no. 1, http://doi.org/10.1109/TEC.2012.2230328, 106–116 (see page 53).

[81] D. Remon, C. A. Cañizares, and P. Rodriguez, **Impact of 100-mw-scale pv plants with synchronous power controllers on power system stability in northern chile**, *IET Generation, Transmission & Distribution*, vol. 11:no. 11, 2958–2964 (see page 53).

[82] L. Zhou, X. Yu, B. Li, C. Zheng, J. Liu, Q. Liu, and K. Guo, **Damping inter-area oscillations with large-scale pv plant by modified multiple-model adaptive control strategy**, *IEEE Transactions on Sustainable Energy*, vol. 8:no. 4, 1629–1636 (see page 53).

[83] S. A. Hosseini, M. Toulabi, A. Ashouri-Zadeh, and A. M. Ranjbar, **Battery energy storage systems and demand response applied to power system frequency control**, *International Journal of Electrical Power & Energy Systems*, vol. 136, 107680 (see page 53).

[84] Z. A. Obaid, L. Cipcigan, M. T. Muhssin, and S. S. Sami, **Control of a population of battery energy storage systems for frequency response**, *International Journal of Electrical Power & Energy Systems*, vol. 115, 105463 (see page 53).

[85] Y. Meng, X. Li, X. Liu, X. Cui, P. Xu, and S. Li, **A control strategy for battery energy storage systems participating in primary frequency control considering the disturbance type**, *IEEE Access*, vol. 9, 102004–102018 (see page 53).

[86] Q. Hou, E. Du, N. Zhang, and C. Kang, **Impact of high renewable penetration on the power system operation mode: A data-driven approach**, *IEEE Transactions on Power Systems*, vol. 35:no. 1, http://doi.org/10.1109/TPWRS.2019.2929276, 731–741 (see page 53).

[87] M. S. Hossain, N. Abboodi Madlool, A. W. Al-Fatlawi, and M. El Haj Assad, **High penetration of solar photovoltaic structure on the grid system disruption: An overview of technology advancement**, *Sustainability*, vol. 15:no. 2, 1174 (see page 57).

[88] H. Bevrani, **Robust power system frequency control**. Springer, 2014, vol. 4 (see page 57).

[89] M. R. Amin, M. Negnevitsky, E. Franklin, K. S. Alam, and S. B. Naderi, **Application of battery energy storage systems for primary frequency control in power systems with high renewable energy penetration**, *Energies*, vol. 14:no. 5, http://doi.org//10.3390/en14051379, ISSN: 1996-1073 (see page 58).

[90] H. Saadat, *Power system analysis, wcb mcgraw-hill series in electrical and computer engineering*, 1999 (see page 58).

[91] J. Riesz, **The future power system security program**, *Australian Energy Market Operator: Melbourne, Australia* (see page 59).

[92] X. Lu, K. Sun, J. M. Guerrero, J. C. Vasquez, and L. Huang, **State-of-charge balance using adaptive droop control for distributed energy storage systems in dc microgrid applications**, *IEEE Transactions on Industrial Electronics*, vol. 61:no. 6, http://doi.org/10.1109/TIE.2013.2279374, 2804–2815 (see page 60).

[93] P. P. Mercier, R. Cherkaoui, and A. Oudalov, **Optimizing a battery energy storage system for frequency control application in an isolated power system**, *IEEE Transactions on Power Systems*, vol. 24, 1469–1477 (see page 61).

[94] S. Akkari, J. Dai, M. Petit, and X. Guillaud, **Interaction between the voltage-droop and the frequency-droop control for multi-terminal hvdc systems**, *IET Generation, Transmission & Distribution*, vol. 10:no. 6, 1345–1352 (see page 63).

[95] P. T. Moseley, **Energy storage in remote area power supply (raps) systems**, *Journal of Power Sources*, vol. 155:no. 1, 83–87 (see page 66).

[96] G. J. May, A. Davidson, and B. Monahov, **Lead batteries for utility energy storage: A review**, *Journal of energy storage*, vol. 15, 145–157 (see page 66).

[97] U. Datta, **Battery energy storage system for renewable energy integrated power system stability enhancement**, Ph.D. dissertation, Victoria University, 2020 (see page 66).